ANALYSIS OF CREEP IN A VARIABLE THICKNESS ROTATING DISC MADE OF FUNCTIONALLY GRADED COMPOSITE

A Thesis

submitted for the award of degree of

DOCTOR OF PHILOSOPHY

IN

MECHANICAL ENGINEERING

by

KISHORE KHANNA

Registration No. 950908008

Under the Guidance of

Dr. S. P. Nigam
Former Visiting Professor
Mechanical Engg. Department
Thapar University,
Patiala – 147004 (India)

Dr. Vinay Kumar Gupta
Professor
Department of Mechanical Engg.
Punjabi University,
Patiala – 147002 (India)

MECHANICAL ENGINEERING DEPARTMENT

THAPAR UNIVERSITY, PATIALA-147004, INDIA

(Established under Section 3 of UGC Act, 1956 vide Notification No. F9-12/84-U.3 of G.O.I.)

August 2017

Dedicated to

my family

CERTIFICATE

I, **Kishore Khanna**, hereby certify that the work presented in the thesis entitled, **"ANALYSIS OF CREEP IN A VARIABLE THICKNESS ROTATING DISC MADE OF FUNCTIONALLY GRADED COMPOSITE"**, which is being submitted for fulfillment of the requirement for the award of the degree of **DOCTOR OF PHILOSOPHY**, in the Mechanical Engineering Department, Thapar University, Patiala, is an authentic record of my own work and refers other researchers' work, which is duly listed in the reference section. The matter presented in this thesis has not been submitted either partially or fully to any other University or Institute for the award of any other degree.

(Kishore Khanna)
Registration No. 950908008

This is to certify that the above statement made by the candidate is correct and true to the best of our knowledge.

Dr. S. P. Nigam
Former Visiting Professor
Mechanical Engineering Department
Thapar University,
Patiala – 147004 (India)

Dr. Vinay Kumar Gupta
Professor
Department of Mechanical Engineering
Punjabi University,
Patiala – 147002 (India)

ACKNOWLEDGEMENT

A formal acknowledgement will hardly meet the end of justice in the expression of my deep sense of gratitude and obligation to all those who helped me in completion of this research. This research is the outcome of the guidance, assistance and inspiration of several people throughout the study.

Above all, with all humility, I would like to thank God, the almighty, the compassionate, who bestowed me with good health and enough courage to reach at this crucial juncture.

I express my heartfelt gratitude to my research supervisors, Dr. Vinay Kumar Gupta, Professor, Department of Mechanical Engineering, Punjabi University, Patiala, and Dr. S. P. Nigam, Former Visiting Professor, Thapar University, Patiala, who supervised my study with enduring interest, concern, faith, friendship and enthusiasm. It has been a great honor for me to work under their guidance and to learn the intricacies of research from them. I have great privilege and pleasure to express my sense of gratitude to both of them for their valuable guidance.

I wish to express my heartfelt gratitude to Dr. S. K. Mohapatra, Senior Professor and Head, Mechanical Engineering Department, for his support and motivation for the smooth progress of my Ph.D. work. My deepest regards and gratitude are also due to Dr. O. P. Pandey, Dean of Research & Sponsored Projects and Dr. Prakash Gopalan, Director, Thapar University for providing a healthy research environment. I wish to further extend my thanks to all the faculty members of the Mechanical Engineering Department, Thapar University, Patiala, for helping me in one or other way to carry out my Ph.D. work successfully.

I sincerely acknowledge the valuable support extended by Dr. Manish Garg during the course of this research work. I am indebted to my mother for showering her love, emotional support, prayers and endless encouragement to pursue the research work. The work would not have been possible without the blessings of my father, Late Sh. Thakur Dass. A special thank must go to my wife Kiran and my sons Ishan and Rohan, who have been the driving force behind this work and acted as an incessant source of inspiration and support. Their infinite affection and faith have kept me in high spirits throughout the work. I express my sincere gratitude for their forbearance and stoicism in the face of many inconveniences and long absences. Thanks are also due to my brothers, Mr. Rajinder Khanna and Mr. Gulshan

Khanna, and my sister Mrs. Geeta Gandhi and their family members for their support and encouragement.

At last, I would also like to thank all my office and technical staff members for extending their help and support in carrying out the present work.

(Kishore Khanna)

TABLE OF CONTENTS

LIST OF PUBLICATIONS

(A) International Journals:

PUBLISHED:

[1] Khanna K., Gupta V. K. and Nigam S. P. (2015), Creep Analysis of a Variable Thickness Rotating FGM Disc using Tresca Criterion, *Defence Science Journal*, 65(2), 163-70 **(Impact factor: 0.428, Publisher: DRDO, India)** .

[2] Khanna K., Gupta V. K. and Nigam S. P. (2015), Investigating Creep Performance and Predicting Rupture Time for Rotating FGM Disc under Different Thermal Gradients, *Computers Materials & Continua*, 48 (3), 147-61 **(Impact factor: 0.500, Publisher: Tech Science Press)**.

[3] Khanna K., Gupta V. K. and Nigam S. P. (2017), Modeling and Analysis of Creep In a Variable Thickness Rotating FGM Disc Using Tresca and Von-Mises Criteria, *Iranian Journal of Science and Technology-Transactions of Mechanical Engineering*, 41(2), 109-19 **(Impact factor: 0.595, Publisher: Springer).**

[4] Khanna K., Gupta V. K. and Nigam S. P. (2017), Creep Analysis in Functionally Graded Rotating Disc Using Tresca Criterion and Comparison with Von-Mises Criterion, *Materials Today: Proceedings*, 4, 2431–38 **(Publisher: Elsevier).**

COMMUNICATED:

[5] Khanna K., Gupta V. K. and Nigam S. P., Effect of Varying Anisotropy on Creep Response of a Rotating FGM Disc having Variable Thickness, *Mechanics Research Communications* **(Impact factor: 1.667, Publisher: Elsevier).**

(B) National Conference:

[6] Kishore Khanna, S. P. Nigam and V. K. Gupta, On the Comparison of Creep in a Variable Thickness Rotating Functionally Graded Disc using Tresca and Von-Mises Criteria", *National Conference on Advances in Materials and Material Processing (AMMP-15)*, 27-28th March 2015, NIT Srinagar.

LIST OF FIGURES

LIST OF TABLES

LIST OF SYMBOLS

$A^{'}$	:	Structure dependent material parameter
a	:	Inner radius
B	:	Materials constant
b	:	Outer radius
E	:	Young's modulus
E_d	:	Young's modulus of reinforcement
E_m	:	Young's modulus of matrix
e	:	Normal strain
e_{ii}^{A}	:	Principle Almansi finite strain components
F, G, H, L, M, N	:	Hill's anisotropic constants
f	:	Transition function
h	:	Disc thickness
h_a	:	Disc thickness at inner radius
h_b	:	Disc thickness at outer radius
I	:	Invariant of stress tensor
J	:	Invariant of deviatoric stresses
k	:	Disc thickness index
M	:	Creep parameter
m	:	Reinforcement gradation index
m_I	:	Irreversibility index
n	:	True stress exponent
n_m	:	Measure
n_T	:	Temperature exponent
P	:	Reinforcement size
Q	:	True activation energy
R	:	Gas constant
r	:	Disc radius
T	:	Operating temperature
t	:	Time
T_m	:	Melting point

t_r	:	Rupture time
u	:	Radial deformation
$\dot{u}_a$	:	Radial deformation rate at the inner radius
$\dot{u}_r$	:	Radial deformation rate
V	:	Reinforcement content
V_{avg}	:	Average content of reinforcement
V_{max}	:	Maximum content of reinforcement
V_{min}	:	Minimum content of reinforcement
x	:	Ratio of radial and tangential stresses

Greek Symbols:

α, β	:	Anisotropic constants
ε	:	Strain
ε^0	:	Instantaneous elastic strain
ε_t	:	Total creep strain
$\dot{\varepsilon}$	:	Creep rate
$\dot{\varepsilon}_s$	:	Steady state creep rate
$\dot{\varepsilon}_r$	:	Radial strain rate
$\dot{\varepsilon}_\theta$	:	Tangential strain rate
$\dot{\varepsilon}_z$	:	Axial strain rate
$\dot{\bar{\varepsilon}}$	:	Effective strain rate
γ	:	Shear strain
v	:	Poisson's ratio
ρ	:	Density
ρ_d	:	Density of SiC_p reinforcement
ρ_m	:	Density of pure Al matrix
σ	:	Normal stress
σ_0	:	Threshold stress
σ_r	:	Radial stress
σ_y	:	Yield strength
σ_z	:	Axial stress
σ_θ	:	Tangential stress

$\sigma_\theta(avg)$	:	Average tangential stress
σ_{ry}	:	Yield strength along radial direction
σ_{zy}	:	Yield strength along axial direction
$\sigma_{\theta y}$	:	Yield strength along tangential direction
$\tau_{\max}$	:	Maximum shear stress
$\bar{\sigma}$	:	Effective stress
$\bar{\sigma}_r$	:	Non-dimensional radial stress
$\bar{\sigma}_\theta$	:	Non-dimensional tangential stresses
Ω^2	:	Non-dimensional angular velocity
ω	:	Angular velocity

ABSTRACT

Metal matrix composites consisting of aluminum/aluminum alloy matrix reinforced with ceramics like silicon carbide (SiC) exhibit higher specific strength and stiffness, and superior thermal resistance and hence may be employed in rotating disc of turbine rotor and disc brakes. The conventional metal matrix composites sometimes fail under extreme service conditions of temperature and mechanical loads. To meet such stringent loading condition, a new class of composites, known as Functionally Graded Materials (FGMs), have been developed. The contents of constituent phases in FGM are gradually varied with respect to position coordinates to attain smooth and continuous variation in the desired properties. The present study is an attempt to investigate the steady state creep behavior of a variable thickness rotating disc made of aluminum or its alloy matrix reinforced with SiC (particles or whiskers).

The first segment of the study deals with the analysis of the steady state creep in a rotating FGM disc yielding according to Tresca criterion. The creep behavior of the disc has been described by a threshold stress based law, with the value of stress exponent equals to 5. The disc thickness and distribution of SiC_p reinforcement are assumed to decrease linearly on moving from the inner to outer disc radius. The stresses and strain rates are estimated from the analysis and compared with those available in literature for a similar FGM disc yielding according to von Mises criterion. The study reveals that the use of Tresca criterion gives much safer design of a variable thickness rotating FGM disc as compared to FGM disc designed on the basis of von Mises criterion.

The second segment of the study investigates the effects of varying disc geometry, radial distribution of SiC_p and radial thermal gradient on the steady state creep behavior of a rotating disc, yielding according to Tresca criterion. The study indicates that by varying the disc thickness gradient from 0 to 29.9 *mm*, the strain rates in a uniform composite disc reduce over the entire disc radius. On increasing the SiC_p gradient in a variable thickness disc, the radial stress increases throughout and the tangential stress increases near the inner radius but decreases towards the outer radius. The strain rates are observed to reduce significantly over the entire disc radius with the increase in the SiC_p gradient. The imposition of radially increasing temperature profiles (linear, parabolic and exponential), with increasing radius,

leads to considerable reduction in the radial and tangential strain rates in a variable thickness FGM disc, with the lowest and relatively more uniform distribution of strain rates observed for exponential temperature profile.

The third segment of the study examines the effect of varying materials' anisotropy on the creep performance of rotating disc made of functionally graded 6061Al-SiC_w composite. The disc thickness and distribution of SiC_w reinforcement are assumed to decrease non-linearly with increasing disc radius. The yielding of the disc material is described by Hill's criterion and the extent of anisotropy is defined by the ratio of yield strength of the disc material along the radial, tangential and axial directions (*i.e.* $\sigma_{ry} : \sigma_{\theta y} : \sigma_{zy}$). The study reflects that an orthotropic disc in which the yield strength decreases in the order $\sigma_{zy} > \sigma_{ry} > \sigma_{\theta y}$ exhibits the lowest radial stress over the entire radius and the lowest tangential stresses near the inner and outer radii. However, the strain are observed to be the lowest in an orthotropic disc wherein the yield strength decreases in the order $\sigma_{zy} > \sigma_{\theta y} > \sigma_{ry}$.

The last segment of the study uses Seth's transition theory to analyze the steady state creep response of a variable thickness rotating FGM disc. The effect of varying the radial distribution of reinforcement (SiC_p) has been investigated on the stresses and strain rates. The study indicates that the stresses as well as strain rates in the FGM disc reduce noticeably with the increase in SiC_p gradient in the disc.

The study evolves a better understanding of the effects of geometrical, material and operating parameters, such as disc profile, distribution of reinforcement, materials' anisotropy and thermal gradient, on the creep response of a rotating FGM disc. The study also highlights the advantage of using Tresca yield criterion for the design of rotating FGM disc. Besides using classical approach, the use of Seth's transition theory to analyze the creep problems in rotating FGM disc has also been demonstrated. The results obtained in the study may assist the designers of rotating disc for creep applications.

CHAPTER-1

INTRODUCTION

1.1 PHENOMENON OF CREEP

Creep is defined as an inelastic and progressive time-dependent deformation under the action of constant load and constant temperature. Creep occurs in materials when they are exposed to high stresses, even below the yield strength of the material, for a long-term. The creep deformations do not occur suddenly upon the application of load, rather the strain accumulates as a result of long-term stress exposure, therefore, the creep is termed as a time-dependent deformation. In addition to exposure time, the creep is also dependent upon the material properties, operating temperature and the external load. For many structural materials including steels, the creep is observed beyond a certain critical temperature called homologous temperature, which is around 50% of the melting point temperature of the materials. Sometimes, the creep deformations become so large that the structural component fails to perform the intended function. As an example, the creep induced deformations in a turbine blade may cause the blade to come in contact with the casing, which ultimately may lead to its failure. The creep phenomenon is accompanied by different slow microstructural rearrangements like dislocation movement, grain-boundary cavitation and ageing of microstructure [Dieter (1988), Naumenko and Altenbach (2007) and Meyers and Chawla (2009)].

During creep phenomenon, the states of stress and strain in the material change with respect to time due to applications of external load and temperature. Most of the time, these states of stress and strain are multi-axial and observed to vary from point to point inside the materials. Apart from progressive deformations, the creep can also lead to reduction of material strength locally, relaxation and redistribution of stresses. Due to the importance of creep in number of structural components, viz. turbine rotor, aerospace vehicles, automobiles, nuclear power plants, the researchers have been making attempt to develop mathematical models to predict creep rupture and evolve better understanding of the time-dependent

behavior of the structural components. These mathematical models also help to correlate the material behavior with the stresses and strains induced in the material [Dieter (1988), Meyers and Chawla (2009)].

1.1.1 Creep Curve

In order to evaluate creep behavior of the materials, uni-axial creep tests are conducted wherein a standard cylindrical shaped specimen of the material is subjected to axial tensile load (F) and the operating temperature (T) is raised from 30% to 50% of the melting point temperature (T_m) of the material, Fig. 1.1. During the creep test, the normal stress (σ) induced in the specimen is kept much below its yield strength (σ_y) while the load and the temperature are maintained at constant level. The strain (ε) induced in the material is recorded at various instant of time (t) and the resulting data is plotted in the form of creep curve shown in Fig 1.1. The total strain consists of instantaneous elastic deformation (ε^0), the strain at the instant of application of load, and time-dependent strain (ε), which is observed to vary at different rates with time, as depicted by three stages-I (primary or transient), II (secondary, steady state, constant rate, quasi viscous) and III (tertiary or accelerated creep). During the primary creep, the strain rate (creep rate) decreases to reach a minimum level, which is maintained during the secondary stage of creep. During the tertiary stage, the strain rate starts to accelerate till the rupture of specimen takes place. The steady state (Stage II), with the almost constant strain rates ($\dot{\varepsilon}_s$), is the most important stage for the researchers, as most of the life is spent by a component in this stage. The dashed lines in Fig. 1.1 represents the constant stress creep curve, which is initially identical to constant load creep curve (shown by solid line). As the specimen elongates, the stress increases, due to reduction in cross section area of the specimen, the creep rate also increases at constant load and hence constant load and constant stress creep curves follow different paths beyond stage-II. The failure time under constant stress and constant load can be drastically different. [Dieter (1988)]

The total creep strain (ε_t) is mathematically expressed as,

$$\varepsilon_t = \varepsilon^0 + \varepsilon[1-\exp(-mt)] + \dot{\varepsilon}_s t \qquad (1.1)$$

where the term $\varepsilon[1-\exp(-mt)]$ represents creep strain occurred during stage I in which m is the exponential time parameter and ε is the limiting transient creep strain (strain at end of

stage-I minus ε^0), and the term $\dot{\varepsilon}_s t$ is a linear function of time and defines strain accumulated during stage-II, with $\dot{\varepsilon}_s$ denoting the steady state/minimum creep rate.

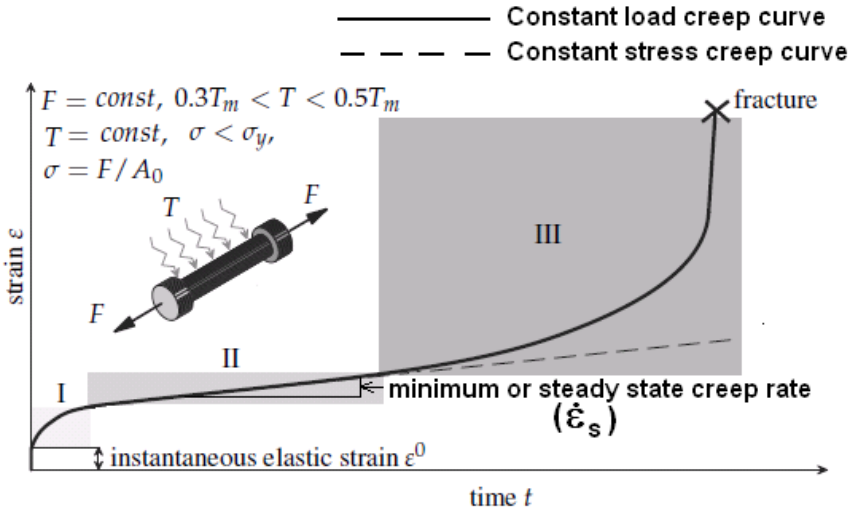

Fig. 1.1: Creep curve at constant load/constant stress and temperature [Naumenko and Altenbach (2007)]

The creep rate of a material is affected by the level of stress and the operating temperature. With the increase in either stress level or the operating temperature, the steady state creep rate is observed to increase, thereby by decreasing the rupture time (t_r), Fig. 1.2 [Naumenko and Altenbach (2007), Meyers and Chawla (2009)]. The magnitude of instantaneous elastic strain (ε^0) is also observed to increase with the increase in stress or operating temperature.

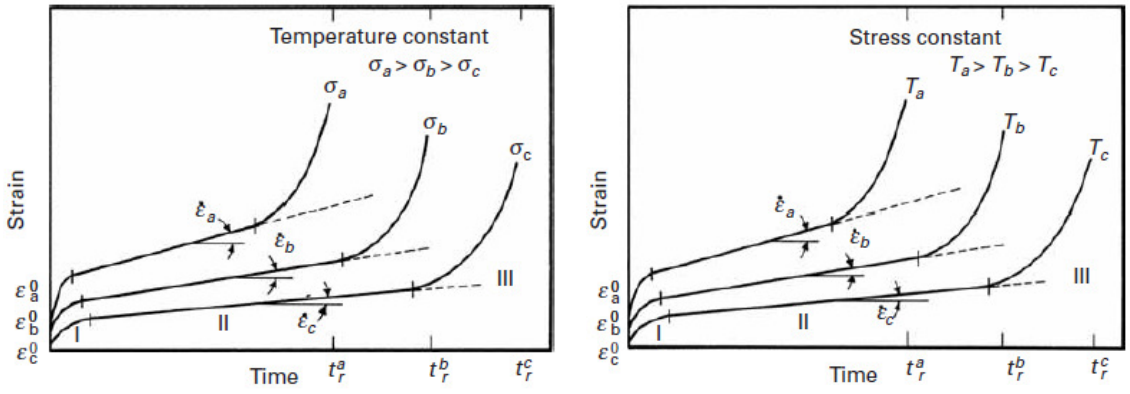

(a) **(b)**

Fig. 1.2: Effect of (a) stress and (b) temperature on creep [Meyers and Chawla (2009)]

1.2 COMPOSITES AND THEIR TYPES

The composite materials came into existence in the early 1900's, with the introduction of particles or fibers reinforced into thermoset phenolics. These are a class of advanced material, obtained by combining two or more materials, with different physical and chemical properties, at macro levels. Composites offer an excellent combination of properties, which are difficult to achieve from any of the constituents alone. The composites consist of two distinct phases: (i) matrix phase, which is the continuous phase, and (ii) reinforcement phase, which may be either continuous or discontinuous in the forms of particles, whiskers and short fibers. The composites have been classified on the basis of matrix materials as metal matrix composites (MMCs), polymer matrix composites (PMCs), ceramic matrix composites (CMCs) and carbon–carbon composites [Alman (2001), Kaw (2006), Mahamood *et al*. (2012)].

1.2.1 Metal Matrix Composites

Amongst all the composites, metal matrix composites (MMCs) are the most popular now a days, as its development has played pivot role in the development of numerous leading technologies. MMCs are the platform for many scientific and technological advances not only in aerospace and shipbuilding technology, but also in mechanical, electronic, power, electrical, construction, transport, and other industries [Nath and Sandeep (1998), Ramnath *et al*. (2014)]. The reinforcements in MMCs are usually a ceramic. The properties of MMCs can be optimized by varying the contents of ceramic and metallic phases, by exploiting the advantages of favorable properties of each constituents and compensating their weaknesses. The presence of metallic phase in MMCs offers the properties like ductility, toughness and environmental resistance combined with high strength and high modulus [Shen (2009), Hasan *et al.* (2011)]. The presence of ceramic phase in MMCs results in properties such as high thermal resistance, improved wear resistance etc., apart from achieving weight reduction, which is beneficial in moving devices where the heavier components are to be replaced by the lighter ones. In comparison to PMCs, MMCs are capable of withstanding higher operating temperatures, possess significantly higher thermal and electrical conductivities, and have greater strength in shear and compression [Park *et al*. (1990)]. Due to numerous advantages offered by MMCs, they are used in variety of engineering and structural applications such as components of combustion engine, turbine rotor, brake systems, load transfer elements in vehicles (sport, personal and utility cars, rail transport), aeronautical (turbine engines, helicopters, spacecrafts, airplanes, missile guidance systems) etc [Hasan *et al.* (2011), Ramnath *et al*. (2014)].

1.2.2 Polymer Matrix Composites

PMCs are the most common advanced composites, which has matrix of polymer (e.g., polyester, epoxy, urethane) reinforced with by thin diameter fibers (e.g., aramids, graphite, boron). These composites possess the advantages like low cost, high strength, and simple manufacturing principles. However, their use is limited due to low operating temperatures, high coefficients of thermal and moisture expansion, and low elastic properties in certain directions [Kaw (2006)].

1.2.3 Ceramic Matrix Composites

CMCs are made of ceramic matrix (e.g., alumina, calcium alumino silicate) reinforced by fibers such as carbon or silicon carbide. These composites offer the advantages like high strength, hardness, high service temperature, chemical inertness, and low density. However, their major drawback is low fracture toughness [Kaw (2006)].

1.2.4 Carbon–Carbon Composites

These composites consist of carbon fibers reinforced in a carbon matrix. Carbon–Carbon composites have high specific strength and can sustain very high-temperature service conditions (up to 3315°C). The major drawbacks of these composites are high cost, low shear strength and poor oxidation resistance at elevated temperatures [Kaw (2006)].

1.3 FUNCTIONALLY GRADED MATERIALS

The conventional composite materials sometimes fail through delamination in applications involving extreme service conditions of temperature and mechanical loads. In order to meet such stringent loading condition, a new class of composite material, known as Functionally Graded Materials (FGMs), has been developed [Wang (1983), Wattanasakulpong (2011), Bui *et al*. (2016)]. FGMs are typically inhomogeneous composite materials made from ceramic and metal. In FGMs the contents of constituent phases are gradually varied to obtain smooth and continuous change in desired properties with respect to position coordinates [Abrate (2006), Viola and Tornabene (2009), Shanmugavel *et al*. (2012), Bhattacharya *et al*. (2014), Shen (2014), Gupta *et al*. (2016), Kennedy *et al*. (2016)]. FGMs are capable of withstanding ultra-high temperatures/large thermal gradients along with severe mechanical loading, as encountered in components of advanced aircraft and aerospace engines, plasma facings of fusion reactors etc. [Aboudi *et al.* (1999), Birman *et al*. (2008), Jagtap *et al*. (2013), Guo *et al*. (2014), Gupta *et al*. (2016)]. As a result of gradual variation in

the content of constituent materials in FGMs, the interfacial issues such as delamination or debonding and thermal stress concentrations are eliminated [Bui *et al.* (2016). Table 1.1 lists some of the major applications of functionally graded MMCs along with the mention of salient properties for the desired applications.

Table 1.1: Applications of functionally graded MMCs

Application areas	Desired properties
Aerospace:	
Aircraft Structure [Pitcher *et al*. (1998), Hunt (2000), Birman *et al*. (2008), Hasan *et al.* (2011), Jagtap *et al*. (2013), Gupta *et al*. (2016)]	Stiffness, Strength, Wear resistance, High temperature stability
Aero-Engine e.g. Gas turbine engines [Hunt (2000), Liu *et al*. (2017a)]	Light weight, Specific stiffness, specific strength at elevated temperature, Creep and fatigue resistance
Space Structures [Yue *et al.* (1998), Pitcher *et al.* (1998), Bache *et al.* (1998), Hunt (2000)]	Specific strength and specific stiffness, Controlled coefficient of thermal expansion, Dimensional stability
Missile Structures, Missile Launcher Pads [Shakesheff and Purdue (1998), Pitcher *et al*. (1998), Jagtap *et al*. (2013)]	High temperature stability, High stiffness and strength, Reduced weight
Automotive:	
Engine [Rohatagi *et al*, 1992, Yue *et al,* 1998, Hunt, 2000]	Increased stiffness, Improved wear resistance, Thermal fatigue resistance
Brake System: Disc brake rotors, brake drums, brake calipers for racecars [Fitzpatrick *et al*. (1998) Hunt (2000), Surappa (2003)]	Wear resistance, High thermal conductivity
Driveshaft [Hunt (2000), Surappa (2003)]	Increased specific stiffness
Others: Brake calipers, pump housings, gears, valves, turbocharger and supercharger compressors, clutch parts [Hunt (2000), Surappa (2003), Liu *et al*. (2017a)]	
Nuclear Plants: Plasma facings of fusion reactors [Jagtap *et al*. (2013)]	
Commercial and Industrial Products:	
Recreational: Golf equipment, bicycle components such as frames, front forks, handlebars [Fitzpatrick *et al.* (1998), Hunt (2000)]	Increased specific stiffness and strength, durability
Computer hard disc drive [Hunt (2000)]	Increasing elastic modulus
Small-scale industrial components: Micro-and nano-scale devices and systems such as thin films, actuators, and MEMS [Liu *et al*. (2017b)]	Higher thermal resistance and better ductility

1.4 ROTATING DISC

Rotating disc is an important structural component that finds widespread applications in many mechanical systems like steam and gas turbine rotors, turbo generators, automotive brakes, flywheels, ship propellers etc. [Gupta *et al.* (2004a), Hojjati and Hassani (2008)]. In some of these applications like turbine rotors and disc brakes, the disc is simultaneously subjected to high temperature and severe mechanical loading, and hence is vulnerable to creep. Under such thermo-mechanical loading, the disc made of monolithic materials may not survive. The use of aluminum/aluminum alloys may save power and fuel due to reduction in payload, and hence may be employed in applications involving rotating disc [Hasan *et al.* (2011)]. However, the low creep resistance offered by aluminum/ aluminum alloys is a big hindrance to such applications. The experiments conducted to evaluate the creep properties demonstrate that the creep resistance of aluminum and its alloys could be significantly improved by using ceramic reinforcement in aluminum and its alloys [Nieh (1984), Nieh *et al*. (1988)]. A variety of ceramic materials are available as reinforcements, but amongst these silicon carbide (SiC) is widely used due to its low density and cost, and excellent potential to improve strength, stiffness and thermal resistance of aluminum/ aluminum alloys based MMCs. Silicon carbide is available in various forms, viz. continuous/discontinuous fibers (aligned or randomly distributed), particles or whiskers. The performance of structural components, such as rotating disc, made of aluminum/aluminum alloy reinforced ceramic composites could be improved at low cost along with reduction in payload by making suitable choice of geometry, size and volume content of the reinforcements [Singh and Ray (2003) Gupta *et al*. (2004a), Deepak *et al*. (2010a) Ramnath *et al*. (2014)].

The studies indicate that besides varying the disc material, the creep performance of the disc could be significantly improved along with the reduction in disc weight by suitably modifying the geometrical parameters, such as disc thickness profile, mean radius, [Guven and Celik (2001)]. The creep rates in a variable thickness rotating disc are observed to reduce appreciably as compared to a uniform thickness disc [Deepak *et al.* (2010a, 2010b), Garg *et al.* (2012, 2013a), Dwivedi *et al.* (2013), Deepak *et al.* (2015)].

1.5 CREEP MODELS FOR ALUMINUM / ALUMINUM ALLOY BASED MMCs

Many creep models have been used to describe steady state creep in aluminum and aluminum alloy based metal matrix composites. These models express creep strain or creep strain rate as a function of stress, time and temperature. Some of the models also use the

accumulated creep strain to model strain hardening. Of the various empirical creep models, Norton's [Singh and Ray (2003a)] and threshold stress based laws have been widely used to describe the steady state creep in aluminum/aluminum alloy based metal matrix composites [Ma and Tjong (2001)]. According the Norton's law, the effective strain rate ($\dot{\bar{\varepsilon}}$) is related to the effective stress ($\bar{\sigma}$) through the following equation,

$$\dot{\bar{\varepsilon}} = B\bar{\sigma}^{n} \tag{1.2}$$

where B is a constant and n is the stress exponent. The values of materials' constant B and n in MMCs depend on the shape, size and content of the reinforcements apart from the operating temperature.

The use of Norton's law to describe steady state creep behavior of aluminum/aluminum alloy matrix composites has been objected, due to its high and often variable values of apparent stress exponent and activation energies observed in these composites [Gupta *et al.* (2005a)]. To overcome these objections, the researchers have used following well-established threshold stress based law to describe steady state creep in aluminum/aluminum alloy matrix composites [Ma and Tjong (2001)],

$$\dot{\bar{\varepsilon}} = [M(\bar{\sigma} - \sigma_0)]^{n} \tag{1.3}$$

where n is the true stress exponent, M is the material parameter and σ_0 is the threshold stress, which is the minimum value of stress beyond which creep starts in a material. The value of creep parameter M appearing in Eq. (1.3) is given by,

$$M = \left[\frac{1}{E}\left(A^{'}\exp\frac{-Q}{RT}\right)^{1/n}\right]$$

In the above expression $A^{'}$, Q, E, R and T denote structure dependent parameter, true activation energy, temperature-dependent Young's modulus, gas constant and operating temperature, respectively. Similar to materials' parameters given in Norton's law, the creep parameters M and σ_0 also depend on the type of reinforcement (shape, size and content) and operating temperature. The value of true stress exponent (n), Eq. (1.3), has been usually selected as 3, 5 and 8, which correspond to different creep mechanisms. The stress exponents 3, 5 and 8 respectively correspond to creep controlled by viscous glide processes of dislocation, creep controlled by high temperature dislocation climb (lattice diffusion) and creep controlled by lattice diffusion with constant structure [Tjong and Ma (2000)]. The

literature reveals that the value of true stress exponent ≈3 or ≈5, rather than 8, better fits the experimental steady state creep data observed for discontinuously SiC reinforced aluminum/aluminum alloy matrix composites [Park *et al*. (1990), Mohamed *et al*. (1992), Park and Mohamed (1995), Cadek *et al*. (1995), Yoshioka *et al*. (1998), Li and Mohamed (1997), Li and Langdon (1997), (1999)].

1.6 YIELD CRITERIA

The successful design of any structure requires efficient and safe use of materials. Therefore, for design purpose it is extremely important to precisely predict the yield strength (*i.e.* the onset of plastic deformation) of a material, under loading conditions prevailing in the service. Several empirical relations, called yield criteria or failure theories, have been proposed to predict the yield strength of a material under multi-axial loading. If the state of stress at a point inside a given material satisfies the yield condition, then at this point the material deforms plastically, otherwise the deformations are within elastic limit. Thus, the yield conditions are mathematically expressed as,

$$f(\sigma_{ij}) < 0 \text{ : for elastic deformation domain}$$

$$f(\sigma_{ij}) \geq 0 \text{ : for plastic deformation domain}$$

where $f(\sigma_{ij})$ is the yield function comprising of six stress components (3-normal and 3-shear stress components) of the stress tensor, which defines the yield surface in the six dimensional stress space isolating the elastic and plastic regions. Different yield criteria have been proposed for isotropic and anisotropic materials. The commonly used yield criteria for isotropic materials are maximum normal stress or Rankine's criterion, maximum shear stress or Tresca criterion), maximum distortion energy or von Mises criterion whereas for anisotropic materials Hill's yield criterion is commonly employed. A brief discussion of these yield criteria is given in the following sub-sections.

1.6.1 Yield Criteria for Isotropic Materials

In isotropic materials, the yielding depends only on the magnitudes of the principal stresses σ_1, σ_2 and σ_3. The yield criterion for such materials could be expressed as,

$$f(\sigma_1, \sigma_2, \sigma_3) = 0$$

or, $$f(I_1, I_2, I_3) = 0$$

where I_1, I_2 and I_3 are the invariants of the stress tensor in terms of principal stresses, as given below,

$$\begin{aligned} I_1 &= \sigma_1 + \sigma_2 + \sigma_3 \\ I_2 &= \sigma_1\sigma_2 + \sigma_2\sigma_3 + \sigma_3\sigma_1 \\ I_3 &= \sigma_1\sigma_2\sigma_3 \end{aligned} \tag{1.4}$$

The experimental data indicates that the hydrostatic stresses have almost negligible effect on the plastic deformation, thus it is possible to express the yield criteria in terms of invariants of the deviatoric stress as,

$$f_3(J_2, J_3) = 0 \tag{1.5}$$

where J_2 and J_3 represent the second and third invariants of the deviatoric stress. The first invariant of the deviatoric stress $J_1 (= I_1)$ is zero. The invariants J_2 and J_3 are given by,

$$J_2 = \frac{I_1^2}{3} - I_2$$

$$J_3 = \frac{2I_1^3}{27} - \frac{I_1 I_3}{3} + I_3 \tag{1.6}$$

Eq. (1.5) represents the general form of a yield function, which satisfies the assumptions of isotropy and plastic incompressibility [Dieter (1988), Khan and Huang (1995), Stouffer and Dame (1996)].

1.6.1.1 Rankine's Criterion

According to this criterion, the plastic flow takes place at a point inside a material subjected to complex state of stress, if the greatest principal stress reaches the flow stress/yield strength (σ_0) of the material, as obtained by conducting uniaxial tensile test. Since the principal stress are assumed to decrease in the order $\sigma_1 > \sigma_2 > \sigma_3$, thus according to this criterion for yielding takes place when [Meyers and Chawla (2009)],

$$\sigma_0\,(tension) < \sigma_1 < \sigma_0\,(compression)$$

1.6.1.2 Tresca Criterion

Tresca yield criterion, also known as maximum shear stress theory, assumes that the plastic yielding would occur in a material if the maximum shear stress reaches the critical value *k* of the material. The mathematical form of Tresca criterion is given by,

$\tau_{\max} < k$: for elastic deformation

$\tau_{\max} \geq k$: for yielding or plastic deformation

In terms of principal stresses, when $\sigma_1 > \sigma_2 > \sigma_3$, this criterion is expressed as,

$$\frac{|\sigma_1 - \sigma_3|}{2} = \frac{\sigma_y}{2} \tag{1.7}$$

The value of constant *k* is again obtained by recording the maximum shear stress of the material from the uniaxial tension and pure shear tests, which are found to be $\frac{\sigma_Y}{2}$ and τ_Y, respectively. Further, Tresca criterion is observed to be unaffected by the intermediate principal stress σ_2 [Dieter (1988)].

Tresca yield surface is represented by a regular hexagon in the principal stress space whereas the von Mises yield surface corresponds to the surface of a cylinder parallel to the hydrostatic stress axis with its locus as a circle of radius $r = \sqrt{2}k$ on the π-plane [Meyers and Chawla (2009)]. Fig. 1.3 shows the graphical comparison of three criteria, together with experimental results (shown by symbols) for ductile e.g. (copper, aluminum, steel) and brittle (e.g. cast iron) materials subjected to plane stress condition (*i.e.* $\sigma_3 = 0$). It is observed that the ductile materials tend to follow the von Mises criterion (and, in a more conservative way, the Tresca criterion), the brittle materials clearly obey the Rankine's yield criterion.

1.6.1.3 Von Mises Criterion

The von Mises yield criterion, also known as distortion-energy criterion, states that the plastic yielding would occur only when the second invariant of the deviatoric stresses (J_2) satisfies the following condition,

$J_2 < k^2$ for elastic deformation

$J_2 - k^2 \geq 0$ for yielding or plastic deformation

where k is a material property, which depends on the yield strength of material, obtained from uniaxial test, and operating temperature.

Using Eqs. (1.4) and (1.6), the von Mises yield criterion could be written in terms of principal stresses as,

$$\frac{1}{6}\left[(\sigma_1-\sigma_2)^2+(\sigma_2-\sigma_3)^2+(\sigma_3-\sigma_1)^2\right]=k^2 \tag{1.8}$$

Since the yield criterion is valid for all combinations of stresses, and hence can also be applied for simple tension as well as for simple shear. The value of constant k is estimated as $\frac{\sigma_Y}{\sqrt{3}}$ from the simple tensile test ($\sigma_1=\sigma_Y, \sigma_2=\sigma_3=0$) and τ_Y from pure shear test, where σ_Y and τ_Y are the yield stresses obtained from simple tension and pure shear tests, respectively [Dieter (1988)].

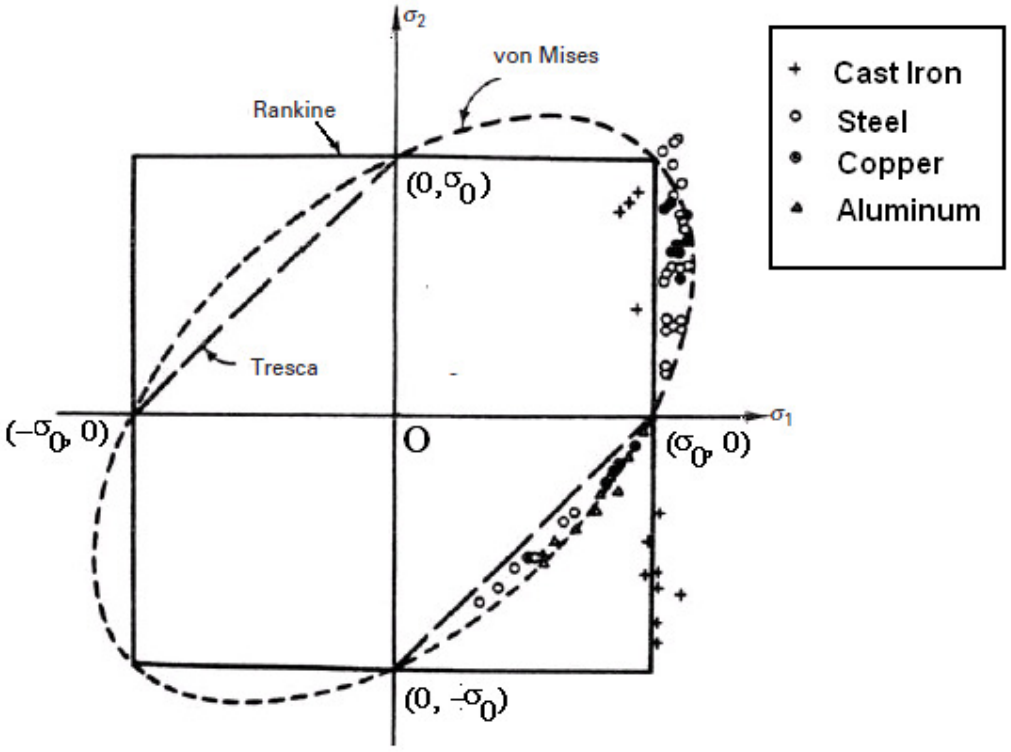

Fig. 1.3: Comparison of yield criteria for isotropic materials [Meyers and Chawla (2009)]

1.6.2 Yield Criteria for Anisotropic Materials

The yield criterion discussed in previous sub-section assumed that the material is isotropic, which might be the case at the start of the plastic deformation. This assumption

may not be valid once the material undergoes appreciable elongation. In addition, fiber-reinforced composite or the components fabricated by processes such as forging, rolling, and extrusion exhibit anisotropy. Hill has generalized the von Mises yield criterion for isotropic material to include the effect of anisotropy. The Hill's yield criterion is based on the following assumptions:

1. The material is orthotropic, *i.e.*, at each point within a material there exists only three mutually orthogonal planes of symmetry. The intersection of these planes is called the principal axes of anisotropy.

2. Yielding is not affected by the hydrostatic stresses.

3. There is no Bauschinger effect, *i.e.*, the yield condition does not change on complete load reversal.

Hill's criterion is expressed by the following equation when the principal axes of anisotropy are along the *x, y* and *z* axes in Cartesian coordinate system,

$$F(\sigma_y-\sigma_z)^2+G(\sigma_z-\sigma_x)^2+H(\sigma_x-\sigma_y)^2 + 2L\tau_{yz}^2+2M\tau_{zx}^2+2N\tau_{xy}^2=1 \tag{1.9}$$

where the parameters *F*, *G*, *H*, *L*, *M* and *N* are material constants characterizing the current state of anisotropic yield behavior.

For principal axes of orthotropic symmetry, the Hill's criterion given in Eq. (1.9) becomes,

$$F(\sigma_2-\sigma_3)^2+G(\sigma_3-\sigma_1)^2+H(\sigma_1-\sigma_2)^2=1 \tag{1.10}$$

where σ_1, σ_2 and σ_3 are the principal stresses.

If *X*, *Y* and *Z* denote the yield stresses along the three principal directions, then the values of constants *F*, *G* and *H* are expressed as,

$$\left.\begin{aligned} 2F &= \frac{1}{Y^2}+\frac{1}{Z^2}-\frac{1}{X^2} \\ 2G &= \frac{1}{Z^2}+\frac{1}{X^2}-\frac{1}{Y^2} \\ 2H &= \frac{1}{X^2}+\frac{1}{Y^2}-\frac{1}{Z^2} \end{aligned}\right\} \tag{1.11}$$

And the values of material constants *L*, *M* and *N* are obtained from the following relations,

$$2L = \frac{1}{R^2},\ 2M = \frac{1}{S^2},\ 2N = \frac{1}{T^2} \tag{1.12}$$

where *R*, *S* and *T* represent the yield stresses in pure shear on each of the orthogonal planes of anisotropy [Dieter (1988), Backofen (1972)].

1.7 SETH's TRANSITION THEORY

The use of classical theory for finding the closed form solutions of the elasticity and plasticity problems (*e.g*. elastic-plastic deformation, creep, relaxation, fatigue and shocks) involves the use of several assumptions like the incompressibility condition and semi-empirical laws (such as yield criteria). Seth (1966) developed a transition theory to obtain a more general solution of elasticity and plasticity problems. The transition theory, unlike classical theory does not require assumptions, as mentioned above. The theory uses the concept of generalized strain measure and asymptotic solution at turning (transition) points of the governing differential equations describing the deformed field [Gupta and Shukla (1994), Shukla (1996)].

According to Seth's transition theory (1966), the generalized principal strain measure is given by,

$$e_{ii} = \int_0^{e_{ii}^A} \left[1-2e_{ii}^A\right]^{\frac{n_m}{2}-1} de_{ii}^A = \frac{1}{n_m}\left[1-(1-2e_{ii}^A)^{\frac{n_m}{2}}\right], \qquad (i = 1,2,3) \tag{1.13}$$

where e_{ii}^A are the principle Almansi finite strain components and n_m is the measure.

Apart from estimating the values of well-known strain measures, the generalized strain measure can also be used to find the stresses (elastic, elastic-plastic, plastic) when it is combined with the analysis of transition points of the governing differential equations defining the deformed shape. The asymptotic solution of the governing differential equations corresponding to the transition point yields the solutions, as estimated by using the yield criteria, if these exist. Seth's transition theory has been successfully employed to solve a large number of problems [Gupta and Shukla (1994), Shukla (1996), Gupta *et al*. (2000a, 2000b), Gupta and Pankaj (2007a), Pankaj and Bansal (2008a), Sharma and Sahni (2008), Thakur (2010a), Sharma *et al*. (2013)].

1.8 ORGANIZATION OF THE THESIS

The entire work carried out has been presented into seven chapters. A brief description of the content of these chapters is given below:

Chapter 1 starts with the introduction of creep followed by the introduction to composite materials, with a special emphasis on metal matrix composites (MMCs). The introduction to FGMs, a new class of composites, is also given in the chapter, along with its salient applications. The gives a brief outline of rotating disc, an important structural components in numerous engineering applications. The chapter also presents a brief discussion of various creep models applicable to MMCs, especially ceramic reinforced aluminum/aluminum alloy matrix composites, which has been chosen as the material of rotating disc in this study. The different yield criteria applicable to isotropic and anisotropic materials are also discussed in the chapter. A brief overview of the thesis is given at the end.

Chapter 2 highlights the summary of the salient research works, carried out by several researchers, dealing with the analysis of elastic, thermo-elastic, elastic-plastic and creep behavior of a rotating disc. The research works carried out by using classical approach and Seth's transition theory are reported into different sections. The chapter identifies the existing research gaps and defines the problem undertaken. In the end, the chapter outlines proposed objectives of the study.

Chapter 3 presents analysis of the steady state creep in a rotating FGM disc (Al-SiC_p) having linearly varying thickness by using Tresca yield criterion and undergoing creep according to threshold stress based creep law. The analysis carried out in the chapter is validated with the published experimental work as well as with the results estimated for FGM disc using commercially available FEM package. The results estimated from the analysis are compared with those available in literature obtained using von Mises yield criterion.

Chapter 4 comprises analysis of steady state creep in a rotating FGM (Al-SiC_p) disc having radially varying distribution of SiC_p reinforcement, $V(r)$, and radially decreasing thickness, $h(r)$, both varying according to power law. The disc has been assumed to yield according to Tresca criterion and is subjected to radial thermal gradient. The analysis carried out has been used to investigate effect of varying: (i) the thickness profile, (ii) the distribution of reinforcement and (iii) radial thermal gradients on the creep stresses and strain rates in the composite disc.

Chapter 5 deals with the analysis of steady state creep in a rotating disc made of anisotropic FGM (6061Al-SiC_w) and having non-linearly variable thickness. The yielding of

the disc material is described by Hill's anisotropy criterion. The analysis has been used to investigate the effect of varying the extent of anisotropy, defined in terms of the ratio of yield strength of the disc material along the radial, tangential and axial directions, on the creep response of variable thickness FGM disc.

Chapter 6 gives analysis of creep in a variable thickness rotating FGM disc using Seth's transition theory. The analysis developed has been validated by comparing the results estimated with the earlier published work based on Seth's transition theory for similar type of disc. The steady state stresses and strain rates have been estimated and compared for FGM disc having different types of radial distribution of reinforcement.

Chapter 7 highlights the important conclusions derived from the present study. The chapter also identifies the research areas for future work.

CHAPTER-2

LITERATURE REVIEW

Rotating disc is an important structural component in many engineering applications like gas turbine rotor, turbo generators, automotive brakes, centrifugal pumps etc. In most of these applications, the disc is subjected to heavy mechanical loads as well as it has to operate under high temperature and hence susceptible to creep. Owing to this fact, the disc has provided a research area intensively pursued by the researchers in the recent past. The researchers have carried out analysis of stresses, strains and deformations in rotating disc, including elastic, thermo-elastic, elastic-plastic and creep analyses. The study reveals that by suitably changing the disc geometry and the parameters of the disc material, the optimal and more reliable design of a rotating disc can be achieved for given operating conditions of load, speed and operating temperature. The general parameters varied in the optimization process involve geometrical parameters like thickness profile of the disc, and material properties, such as elastic modulus, density and Poisson's ratio, of the disc material [Guven and Celik (2001)]. In these different studies, the researchers have used different yield criteria, depending on the type of disc material chosen, viz. isotropic, or anisotropic. Some of the researchers have also analyzed elastic, elastic-plastic and creep analyses in rotating disc by using Seth's transition theory, which does not involve the use of assumptions like yield criterion, incompressibility condition, as employed during analysis based classical approach.

An extensive literature review, related to the area of the current research work, has been undertaken to assess the level of current research and to identify the existing research gaps. Some of the salient studies carried out are reported in this chapter.

2.1 ELASTIC/THERMO-ELASTIC ANALYSIS

Analysis of stresses and strains in thin isotropic disc are available in the literature [Malkin (1934), Finnie and Heller (1959), Lubhan and Felger (1961)]. Timoshenko and Goodier (1970) were the first to obtain a closed form solution for a rotating disc made of homogeneous material and operating at constant temperature.

Reddy and Srinath (1974) and Chang (1976) investigated the stresses and displacements in rotating disc made of orthotropic material to examine the effect of varying material density. Yeh and Han (1994) obtained solutions to estimate the elastic stresses in a constant thickness rotating disc made of inhomogeneous material and subjected to thermal load.

Tutuncu (1995) investigated the stresses and deformations in a rotating circular plate made of orthotropic material. Durodola and Adlington (1997) analyzed the elastic stresses and strains in a rotating disc and investigated the effect of radially varying the disc properties on the performance of the disc. Horgan and Chan (1999) also analyzed the effect of material inhomogeneity on the elastic stresses in isotropic rotating solid disc. The elastic stresses in the disc are observed to be significantly affected by varying material inhomogeneity.

Jain *et al.* (1999) developed a design approach to obtain uniform strength rotating composite disc by suitably tailoring the anisotropic elastic constants along the radial direction. The study also compared analytical and FEM results estimated for anisotropic and isotropic discs with radially varying elastic modulus. The FGM disc with tailored elastic modulus is observed to have optimum use of material.

Durodala and Attia (2000) analyzed the stresses and displacements in rotating hollow and solid discs made of orthotropic FGMs. The disc was assumed to be made of metal matrix reinforced composite having non-uniform distribution of long fiber reinforcement. The analytical results, obtained by direct integration of the governing differential equations, were observed to be in close agreement with the FE results. The distributions of stresses and displacements in the disc are observed to change significantly on varying the radial distribution of reinforcement in the FGM discs, with higher variation noticed for hollow disc as compared to solid disc. Zhou and Ogata (2002) used direct displacement method to estimate stresses, strains and displacement in a rotating disc composed of anisotropic material.

Callioglu (2004) performed analysis to estimate thermal stresses in an orthotropic rotating hollow disc made of glass-fiber reinforced epoxy matrix composite. The disc was assumed to operate under a radial temperature distribution having parabolic profile. The study reveals that with the increase in temperature, the radial stress reduces throughout and the tangential stress decreases near the inner radius but increases near the outer radius.

Jahed *et al*. (2005) presented an approach to optimize the mass of a rotating FGM disc having non-linear thickness profile and subjected to elevated temperature. Zenkour (2006) investigated the effect of varying the disc profile on thermo-elastic stresses and displacements in an annular disc subjected to steady radial temperature gradient, with the temperature at the inner surface being higher than the outer surface. The study used disc with parabolic and exponential thickness profiles.

Bayat *et al.* (2007) used small deflection theory to obtain exact solution for displacement in a rotating FGM disc subjected to axisymmetric bending and steady-state thermal loading. The properties of the disc were assumed to vary radially according to power law distribution of content of the reinforcement. You *et al*. (2007) analyzed stresses and deformations in a rotating FGM disc operating at constant temperature. The study investigated the effect of varying density, material properties (viz. Young's modulus, coefficients of thermal expansion), disc thickness profile and temperature on the performance of disc.

Zenkour (2007, 2009) investigated the effect of radially varying the density and material properties on the stresses in a constant thickness rotating FGM disc. The study reveals that the FGM disc having higher elastic modulus and density near the inner radius exhibits lower stresses and deformations. Bayat *et al*. (2008) analyzed stresses and displacements in a variable thickness rotating FGM disc. The study investigated the effect of radially varying the material properties and disc thickness profile on the performance of the disc. The study indicates that a rotating FGM disc having parabolic concave or hyperbolic convergent thickness profile has lower stresses and deformations than a constant thickness FGM disc.

Callioglu (2008) estimated stresses and deformations in a rotating FGM subjected to internal and external pressure. The study assumed elastic modulus and density to vary radially according to different power law functions. The stresses and deformations in the disc are observed to be significantly affected by varying the material properties along the disc radius. Hojjati and Hassani (2008) used variable material properties (VMP) approach to analyze stresses and strains in a variable thickness rotating FGM disc. The study obtained solutions for similar FGM disc using numerical technique based on solution of governing differential equation using Runge-Kutta's method, and FE analysis. The results estimated using VMP approach, numerical techniques and FEM are observed to be in close agreement.

The VMP method is observed to be a reliable solution technique for solving the complex disc problems, which do not have exact solution.

Bayat *et al*. (2009a) used first-order shear deformation theory (FSDT) to analyze thermo-mechanical response of a variable thickness rotating FGM disc. The material properties and thickness of the disc were assumed to radially vary according to power law functions. The gradation in material properties and disc thickness profile are assumed to have significant effect on the stresses and displacements in the disc. Bayat *et al*. (2009b) in another study obtained elastic and thermo-elastic solutions for rotating FGM disc operating under steady state temperature field. The response of the disc was estimated for different types of thickness profile and different radial gradation of material properties. The study again reveals that the FGM disc having parabolic or hyperbolic convergent thickness profile is superior to a uniform thickness FGM disc. The variable thickness FGM disc also performs better than the constant thickness FGM disc when both the discs operate under similar temperature field.

Afsar and Go (2010) used FEM to analyze the thermo-elastic response of a rotating FGM disc operating under varying thermal loading. The response of the disc is observed to be significantly affected by varying the thermal loading, disc thickness profile and angular speed of the disc.

Asghari and Ghafoori (2010) used a semi-analytical approach to generalize the available two-dimensional plane-stress elasticity solution for a rotating FGM disc and obtained solutions for three-dimensional elasticity problem. The study indicates that for a thin rotating disc the two-dimensional solution provides appropriate results, but for a thick rotating disc, the results of three-dimensional elasticity solution are more appropriate.

Nie and Batra (2010) analyzed stresses and displacements in a variable thickness rotating solid and hollow FGM discs under different boundary conditions (free-free, fixed-free). The disc thickness and material properties (density, shear modulus, coefficient of thermal expansion) were assumed to vary according to power law functions of disc radius. As compared to hollow FGM disc with free-free condition, the maximum hoop stress in hollow FGM disc with fixed-free condition is considerably lower, though it has higher value of peak radial stress. In hollow FGM discs with fixed-free boundary condition the value of peak radial stress is observed to be higher than the maximum hoop stress. However, the results are opposite for FGM disc with free–free condition. The study also attempts to find the desired

tailoring of the material properties (shear modulus or thermal expansion coefficient) so as to achieve a uniform distribution of either the hoop or the in-plane shear stress or a linear combination of the radial and the hoop stresses in the disc.

Zenkour and Mashat (2010) obtained analytical and numerical solutions for variable thickness rotating hollow and solid discs. The study indicates that the radial displacement in the FGM disc decreases over the entire disc radius when its thickness profile has much steeper variation.

Bayat *et al*. (2011) investigated the effect of varying the disc profile and material properties, along the radial direction, on the stresses and displacements in rotating discs made of metal-ceramic and ceramic-metal FGMs. The radial displacement in ceramic-metal FGM disc is observed to be lower than that observed in metal-ceramic FGM disc. The study also indicates the performance of rotating FGM disc with concave thickness is superior to a uniform thickness FGM disc.

Callioglu (2011) used infinitesimal deformation theory to estimate thermo-mechanical response of a rotating FGM disc, having radial variation of material property. The performance of the FGM disc was analyzed corresponding to different values of internal and external pressure, centrifugal force and steady state temperature. It is revealed that by suitably tailoring the material properties, the optimal design of the FGM disc could be attained under given thermo-mechanical loading. Callioglu *et al*. (2011a) investigated the effect of material tailoring on the stresses and displacements in a rotating FGM disc. The stresses and displacements were estimated in the FGM disc for different values of material gradient index (n) ranging between 0 to 1. The FGM disc was observed to sustain higher rotating speed as compared to disc made of uniform material properties. Further, the FGM disc with material index (n) =1, exhibits the lowest radial stress. Callioglu *et al.* (2011b) in another study investigated the stresses and displacements in a rotating FGM disc subjected to different kinds of radially decreasing parabolic temperature profiles. The study indicates that with the increase in temperature gradient, the tangential stress decreases near the inner surface but increases towards the outer disc radius. However, the radial stress in the disc reduces gradually on imposing the radial thermal gradient. The radial displacement at the outer radius FGM disc is always higher as compared to that noticed near the inner radius. Callioglu *et al*. (2011c) further performed study to analyze stresses in rotating FGM disc operating under internal pressure and radially varying temperature profiles (uniform, linearly increasing, linearly decreasing). The study indicates that the radial displacement in the FGM

disc subjected to radial thermal gradient is observed to be lower than that of the FGM disc operating at uniform temperature.

Sharma *et al*. (2012) employed FEM to analyze thermo-elastic stresses, displacements and strains in a thin rotating FGM disc subjected to radially varying temperature. The material of the disc was assumed to be made of functionally graded Al-Al_2O_3 composite. The stresses, strains and displacements in the FGM disc are observed to have significant dependence on the radial temperature profile.

Peng and Li (2012) analyzed elastic behavior of a rotating solid disc made of FGM having different kinds of radial gradation of material properties. The numerical results are observed to be in close agreement with the exact results for some specific types of gradation of material properties. The results of the study are helpful in selecting the appropriate gradation of material properties in order to achieve the optimal disc performance.

Nejad *et al*. (2013) obtained closed form elastic solutions for a rotating FGM disc subjected to internal and external pressures. The material properties were assumed to vary radially according to an exponential law. The stresses, strains and displacements in the FGM disc were estimated for different types of material inhomogeneity. The analytical results obtained in the study were observed to have good agreement with the results estimated using FEM.

Zafarmand and Hassani (2014) obtained elastic solutions for a variable thickness rotating hollow and solid discs made of two-dimensional FGM by using the graded finite element method. The material properties were assumed to vary continuously along the radial and axial directions of the FGM disc. The study reveals that the stresses in FGM disc made of two-dimensional FGM are lower than that induced in FGM disc made of conventional one-dimensional FGM.

Garg and Gupta (2015) analyzed stresses and strains in a rotating FGM disc having linearly varying thickness profile. The Young's modulus and density of the disc were assumed to vary radially according to power law. The study indicates that the performance of the variable thickness FGM disc is superior to constant thickness FGM disc.

Dai and Dai (2015) used Runge-Kutta and shooting methods to obtain the numerical solutions of elastic stresses and displacements in a rotating FGM disc. The modulus of elasticity and density of the disc material were assumed to vary along the radius. The study reveals that the parameters like property gradation index, angular speed and disc geometry

have noticeable impact on the mechanical behavior of the disc. The stresses and displacements in the FGM disc are observed to reduce with the increasing value of property gradation index. Dai and Dai (2016) further extended the analysis to investigate the thermo-elastic stresses and displacements in a variable thickness rotating FGM disc operating under a radially varying temperature field. The study also indicates the dependence of the stresses and displacements in the disc on the property gradation index, disc geometry and angular speed, apart from the radial temperature profile. The FGM disc with higher value of property gradation index and thickness near the bore exhibits the lowest stresses and displacements. The displacement in the FGM disc is noticed to reduce with the increase in radial thermal gradient, although the radial and circumferential stresses show increase.

Jabari *et al.* (2016) estimated thermo-elastic behavior of a rotating FGM disc subjected to internal pressure and having different thickness profiles. The analysis was carried out by assuming material properties (except Poisson's ratios) and disc profile to vary according to power and exponential functions of disc radius. The analytical results were observed to be in close agreement with the FEM results. The stresses and displacements in the FGM disc were calculated for different disc thickness profile and at different angular velocity. The disc having variation of material properties and thickness according to power law function is observed to perform better than that having exponential variation, for specified thermal and centrifugal loading. However, for discs subjected to internal pressure, the use of exponential function is recommended.

Mirzana *et al.* (2016) analyzed the elastic stresses and deformations in a hollow disc made of functionally graded aluminum-zirconia composite using analytical and FEM techniques. The disc was subjected to the internal and external pressures of equal magnitude. The numerical and FEM results were observed to be in good agreement. The stresses and deformations in the FGM disc were noticed to be considerably affected by varying the radial distribution of Young's modulus of the disc material.

Thawait *et al.* (2017) used FEM to analyze elastic response of a variable thickness rotating FGM disc under fixed-free conditions. The material properties were assumed to vary radially according to the exponential law. The results were estimated for FGM disc with uniform, linearly varying and concave thickness profiles. The displacements and stresses are observed to be lower in the variable thickness FGM disc as compared to the uniform thickness disc.

2.2 ELASTIC-PLASTIC ANALYSIS

Gamer (1983) analyzed elastic-plastic response of a rotating solid disc of constant thickness using Tresca's yield criterion. Kollman (1981, 1984) obtained solutions for the problem of shrink fitted rotating and non-rotating disc using Tresca's criterion. Gamer (1984) extended the work by analyzing the elastic-plastic deformation in a rotating solid disc using Tresca's criterion and linear strain-hardening material behavior. Güven (1992, 1995) further extended the analysis for variable thickness hollow and solid FGM disc undergoing fully plastic deformation. Rees (1999) presented the analysis of elastic-plastic stresses in a constant thickness rotating hollow and solid discs using von Mises and Tresca's yield criteria.

You *et al*. (2000) estimated the elastic-plastic stresses and deformations in variable thickness rotating FGM disc. The comparison of results estimated using numerical technique with those obtained using FEM show good agreement.

Guven and Altay (2000) estimated the exact solution for elastic-plastic stresses in a solid disc subjected to external pressure and varying temperature. Eraslan and Argeso (2002) and Eraslan (2003) analyzed elastic-plastic behavior of a rotating hollow disc subjected to different boundary conditions and having parabolic thickness profile. Orcan and Eraslan (2002) analyzed stresses and deformations in a variable thickness rotating disc. The study indicates that the stresses and deformations in the disc reduce and the plastic limit angular velocity increases as the thickness of the disc is reduced.

Alexandrova and Alexandrov (2004) used Hill's orthotropic yield criterion and the associated flow rule to investigate the effect of anisotropy on the elastic-plastic stresses in a rotating hollow disc. The stress distribution in the disc is observed to be appreciably modified on varying the extent of anisotropy in the disc material.

Sayman (2006) estimated elastic-plastic stresses and deformations in a rotating disc in the presence of a radial thermal gradient. The study indicates that with the increase in operating temperature, the region of plastic deformation zone in the disc expands around the inner as well as outer radius. The plastic deformation is observed to be maximum at the inner disc radius.

Callioglu *et al*. (2006), using strain-hardening material behavior, analyzed the elastic-plastic response of a rotating disc made of orthotropic material and rotating at different angular velocity. The hoop stress in the disc is observed to be higher than the radial stress. The residual stress component of the circumferential stress and plastic deformation are

noticed to be the maximum at the inner disc radius. At all angular velocities, the radial displacement corresponding to elastic and plastic solutions are observed to be the maximum at the inner disc radius.

Sen and Sayer (2006) used FEM techniques to estimate elastic-plastic thermal stresses in a composite disc, made of thermoplastic matrix having reinforcement of steel fibers, subjected to constant temperature. The magnitude of elastic/elasto-plastic tangential stress is noticed to be higher than the radial stress in the disc, which is observed to be compressive at the inner and outer disc radii. The presence of thermal stresses in the disc was attributed to the mismatch in coefficient of thermal expansion of the disc material along the radial and tangential directions. The location of thermal and residual stresses is observed to change significantly with increasing temperature.

Sen *et al.* (2007) estimated elastic-plastic thermal stresses in a thermoplastic composite disc having reinforcement of steel fibers and subjected to radially varying parabolic temperature profile. The magnitude of tangential stress is observed to be higher than the magnitude of radial stress in the disc. The magnitude of tangential residual stress is noticed to be maximum at the inner disc radius. Altan *et al.* (2008) also analyzed elastic-plastic thermal stresses in a hollow disc made of an orthotropic composite consisting of reinforcement of steel fibers in aluminum matrix. The disc was assumed to operate under a parabolic thermal gradient along the disc radius. The study again indicates that the magnitude of tangential stress in the disc is higher than the radial stress.

Sen and Aldas (2009) used FEM to analyze elastic-plastic thermal stresses in a thermoplastic composite disc subjected to linearly varying radial temperature profile. The study also reveals that the magnitude and distribution of thermal and residual stresses in the disc are significantly affected on increasing the linear thermal gradient.

Hassani *et al.* (2012) analyzed thermo-elasto-plastic stresses and strains in a variable thickness rotating FGM disc. The results were also estimated by using semi-exact technique (Liao's homotopy) and FEM. The comparisons of results estimated by using above mentioned three different techniques are observed to be in close agreement.

Pei *et al.* (2013) analyzed elastic-plastic stresses in a rotating disc subjected to increasing edge temperature and torque, transmitted at the inner and the outer clamped edges. The study investigated the effect of varying disc speed and torques, and increase in edge temperatures on the elastic-plastic behavior of the disc. The effective stress in the disc is

observed to increase with the increase in edge temperature. The increase in effective stress is noticed to be relatively higher with the increase in outer edge temperature as compared to those noticed with the corresponding increase in the inner edge temperature.

Sharma and Yadav (2013) used finite difference method and von Mises yield criterion to analyze elastic-plastic behavior of a thin rotating disc having with radially varying thickness and density profiles (exponential and power law). The study indicates that the disc having radially decreasing thickness but radially increasing density, with power law profiles, is safe as compared to disc having exponentially varying thickness and density profiles as well as to constant thickness disc.

Callioglu *et al.* (2015) investigated the elastic–plastic stresses in a functionally graded disc subjected to constant angular velocity. The yielding of the disc material was described by von Mises criterion and the material properties (viz. elasticity modulus, density and yield strength) were assumed to vary radially according to a power law function. The study indicates that the yielding of the disc starts at the inner surface as its angular velocity is increased to a certain level. With further increase in angular velocity of the disc, the yielding region expands towards the outer radius. The FGM disc with radially decreasing material properties has almost homogenous distribution of stresses and more load carrying capacity as compared to the FGM disc having radially increasing material properties.

Singh and Sahni (2016) obtained closed form analytical solutions for elastic-plastic stresses in a variable thickness rotating FGM disc subjected to both internal and external pressure. The Young's modulus and thickness of the disc were assumed to increase with increasing radial distance according to a power law function. The radial and tangential stresses in the disc are observed to increase appreciably at higher values of pressure. The tangential stress in the FGM disc is noticed to be lower than that in the uniform composite disc.

Demir *et al.* (2017) investigated the elasto-plastic stresses in a rotating functionally graded disc having hyperbolic thickness profile and operating at a constant temperature. The study indicates that a variable thickness FGM disc has lower weight and can operate at higher temperature in comparison to a constant thickness FGM disc. The FGM disc in which the rigidity of the disc material decreases radially, has almost homogenous stress distribution and hence could be operated at higher temperature.

2.3 CREEP ANALYSIS

Wahl *et al*. (1954) developed a mathematical model to analyze the steady state creep response of a constant thickness rotating hollow disc made of forged alloy steel and operating at constant temperature of 1000^0F. The creep behavior of the disc material was described by Norton's creep law. The results were estimated using Tresca and von Mises yield criteria and compared with the experimental results obtained by conducting the creep tests on the same rotating disc. The theoretical results based on Tresca yield criterion are observed to be in better agreement with the experimental one. Wahl (1957) used Tresca yield criterion to further analyze the steady state creep in a rotating hollow disc having constant and variable thickness, and operating under either constant or radially varying temperature. The study also investigated the effect of varying stress exponent (n), appearing in the creep law, and varying the ratios of outer to inner disc radius on the creep performance of the disc. The variable thickness disc is observed to have lower values of tangential stresses than the constant thickness disc. For lower value of stress exponent in power law, the disc is observed to have lower creep rupture under long time loading conditions, due to considerable non-uniformity in the stress distribution. Wahl (1958) further extended his previous work (Wahl *et al*. 1954), and analyzed the steady state creep in rotating discs having constant and variable thickness profiles. The study assumed that the radial and tangential stresses are uniform either over the entire disc radius or over some portion of the disc. The study also confirmed that a variable thickness rotating disc is superior to a similar disc but having constant thickness.

Ma (1959) analyzed steady state creep in a variable thickness rotating turbine disc operating at a constant elevated temperature. The yielding of the disc material was described by Tresca criterion while the creep behavior of the disc material was described by either the power or the exponential law. Ma (1960) further extended the analysis for gas turbine and jet engine discs. The study indicates that the distribution of stress over the central portion of a variable thickness disc is significantly different from that noticed in a constant thickness disc. Ma (1961, 1964) in his subsequent studies further analyzed the steady state creep in a variable thickness disc by using either power [Ma (1964)] or exponential [Ma (1961)] creep law. The closed form solutions were obtained to estimate the creep stresses in the disc.

Arya and Bhatnagar (1979) investigated the effect of material anisotropy on the steady state creep stresses and deformations in a rotating disc. The study reveals that with the increase in materials' anisotropy, the tangential stress decreases throughout and the tangential strain decreases near the inner radius. Bhatnagar *et al*. (1986) further extended the analysis to

investigate the effect of varying disc profile (constant, linear and hyperbolic) on the steady state creep behavior of rotating disc made of anisotropic material. The disc material was assumed to creep according to Norton's power law. The study indicates that the design of disc could be improved by selecting a particular type of material anisotropy and disc thickness profile.

Singh and Ray (2001, 2003b) analyzed steady state creep in a constant thickness rotating FGM disc subjected to a constant temperature. The disc was assumed to be made of Al-SiC_P, wherein the content of SiC_p was assumed to decrease linearly with the increasing radius. The steady state creep rates in FGM disc were observed to be significantly lower than those observed for a uniform composite disc having uniform distribution of SiC_p reinforcement along the disc radius. The analysis was further extended to analyze the effect of material anisotropy on the steady state creep behavior of rotating disc made of homogeneous 6061Al-SiC_w composite (Singh and Ray, 2002) and inhomogeneous Al-SiC_p (Singh and Ray, 2003a). It is observed that the presence of anisotropy in the disc material significantly reduces the strain rates in the disc.

Jahed and Bidabadi (2003) used variable material properties (VMP) approach to analyze primary and secondary creep in a rotating disc subjected to different types of centrifugal and radially varying thermal loading. The approach used the basic solution for a rotating disc made of isotropic homogeneous material and obtained solution for FGM disc. The creep results estimated from the analysis schemes were compared to those obtained using the FEM techniques. The study indicates a close agreement between the results.

Gupta *et al.* (2003, 2004a) examined the effect of varying reinforcement content and size, and operating temperature on the steady state creep behavior of a rotating FGM disc. The disc was assumed to be made of linearly functionally graded Al-SiC_p composite and undergoing steady state creep according to Sherby's law and yielding according to von Mises criterion. The study reveals that by varying the reinforcement size and content, and operating temperature, the distribution of radial stress in the FGM disc is not affected significantly but their effect on the tangential stress is sizable. The strain rates in the disc are observed to reduce with the decrease in reinforcement size, increase in reinforcement content and decrease in operating temperature. Gupta *et al*. (2005a) further examined the steady state creep behavior of the rotating Al-SiC_p disc having radially varying (linear and quadratic) distribution of SiC_p reinforcement along the disc radius and subjected to a radial temperature

distribution. The FGM disc having radially varying quadratic distribution of SiC_p is observed to have lower strain rates compared to linear FGM and uniform composite discs.

Gupta *et al*. (2004b, 2005b) extended the study conducted by Singh and Ray (2001) and analyzed the steady state creep response of a constant thickness rotating FGM disc subjected to radially varying temperature. The disc material was assumed to creep according to Sherby's law and yield according to von Mises criterion. The study reveals that the FGM disc operating under a radially varying temperature profile has lower strain rates than that observed in a similar FGM disc, but operating at constant temperature, which is assumed to be the average of the imposed radial temperature profile.

Gupta *et al*. (2007) analytically estimated the steady state creep behavior of a rotating disc made of Al-SiC_p, by using the Sherby's creep law. The stresses and strain rates in the disc were estimated for various combinations of reinforcement size, reinforcement content and operating temperature. The results, thus obtained, were used to train the ANN based on back propagation learning algorithm by keeping the reinforcement size, reinforcement content and operating temperature as the input parameters, and the stresses and strain rates as the output parameters. The developed ANN model was then used to predict the stresses and strain rates in the disc, which were observed to be in excellent agreement with the analytical results.

Farshi and Bidabadi (2008) investigated steady state creep in a rotating FGM disc operating under a high radial thermal gradient. The efforts were made to minimize weight of the disc by varying the disc thickness profile in such a way that the value of equivalent creep stresses over the entire disc radius simultaneously approach the allowable stress of the disc material.

Gun (2008) used quadratic boundary element (BE) formulation to analyze elasto-plastic creep damage in a rotating disc. The prediction of creep rupture life was made by using the continuum damage mechanics approach. The study reveals that BE technique is an accurate alternative approach for solving the elasto-plastic creep damage problems.

Singh (2008), using Norton's power law and Hill's yield criterion, analyzed the steady state creep behavior of a rotating disc made of anisotropic 6061 Al-SiC_w composite. The study indicates that the presence of anisotropy significantly affects the distribution of strain rates in the disc, although its effect on stress distribution is not prominent.

Deepak *et al*. (2009) analyzed the steady state creep behavior of a constant thickness rotating Al-Si_p disc. The creep behavior of the composite was described by threshold stress based law for three different values of stress exponents (3, 5 and 8). The stresses and strain rates in the disc are observed to vary significantly on varying the value of stress exponent. The strain rates in the disc are observed to increase by around about two orders of magnitude as the value of stress exponent is increased from 3 to 8.

Gupta *et al.* (2009a) analyzed the steady state creep behavior of a constant thickness rotating functionally graded Al-SiC_p disc having radially varying (linear and quadratic) distribution of SiC_p reinforcement. The disc was assumed to creep following Sherby's law and subjected to a radial thermal gradient. The study indicates that the stresses and strain rates in the FGM disc could be reduced to a large extent by employing more SiC_p reinforcement in the middle region as compared to the inner and the outer regions. Similar observations were also made by Rattan *et al.* (2010) in their study on rotating functionally graded Al-SiC_p disc having radially varying parabolic distribution of SiC_P reinforcement.

Gupta *et al.* (2009b) developed a mathematical model to investigate the effect of varying the morphology (particle/whisper) of SiC reinforcement on the steady state creep behavior of a rotating disc made of 6061Al-$SiC_{w,p}$ ('w' for whisker, 'p' for particle) composite. The study reveals that the stresses and strain rates in the composite disc are significantly affected by varying the morphology of SiC reinforcement. The whisker reinforced composite disc develops appreciably lower strain rates as compared to a particle reinforced composite disc, when both the discs are subjected to similar loading condition.

Chamoli *et al*. (2010) investigated steady state creep response of a constant thickness rotating disc made of anisotropic composite by using Sherby's creep law. The effect of varying the extent of materials' anisotropy was investigated on the creep stresses and strain rates. It is observed that the presence of anisotropy significantly affects the creep response of the composite disc. The strain rates in the disc could be reduced significantly by selecting a particular type of material anisotropy.

Deepak *et al*. (2010a) analyzed the steady state creep behavior of a rotating FGM disc having a radially varying linear thickness profile and subjected to a constant temperature. The strain rates in the FGM disc are observed to be significantly lower than that noticed in the homogeneous composite disc. Deepak *et al.* (2010b) further extended their work to investigate the effect of varying disc thickness profile on the steady state creep stresses and

creep rates in a rotating disc made of homogeneous Al-SiC_p composite. The composite disc having linearly varying thickness is observed to have lower strain rates as compared to similar composite disc having either constant or hyperbolic thickness profile.

Singh and Rattan (2010) analyzed steady state creep behavior of a rotating Al-SiC_p composite disc in the presence of thermal residual stresses. The yielding of the disc material was described by isotropic Hoffman yield criterion. The presence of thermal residual stress is observed to have a little effect on the distribution of stresses in the disc. However, the tangential and radial strain rates in the disc are observed to increase significantly, especially near the outer radius of the disc, in the presence of residual stresses. The presence of residual stress is also observed to change the nature of radial strain rate from compressive to tensile in the middle region of the disc.

Loghman *et al*. (2011) used Mendelson's method of successive elastic solution and Sherby's creep law to analyze time-dependent creep stress in a rotating Al-SiC_p composite. The results were estimated by varying the radial distribution of SiC_p reinforcement in the disc. The study indicates that the FGM disc having 0% SiC at inner radius and 40% SiC at the outer radius exhibits the minimum and more uniform distribution of tangential and effective stresses.

Garg *et al.* (2012) investigated the steady state creep in a rotating functionally graded Al-SiC_p disc having radially decreasing (linear and non-linear) distribution of SiC_p reinforcement and radially decreasing linear thickness profile. The disc material was assumed to creep according to the threshold stress based law and yield following von Mises criterion. As compared to the uniform composite disc, the FGM discs (linear and non-linear) show slightly higher values of radial stress over the entire radius and appreciably higher tangential and effective stresses near the inner radius but considerably lower values of the tangential and effective stresses near the outer radius. The increase or decrease observed in the stresses is more for non-linear FGM disc than the linear FGM or uniform composite disc. The strain rates in the FGM discs are observed to be lower and relatively more uniform over the entire disc radius than that noticed in the uniform composite disc. The non-linear FGM disc is observed to have the least chances of creep induced distortions.

Goel *et al.* (2012) analyzed the creep response of a rotating functionally graded Al-SiC_p disc using finite element-based Abaqus software. The content of SiC_p reinforcement in the disc was assumed to decrease linearly with increasing radius. The FGM disc shows

relatively higher radial stress throughout as compared to uniform composite disc. However, the tangential and effective stresses in the FGM disc are observed to be noticeably higher near the inner radius but significantly lower near the outer radius, when compared to a uniform composite disc. The FGM disc shows considerably lower values of the strain rates in comparison to a uniform composite disc.

Gupta and Singh (2012) investigated the effect of varying anisotropy on the steady state creep behavior of a rotating Al-SiC_p composite disc having hyperbolic thickness profile. The study also reveals that the anisotropy has significant impact on the creep response of the composite disc.

Dwivedi *et al.* (2013) investigated the effect of varying disc thickness gradient on the steady state creep response of a rotating FGM disc having linearly varying thickness along the disc radius. The study shows that with the increase in disc thickness gradient, the stresses as well as the strain rates in the FGM disc reduce, with significant reduction observed in the strain rates. Garg *et al*. (2013a, 2013b) in similar studies, but for non-linear FGM discs with linear thickness profiles, also noticed that the increase in disc thickness gradient [Garg *et al.* (2013a)] or reinforcement gradient [Garg *et al.* (2013b)] reduces the stresses and strain rates in the disc, and hence reduces the possibility of creep distortions in the disc. Garg *et al.* (2013c) further extended their analysis to investigate the effect of imposing radially increasing linear thermal gradient on the steady state creep performance of a non-linear FGM disc having linear thickness profile. With the increase in radial thermal gradient in the FGM disc, the radial stress increases throughout and the tangential stress increases near the inner radius but decreases towards the outer radius. The creep rates in the FGM disc are observed to reduce appreciably with the increasing radial thermal gradient. Deepak *et al.* (2015) further extended their earlier work [Dwivedi *et al.* (2013)] to investigate the steady state creep in a variable thickness rotating FGM disc having different thickness profiles, viz. constant, linear and hyperbolic. The study indicates that by using the FGM disc with hyperbolic thickness profile, the stresses and strain rates in the disc could be reduced significantly.

Gupta and Singh (2014) investigated the influence of anisotropy on the steady state creep response a variable thickness (linear/hyperbolic) rotating composite disc in the presence of residual thermal stresses. The disc material (Al-SiC_w) was assumed to creep according to the Sherby's law and yield following isotropic/anisotropic Hoffman criterion. The strain rates in the rotating anisotropic disc having hyperbolic thickness profile and residual thermal stresses are observed to be lower by about three orders of magnitude as

compared those noticed in an isotropic composite disc with linear thickness profile. The anisotropy is found to have a little effect on the distribution of stresses in the disc.

Garg *et al.* (2015) analyzed the steady state creep performance of a rotating functionally graded Al-SiC_p composite disc having linearly varying radial distribution of SiC_p reinforcement and subjected to varying radial thermal gradients. The disc material was assumed to creep according to threshold stress based law and yield following von Mises criterion. The study reveals that on increasing the thermal gradient in the FGM disc, the strain rates in the rotating FGM disc reduce significantly.

Rattan *et al.* (2016) investigated the effect of thermal residual stresses on the steady state creep behavior of a rotating Al-SiC_p FGM disc subjected to different radial temperature profiles (uniform, linear and parabolic). The disc material was assumed to yield according to isotropic Hoffman yield criterion and undergo creep following Sherby's law. The radial stress in FGM disc operating under different temperature profiles is observed to decrease in the presence of thermal residual stresses. The presence of residual stresses tend to increase the tangential and radial strain rates in the FGM disc, as compared to those observed in the FGM disc without residual stresses.

Bose *et al.* (2017), using Sherby's creep law, analyzed the steady state creep behavior of a constant thickness rotating disc made of functionally graded Al-SiC_p composite. The stresses and strain rates in the FGM disc, with linearly increasing SiC_p content along the disc radius, were estimated for various types of radially decreasing temperature profiles. The study reveals that the presence of thermal gradient does not have significant effect on the radial and tangential stresses in the disc, but its effect on the strain rates is appreciable. With the increase in radial thermal gradient in the FGM disc, the radial and tangential strain rates increase near the inner radius but decrease towards the outer radius.

2.4 ANALYSIS BASED ON SETH'S TRANSITION THEORY

This section gives a brief overview of the research work conducted to analyze elastic-plastic and creep response of rotating disc based on Seth's transition theory.

2.4.1 Elastic-Plastic Transition

Gupta and Shukla (1994) investigated the effect of varying material inhomogeneity on the elastic-plastic transition in a thin hollow rotating disc using Seth's transition theory. The disc made of inhomogeneous material is observed to yield at higher angular velocity as compared to those observed for disc made of homogeneous material. The disc having higher

material inhomogeneity requires less percentage increase in angular velocity to reach fully plastic stage against initial yielding. The percentage increase in angular velocity, corresponding to initiation of yielding, is observed to decrease with the increase in material inhomogeneity.

Shukla (2000) estimated elastic-plastic transitional stresses in a variable thickness FGM disc operating under internal pressure. The inhomogeneity of the disc material was described in terms of varying Poisson's ratio of the disc material. The presence of non-homogeneity and thickness gradient of the disc are observed to have significant effect on stresses in the disc and on the operating pressure for the initiation of yielding.

Gupta and Pankaj (2007b) analyzed the elastic-plastic and fully plastic behavior of a thin rotating disc mounted on a shaft and subjected to different operating temperatures. As compared to the disc made of incompressible material, the disc made of compressible material exhibits the start of yielding (at the inner radius) at lesser angular speed. However, the disc made of compressible material requires higher percentage increase in angular speed to reach fully plastic state, as compared to the disc made of incompressible material.

Pankaj and Bansal (2008a) analyzed elastic-plastic transition in a thin rotating disc with inclusion. The study also reveals that a rotating disc made of compressible material exhibits yielding at lower angular speed but requires higher percentage increase in angular speed to become fully plastic, when compared to a similar disc, but composed of incompressible material.

Pankaj (2009) used Seth's theory to analyze elastic-plastic transition in a variable thickness rotating disc under internal pressure. The study indicates that a variable thickness disc made of compressible yields at some intermediate radius and at higher operating pressure in comparison to a similar disc but made of incompressible material, which exhibits yielding at the outer radius. However, a constant thickness disc made of incompressible material yields at the inner radius at high value of operating pressure as compared to disc consisting of compressible material.

Thakur (2009) investigated elastic-plastic transition in a thin rotating disc with inclusion and having variable density. The rotating disc made of compressible material and having radially varying density is more prone to fracture at the bore. The variable density disc is observed to have higher values of radial and tangential stresses at the inner radius for fully-plastic state, as compared to a similar disc having constant density.

Sharma and Sahni (2009) used Seth's transition theory to analyze elastic-plastic stresses in a transversely isotropic thin rotating disc. The disc made of transversely isotropic material is observed to yield at a higher angular speed, as compared to a similar disc but having isotropic properties. The study also indicates that the rotating disc made of transversely isotropic material is much safer as compared to the disc made of isotropic material.

Thakur (2010a) carried out analysis of elastic-plastic and fully plastic behavior of a thin rotating disc mounted on a rigid shaft and subjected to different temperatures. At room temperature, the disc made of compressible material and having smaller value of ratio of inner to outer radius exhibits yielding at the inner radius at high value of angular speed, when compared to a similar disc made of incompressible material. With the increase in operating temperature, the yielding is observed to occur at the outer radius and at lesser angular speed.

Sharma and Sahni (2011) employed Seth's transition theory to obtain solutions for elastic-plastic and transitional stresses in a variable thickness rotating disc. The rotating disc made of incompressible material is observed to yield at the inner surface at higher angular speed in comparison to disc made of compressible material. As compared to a constant thickness disc, the rotating disc having exponentially varying thickness exhibits yielding at the inner surface at higher angular speed.

Thakur (2011) estimated elastic-plastic transitional stresses in a variable thickness hollow disc having radially varying Poisson's ratio and operating under an internal pressure. The stresses induced in the disc and the value of pressure required for initial yielding are observed to depend significantly on the radial variation of Poisson's ratio and disc thickness profile.

Thakur (2012) investigated elastic-plastic transitional stresses in a rotating disc mounted on shaft and having variable thickness profile. The disc made of incompressible material is observed to undergo yielding at the inner radius and at higher angular speed, when compared to similar disc composed of compressible material. The increase in disc thickness gradient is observed to induce maximum tangential stress at the outer radius but maximum radial stress is noticed at the inner radius. The disc made of isotropic compressible material is observed to be much safer that a similar disc made of isotropic incompressible material.

Thakur *et al*. (2013), using finite deformation and Seth's transition theories, investigated the effect of varying disc thickness profile on the elastic-plastic transitional

stresses of a thin rotating disc. The study indicates that the variable thickness disc made of incompressible material needs higher percentage increase in angular speed to reach fully plastic stage, as compared to a similar disc, but made of compressible material. The effect of varying disc thickness on the circumferential stresses is maximum at the outer radius for compressible materials as compared to incompressible materials. However, for a constant thickness disc of incompressible material the circumferential stresses are maximum at the inner radius as compared to similar disc made of compressible materials. For fully plastic state, the circumferential stress at the outer disc radius is observed to increase with the increase in the disc thickness near the inner radius.

Thakur *et al*. (2014) used Seth's transition theory to analyze steady thermal stresses in a rotating disc with shaft having density variation parameter. The study reveals that the disc made of compressible material requires higher percentage increase in angular speed to become fully plastic as compared to a rotating disc made of incompressible material. The introduction of thermal effect is observed to decrease the value of radial and circumferential stresses at the inner and outer radii of the disc for fully-plastic state.

Thakur *et al.* (2015) used Seth's transition theory to analyze the plastic stresses and deformations in a thin rotating disc made of non-homogeneous isotropic material and attached to a shaft. The study indicates that the rotating disc consisting of non-homogenous material having higher non-homogeneity at the bore than at the rim undergoes yielding at a lower angular velocity as compared to non-homogeneous disc with less non-homogeneity at the bore than at the rim.

2.4.2 Creep Transition

Shukla (1996) used transition theory to investigate creep in a thin rotating disc made of non-homogeneous material. The presence of material non-homogeneity, which increases with increase in radius, is observed to reduce the stresses in the disc and the angular velocity required to initiate steady state creep in the disc, as compared to those observed in a homogeneous disc. Increasing the value of non-homogeneity at the inner radius of the disc tends to further increase the magnitude of angular velocity and creep stresses, and increases the probability of disc fracture in the vicinity of bore.

Gupta *et al.* (2000a) investigated creep in a variable density thin rotating disc using Seth's transition theory. The study reveals that the disc made of incompressible material with radially decreasing density and rotating at higher angular speed are more prone to fracture at

the bore, as compared to rotating disc having radially increasing density or having uniform density. The creep deformations are observed to be significant in variable density disc when it rotates at higher angular speed. Gupta *et al*. (2000b) further extended the analysis for a thin rotating disc having variable thickness and density. The study indicates that the rotating disc whose density and thickness ratio decreases radially is much safer as compared to a variable density disc having constant thickness.

Gupta and Pankaj (2007a) used Seth's transition theory to analyze creep in a thin rotating disc mounted on a solid shaft. The study indicates that the disc made of incompressible material exhibits the maximum value of radial stress at the inner radius as compared to circumferential stress in the disc. The radial stress is observed to further increases with the increase in angular speed of the disc. The creep rates in a rotating disc made of compressible material are observed to be maximum at the inner radius.

Pankaj and Bansal (2008b) investigated creep stresses and strains in a thin rotating disc with radially varying density and attached to a solid shaft. It is revealed that the disc rotating at higher speed and having radially increasing density is safer than the disc rotating at the same speed but having radially decreasing density.

Sharma and Sahni (2008) performed analysis of creep, using Seth's transition theory, in a rotating disc made of transversely isotropic and isotropic materials. The study indicates that the disc made of transversely isotropic material and rotating at higher angular speed has more chances of fracture at the bore as compared to disc made of isotropic material and operating at the same speed.

Thakur (2010b) used Seth's transition theory to investigate the effect of imposing different types of radial thermal gradient on the creep performance of a thin rotating disc. The presence of radial thermal gradient in the disc is observed to increase the maximum value of radial stress, noticed at the inner radius, as compared to similar disc operating at uniform temperature.

Sharma *et al*. (2013) analyzed creep performance of a thin rotating disc subjected to edge load and mounted on a shaft, and having exponential thickness profile. The study indicates that in a rotating disc made of incompressible material the radial stress is observed to be maximum at the inner radius as compared to circumferential stress. The magnitude of radial stress is observed to further increase with the increase in angular speed of the disc. The

study also reveals that the disc has possibility to fail by cleavage close to the bore. The presence of edge load is observed to increase the strength of the disc against fracture.

2.5 PROBLEM FORMULATION

The literature consulted reveals that a number of studies have been undertaken to investigate the creep behavior of rotating disc made of monolithic or uniform composite materials. The studies pertaining to the creep behavior of rotating disc made of FGMs are rather limited. In most of the work, the yielding has been described by von Mises yield criterion. But a limited number of studies [Wahl *et al.* (1954), Wahl (1956)] confirm that the results obtained using Tresca criterion are much closer to the experimental one, as compared to those estimated by using von Mises criterion.

In some of the real life applications, viz. turbine rotor and disc brake, the disc has to operate under different kinds of radial thermal gradient, rather than at uniform temperature. But in the studies conducted on FGM disc of constant thickness, the disc is assumed to operate at a constant temperature. In this light, it is imperative to consider the effect of imposing different kinds of radial thermal gradient on the creep performance of rotating FGM disc.

Deformation processing of composites by processes such as forging, rolling or extrusion often results in alignment of reinforcement, which leads to anisotropic flow behavior. Some of the investigators have considered the effect of anisotropy on the creep behavior of a rotating disc. But these studies are based on constant thickness disc made of monolithic material, uniform composite or FGM. The literature consulted does not reveal any study that considers the effect of anisotropy on the steady state creep behavior of rotating FGM disc having variable thickness. In view of this, it is necessary to investigate the consequences of anisotropy on the creep behavior of FGM disc having variable thickness.

The literature also reveals that Seth's transition theory can also be used to analyze the creep behavior of rotating disc made of monolithic material. The transition theory does not require a number of assumptions that are made during the analysis of creep in rotating disc using classical approach. Therefore, it may be interesting to carry out creep analysis of the rotating FGM disc having variable thickness by employing Seth's transition theory.

2.6 OBJECTIVES OF STUDY

On the basis of literature consulted and research gaps noted, the following objectives have been identified for the present study:

1. To analyze steady state creep in the FGM disc using Tresca yield criterion and to compare the results with that obtained by using von Mises criterion.
2. To investigate the effect of imposing different kinds of thermal gradients on the creep performance of the FGM disc with variable thickness.
3. To analyze steady state creep in a variable thickness disc made of orthotropic FGM and to investigate the effect of varying anisotropy on the creep performance of the FGM disc.
4. To analyze creep in a variable thickness disc made of FGM by using Seth's transition theory.

2.7 METHODOLOGY

The step-wise description of the methodology followed during the course of present study is given below:

[I]. Development of the constitutive equations for a rotating FGM disc subjected to plane stress condition on the basis of creep law and different yield criteria, Tresca for isotropic and Hill for anisotropic. The basic equations for an isotropic rotating disc subjected to multi-axial creep are given below,

$$\dot{\varepsilon}_r = \frac{\dot{\bar{\varepsilon}}}{2\bar{\sigma}}\left[2\sigma_r - \sigma_\theta - \sigma_z\right]$$

$$\dot{\varepsilon}_\theta = \frac{\dot{\bar{\varepsilon}}}{2\bar{\sigma}}\left[2\sigma_\theta - \sigma_r - \sigma_z\right] \qquad (2.1)$$

$$\dot{\varepsilon}_z = \frac{\dot{\bar{\varepsilon}}}{2\bar{\sigma}}\left[2\sigma_z - \sigma_r - \sigma_\theta\right]$$

where $\dot{\varepsilon}_r$, $\dot{\varepsilon}_\theta$, $\dot{\varepsilon}_z$ and σ_r, σ_θ, σ_z are the strain rates and the stresses, respectively along the *r*, θ and *z* directions of the disc, as indicated by the subscripts, $\bar{\sigma}$ is the effective stress and $\dot{\bar{\varepsilon}}$ is the effective strain.

The steady state creep behavior of the disc material (Al-SiC) has been described by the threshold stress (σ_0) based creep law [Deepak *et al*. (2010a)],

$$\dot{\bar{\varepsilon}} = \left[M\,(\bar{\sigma} - \sigma_0)\right]^5 \qquad (2.2)$$

where M and σ_0 are the creep parameters of the disc material, which depend on reinforcement size, reinforcement content and operating temperature.

[II]. Mathematical analysis to develop expressions for estimating the distributions of radial and tangential stresses in the FGM disc. To obtain these expressions, the force equilibrium equation for a variable thickness rotating FGM disc (refer Eq. 2.3 below) is solved along with the constitutive stress-strain relations (Eq. 2.1), compatibility (strain-displacement) equations and the boundary conditions of the disc,

$$\frac{d}{dr}[h(r)r\sigma_r] - h(r)\sigma_\theta + \rho(r)\omega^2 r^2 h(r) = 0 \qquad (2.3)$$

where $h(r)$ and $\rho(r)$ are thickness and density, respectively, at any radius r of the FGM disc. The radial variation of density, $\rho(r)$, in the FGM disc is estimated from the rule of mixture.

[III]. Obtaining the expressions for estimating the radial and tangential strain rates in the FGM disc, by substituting the equations of stresses, as obtained above, into the constitutive stress-strain equations (Eq. 2.1).

[IV]. Estimating the values of creep parameters for the FGM disc from the available creep results for SiC (particle/whisker) reinforced aluminum/aluminum alloy matrix composites.

[V]. Development of computer code to estimate the stresses and the strain rates in the rotating FGM disc. The computer code is developed by implementing an iterative numerical scheme of computation by following the method of successive approximations and adopting a rapid convergence criterion.

[VI]. Validation of the analysis and the software developed by comparing the estimated results with the published experimental/analytical results and the results obtained through finite element (FE) modeling.

[VII]. Estimation of creep response of the rotating FGM disc corresponding to different objectives, as mentioned in Section-2.6.

[VIII]. Analysis of the results.

CHAPTER-3

ANALYSIS OF CREEP IN A VARIABLE THICKNESS ROTATING FGM DISC: COMPARISON USING TRESCA AND VON MISES CRITERIA

3.1 INTRODUCTION

Rotating disc is a widely used structural component in many mechanical systems like steam and gas turbine rotors, turbo generators, automotive brakes, flywheels, ship propellers, etc. [Gupta *et al.* (2004a), Hojjati and Hassani (2008)]. In some of these applications, such as turbine rotors and disc brakes, the disc is simultaneously subjected to high temperature and severe mechanical loading, and hence is vulnerable to creep. Under such thermo-mechanical loading conditions, the disc made of monolithic materials may not survive. To overcome this problem, Functionally Graded Materials (FGMs) have been evolved, which could sustain severe thermo-mechanical loading [Bui *et al.* (2016)]. FGMs are advanced high performance materials, and are able to withstand the ultra-high temperatures, extremely large temperature gradients which usually happens in spacecraft, nuclear plants, and plasma facing for fusion reactors [Jagtap *et al.* (2013]. Functionally Graded Materials are categorized among one of the high technology materials [Gupta *et al.* (2016)] Owing to this FGMs find applications in components of advanced aircraft and aerospace engines [Aboudi *et al.* (1999), Talha and Singh (2015)], wherein the components operate under severe thermo-mechanical loading. Keeping this in view, investigators have explored the possibility of using FGMs for rotating disc applications.

Several investigators have analyzed the stresses and deformations (elastic, elastic-plastic, creep) in variable thickness rotating disc, which has been found superior to constant thickness disc, as outlined in Section-2.1 [Eraslan and Orcan (2002), Orcan and Eraslan (2002), Bayat *et al.* (2009b, 2011), Zenkour and Mashat (2010), Deepak *et al.* (2010a, 2010b), Garg *et al.* (2012, 2013a), Dwivedi *et al.* (2013), Deepak *et al.* (2015)]. Güven (1992) investigated elastic-plastic stresses and radial displacement in a variable thickness

rotating disc by using Tresca yield criterion. Gupta *et al.* (2005a) used von Mises yield criterion to investigate steady state creep in a constant thickness rotating FGM disc made of Al-SiC_p and subjected to radial thermal gradient. Deepak *et al.* (2010a) investigated steady state creep in a rotating FGM disc having linearly varying thickness by using von Mises yield criterion.

The literature review given in Chapter-2 reveals that most of the researchers have used von Mises criterion for analyzing steady state creep in a variable thickness rotating disc made of FGM. The literature further reveals that as compared to von Mises criterion, Tresca yield criterion could better deal with more complex problems like of rotating disc [Eraslan (2003)]. In addition, due to non-linearity associated with the use of von Mises criterion, a careful choice of numerical treatment is essential for obtaining approximate solutions [Bhowmick *et al.* (2010)]. The superiority of Tresca criterion over von Mises criterion for analyzing rotating disc problem is also confirmed by the earlier studies on steel [Wahl *et al.* (1954), Wahl (1962)] and lead discs [Frank (1960)]. The analytical creep solutions based on Tresca criterion were observed to be much closer to the experimental creep results as compared to the results estimated by using von Mises criterion. In this light, the present analysis uses Tresca criterion to analyze steady state creep in a variable thickness rotating disc. The creep stresses and creep rates are estimated in the FGM disc and compared with those available in literature [Deepak *et al.* (2010a)] for similar FGM disc yielding according to von Mises criterion.

3.2 DISC PROFILE

The present study considers a rotating hollow disc made of FGM having the inner and outer radii as *a(=31.75 mm)*, *b(=152.4 mm)*, respectively, and rotating at a constant speed of 15000 *rpm.*

The FGM disc is assumed to have radially varying thickness (Fig. 3.1), with thickness $h(r)$ at radius r is expressed by,

$$h(r) = h_b + 2c(b - r) \tag{3.1}$$

where $c \left[= \frac{h_a - h_b}{2(b-a)} \right]$ is a constant, and h_a (*=43.22mm*) and h_b (*=13.97mm*) are the disc thicknesses at the inner and the outer radii, respectively. The disc dimensions, thickness profile and the operating speed selected in this study are kept similar to that reported in earlier published work of Deepak *et al.* (2010a) based on von Mises yield criterion.

3.3 DISTRIBUTION OF REINFORCEMENT

The FGM disc under investigation is assumed to be made of silicon carbide (particle shape) reinforced in aluminum matrix composite (Al-SiC_p). Similar to study of Deepak *et al.* (2010a), the present study also assumes that the distribution of SiC_p in the FGM disc decreases linearly on moving from the inner to the outer radius (Fig. 3.2) according to the following relation,

$$V(r) = V_{\max} - \frac{(r-a)}{(b-a)}(V_{\max} - V_{\min}) \tag{3.2}$$

where $V(r)$ is the content of SiC_p (*vol%*) at any radius r, and V_{max} and V_{min} are the maximum and minimum SiC_p content at the inner and the outer radii, respectively. In this investigation, two different FGM discs (Fig.3.2) with V_{max} = 25% and 35% have been assumed. However, for the purpose of comparison both the discs are assumed to have same average content of SiC_p (=20% *vol%*).

Knowing the radial distribution of SiC_p in the disc from Eq. (3.2), the density $\rho(r)$ of the FGM disc at any radius r is estimated by using the rule of mixture [Gupta *et al.* (2005a)] as given below,

$$\rho(r) = \frac{[100 - V(r)]\rho_m + V(r)\rho_d}{100}$$

or,

$$\rho(r) = \rho_m + \frac{(\rho_d - \rho_m)V(r)}{100} \tag{3.3}$$

where ρ_m and ρ_d are the densities of pure Al matrix and SiC_p reinforcement, respectively. The values of ρ_m and ρ_d are taken as 2698.9 kg/m^3 and 3210 kg/m^3, respectively [Gupta *et al.* (2005a)].

In this study, the creep response of rotating Al-SiC_p disc is estimated by assuming the operating temperature T = 623 K, which is well above homologous temperature [≅ 50% of melting point temperature of Al-SiC_p [Dieter (1988)]. At such a high operating temperature significant creep is noticed in Al-SiC_p composite, as the melting point of Al-SiC_p is around 700 ^oC. In a rotating FGM disc, if the size of SiC_P reinforcement (P) and the operating temperature (T) are kept constant, the creep stresses and creep rates will depend on the radial distribution of SiC_p in the disc.

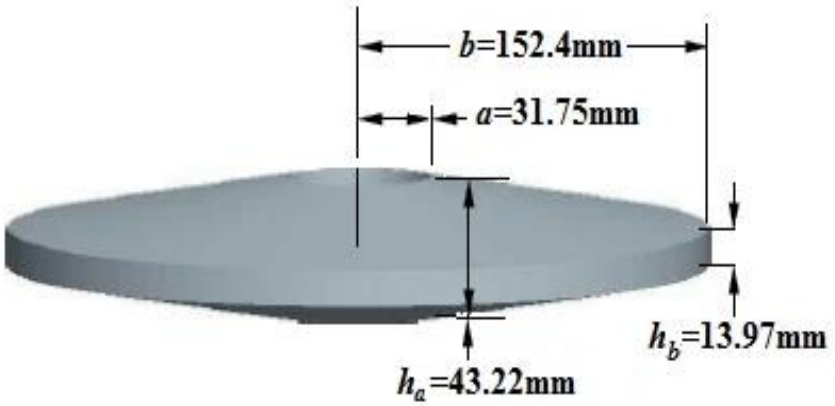

Fig. 3.1: Schematic showing disc dimensions and geometry

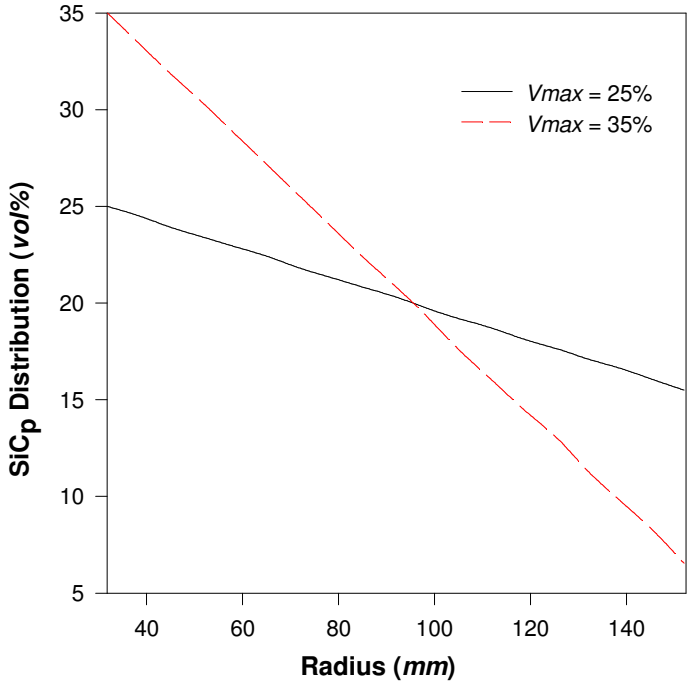

Fig. 3.2: Distribution of SiC_p in FGM discs

3.4 CREEP LAW

The steady state creep behavior of the disc material is described by the following well-established threshold stress based law [Ma and Tjong (2001)],

$$\dot{\bar{\varepsilon}} = [M(r)\{\bar{\sigma} - \sigma_0(r)\}]^n \tag{3.4}$$

where $\dot{\bar{\varepsilon}}$ is the effective strain rate, $\bar{\sigma}$ is the effective stress, $\sigma_0(r)$ is the threshold stress and $M(r)$ is creep parameter of the material. The value of parameter $M(r)$ is given by,

$$M(r) = \frac{1}{E}\left(A' \exp\frac{-Q}{RT} \right)^{1/n}$$

where the symbols A', n, Q, E, R and T denote, respectively, the structure dependent parameter, true stress exponent, true activation energy, temperature-dependent Young's modulus, gas constant and operating temperature. The value of true stress exponent (n) in Eq. (3.4) is taken as 5, which corresponds to creep controlled by high temperature dislocation climb, as observed in Al-SiC_p composite [Deepak *et al.* (2010a)].

The values of creep parameters $M(r)$ and $\sigma_0(r)$ depend on the size of SiC_p reinforcement ($P=1.7\,\mu m$) and SiC_p content $V(r)$, apart from the operating temperature (T = 623 K). The following regression equations, as derived in earlier work [Deepak *et al.* (2010a)], have been used to estimate the value of creep parameters in the FGM disc.

$$M(r) = 0.0288 - \frac{0.0088}{P} - \frac{14.0267}{T} + \frac{0.0322}{V(r)} \tag{3.5}$$

$$\sigma_0(r) = -0.084P - 0.023T + 1.185V(r) + 22.207 \tag{3.6}$$

3.5 MATHEMATICAL ANALYSIS

The analysis carried out is based on the following assumptions:

(i) Material of the disc is incompressible and locally isotropic, *i.e.* at a given radius the properties of disc material remain the same in all the directions.

(ii) The disc is under steady state condition of stress.

(iii) Elastic deformations in the disc, being small, are neglected as compared to creep deformations.

(iv) The disc thickness is small compared to its diameter, therefore, plane stress condition is assumed *i.e.* axial stress (σ_z) is zero throughout the disc.

Taking the reference frame along the principal directions r, θ and z of the disc, the generalized constitutive creep equations under plane stress condition ($\sigma_z = 0$) are given by [Gupta *et al.* (2004a)],

$$\dot{\varepsilon}_r = \frac{\dot{\bar{\varepsilon}}}{2\bar{\sigma}}\left[2\sigma_r(r) - \sigma_\theta(r)\right]$$

$$\dot{\varepsilon}_\theta = \frac{\dot{\bar{\varepsilon}}}{2\bar{\sigma}}\left[2\sigma_\theta(r) - \sigma_r(r)\right] \tag{3.7}$$

$$\dot{\varepsilon}_z = \frac{\dot{\bar{\varepsilon}}}{2\bar{\sigma}}\left[-\sigma_r(r) - \sigma_\theta(r)\right]$$

where $\dot{\varepsilon}_r$, $\dot{\varepsilon}_\theta$ and $\dot{\varepsilon}_z$ are, respectively, the strain rates along *r*, θ and z directions and σ_r and σ_θ are, respectively, the radial and tangential stresses in the disc under steady state condition.

The material of the disc is assumed to yield according to Tresca criterion, as discussed in Section 1.6.1 and expressed by Eq. (1.7) for 3D state of stress. In terms of the effective stress ($\bar{\sigma}$), defined as the uniaxial state of stress equivalent to the multi-axial state of stress, the Tresca criterion for 3D state of stress can be expressed as [Dieter (1988)],

$$\bar{\sigma} = \sigma_y,$$

where the effective stress $\bar{\sigma} = (\sigma_1 - \sigma_3)$, as evident from Eq. (1.7), wherein σ_1 and σ_3 are the maximum and minimum principal stresses, respectively. Under bi-axial state of stress (*i.e.* $\sigma_3 = 0$), the effective stress $(\bar{\sigma}) = \sigma_1$.

Since in a rotating disc since $\sigma_\theta > \sigma_r > \sigma_z$ [Ma (1964)], therefore the effective stress ($\bar{\sigma}$) in a rotating disc under biaxial state of stress (σ_z=0) is given by,

$$\bar{\sigma} = \sigma_\theta \tag{3.8}$$

Substituting $\dot{\bar{\varepsilon}}$ and $\bar{\sigma}$, from Eqs. (3.4) and (3.8), respectively, into the first equation amongst the set of Eqs. (3.7), one gets,

$$\dot{\varepsilon}_r = \frac{d\dot{u}_r}{dr} = [M(r)\{\bar{\sigma} - \sigma_0(r)\}]^n \frac{[2x(r) - 1]}{2} \tag{3.9}$$

where $x(r)\left[= \sigma_r(r) \big/ \sigma_\theta(r)\right]$ is the ratio of radial and tangential stresses, $\dot{u}_r\left[= du \big/ dt\right]$ is the radial deformation rate and *u* is the radial deformation of the disc.

Similarly, the second equation amongst the set of Eqs. (3.7) yields,

$$\dot{\varepsilon}_\theta = \frac{\dot{u}_r}{r} = [M(r)\{\bar{\sigma} - \sigma_0(r)\}]^n \frac{[2 - x(r)]}{2} \tag{3.10}$$

Dividing Eq. (3.9) by Eq. (3.10) and integrating the resulting equation between limits *a* to *r*, one gets,

$$\dot{u}_r = \dot{u}_a . exp\left[\int_a^r \frac{\Phi(r)}{r}\right] dr \tag{3.11}$$

where $\dot{u}_a$ is the radial deformation rate at the inner disc radius and $\Phi(r) = \dfrac{2x(r)-1}{2-x(r)}$

Substituting $\dot{u}_r$ from Eq. (3.11) into Eq. (3.10) and simplifying, one gets,

$$\sigma_\theta(r) = \frac{\dot{u}_a^{1/n}\Psi_1(r)}{M(r)} + \sigma_0(r) \tag{3.12}$$

where,

$$\Psi_1(r) = \Psi_2(r)^{1/n} \quad \text{and} \quad \Psi_2(r) = \frac{2}{r[2-x(r)]} \exp \int_a^r \frac{\Phi(r)}{r} dr$$

The force equilibrium equation for a variable thickness FGM disc, rotating at angular velocity ω, is given by [Deepak *et al.* (2010a)],

$$\frac{d}{dr}[rh(r)\sigma_r(r)] - h(r)\sigma_\theta(r) + \rho(r)\omega^2 r^2 h(r) = 0 \tag{3.13}$$

Earlier investigators have analyzed rotating discs by considering different types of boundary conditions. The boundary conditions of the disc depend on the way it is attached to the shaft. The present study assumes that the disc is connected to the shaft by means of splines, thus radial pressure at the inner and the outer surfaces is zero, *i.e.* free-free boundary conditions, [Wahl *et al.* (1954)] prevail in the disc, as explained below,

$$\text{(i) } \sigma_r(r) = 0 \text{ at } r = a \text{ and } \quad \text{(ii) } \sigma_r(r) = 0 \text{ at } r = \text{b.} \tag{3.14}$$

Substituting $h(r)$ from Eq. (3.1) into the equilibrium Eq. (3.13) and integrating the resulting equation between limits a to b, under the imposed boundary conditions given in Eq. (3.14), one gets,

$$\int_a^b h(r)\sigma_\theta(r)dr = \omega^2\left[\frac{A_\rho M}{3}(b^3-a^3) - \frac{A_\rho N}{4}(b^4-a^4) - \frac{B_\rho M}{4}(b^4-a^4) + \frac{B_\rho N}{5}(b^5-a^5)\right] \tag{3.15}$$

where,

$$M = (h_b + 2bc), \quad N = 2c,$$

$$A_\rho = \rho_m + \frac{(\rho_d - \rho_m)}{100}\left[V_{\max} + \frac{a(V_{\max} - V_{\min})}{(b-a)}\right]$$

and,

$$B_\rho = \frac{(\rho_d - \rho_m)}{100}\frac{(V_{\max} - V_{\min})}{(b-a)}$$

The average tangential stress, $\sigma_\theta(avg)$, in the FGM disc is given by,

$$\sigma_\theta(avg) = \int_a^b \frac{h(r)\sigma_\theta(r)dr}{\int_a^b h(r)dr} \tag{3.16}$$

Putting Eqs. (3.1) and (3.15) in Eq. (3.16), one gets,

$$\sigma_\theta(avg) = \frac{\omega^2\left[\frac{A_\rho M}{3}(b^3-a^3) - \frac{A_\rho N}{4}(b^4-a^4) - \frac{B_\rho M}{4}(b^4-a^4) + \frac{B_\rho N}{5}(b^5-a^5)\right]}{M(b-a) - \frac{N}{2}(b^2-a^2)} \tag{3.17}$$

Integrating Eq. (3.13) once again between limits *a* to *r*, and using the first boundary condition given in Eq. (3.14), one obtains,

$$\sigma_r(r) = \frac{[\int_a^r h(r)\sigma_\theta(r)dr - \int_a^r \rho(r)\omega^2 r^2 h(r)dr]}{rh(r)} \tag{3.18}$$

Multiplying both sides of Eq. (3.12) by $h(r)dr$, and then integrating the resulting equation between limits *a* to *b*, and using Eq. (3.16), one gets,

$$\dot{u}_a^{1/n} = \frac{\sigma_\theta(avg)\int_a^b h(r)dr - \int_a^b h(r)\sigma_0(r)dr}{\int_a^b \frac{h(r)\Psi_1(r)}{M(r)}dr} \tag{3.19}$$

Substituting $\dot{u}_a^{1/n}$ from Eq. (3.19) into Eq. (3.12), one obtains the distribution of tangential stress in the disc as,

$$\sigma_\theta(r) = \frac{\sigma_\theta(avg)\int_a^b h(r)dr - \int_a^b h(r)\sigma_0(r)dr}{M(r)\int_a^b \frac{h(r)\Psi_1(r)}{M(r)}dr}\Psi_1(r) + \sigma_0(r) \tag{3.20}$$

Once the distribution of $\sigma_\theta(r)$ in the disc is known from Eq. (3.20), the radial stress in the disc may be estimated from Eq. (3.18). Thereafter, the strain rates $\dot{\varepsilon}_r$ and $\dot{\varepsilon}_\theta$ in the disc are estimated, respectively, from Eqs. (3.9) and (3.10).

3.6 RESULTS AND DISCUSSION

Following the analysis presented in Section-3.5, the creep stresses and strain rates are estimated for two different FGM discs (Table 3.1) by following an iterative numerical scheme, shown in Fig. 3.3. The iteration is continued till the process converges and yields the values of stresses at different radial locations of the disc. To achieve rapid convergence, 75% of the value of σ_θ obtained in the current iteration (say i^{th} iteration) has been added to 25% of the value of σ_θ obtained in the previous iteration, as given by Eq. (3.21) below, and this

modified value is used in the next cycle of computation. The iteration process is continued until it satisfies the convergence criterion (h=0.01) is satisfied, Fig. 3.3. The choice of h=0.01 is motivated by the earlier works [Gupta *et al.* (2004a), Deepak *et al.* 2010a].

$$[\sigma_\theta]_{(i+1)} = 0.75[\sigma_\theta]_i + 0.25[\sigma_\theta]_{(i-1)} \tag{3.21}$$

Table 3.1: Distribution of SiC_p in variable thickness FGM discs (V_{avg} = 20 *vol %*)

Disc Notation	**SiC_p Content (*vol %*)**		**Particle Gradient**
	V_{max} **(*r* = *a*)**	V_{min}**(*r* = *b*)**	**(PG) = (V_{max} - V_{min}) in *vol %***
D1	25	15.51	9.49
D2	35	6.54	28.46

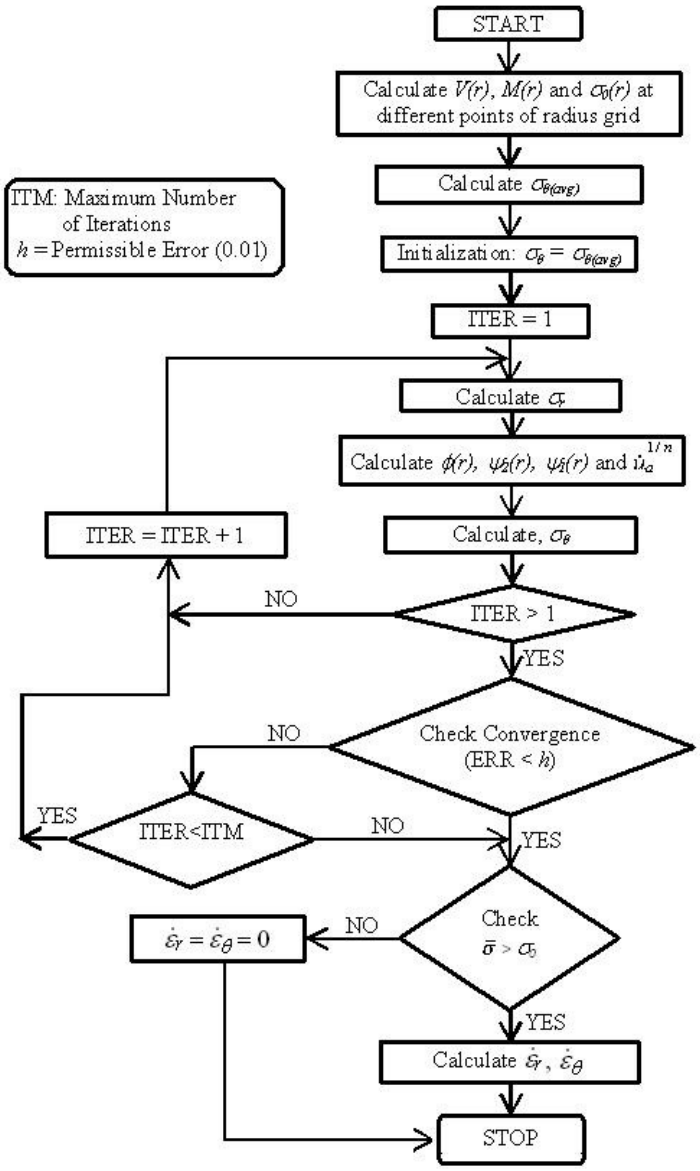

Fig. 3.3: Scheme of computation

3.6.1 Validation

In order to check the validity of analysis carried out and computation scheme followed, the results estimated by using the present analysis are compared with the published experimental results and with the finite element (FE) results obtained using commercially available ANSYS package. The comparisons of the results are presented and discussed in the following sub-sections.

3.6.1.1 Comparison of analytical and experimental results

The radial and tangential strains are estimated for a rotating steel disc by following the current analysis scheme and compared with the experimental results reported by Wahl *et al.* (1954), for the same steel disc. The operating conditions, disc dimensions and creep parameters used in the computation process are taken from the earlier studies [Wahl *et al.* (1954), Gupta *et al.* (2004a)] and are mentioned in Table 3.2.

Table 3.2: Operating conditions, disc dimensions and creep parameters used for validation

Disc Dimensions:	**Operating Conditions:**
Inner radius (a) = 31.75 *mm*	Operating temperature = 810.78 *K*
Outer radius (b) = 152.4 *mm*	Disc speed = 15,000 *rpm*
Disc thickness (t) = 25.4 *mm*	Creep duration = 180 *hrs*
Properties of Steel Disc:	
Creep parameter (M) = 2.0408×10^{-4} $s^{-1/5}/MPa$	Density (ρ) = 7,823.18 kg/m^3
Threshold stress (σ_o) = 37.178 *MPa*	Stress exponent (n) = 5

As evident from Fig. 3.4a, the estimated values of radial and tangential strains are observed to be in good agreement with the corresponding values of experimental strains. Since the order of strains are quite low, thus for better comparison the relative error [Burden and Faires (2011)] is estimated between the estimated and the experimental values of strains by dividing the difference of experimental and estimated values of strain with the experimental value of strain. The maximum value of relative error (Fig. 3.4a) noticed between the experimental strains (average of experimental values of strains at a given

location) and the estimated values of radial and tangential strains are observed to be 0.1 and 0.4, respectively, at the outer radius. Such a low magnitude of relative error between the experimental and the estimated strains establishes the validity of the analysis scheme followed and the software developed.

3.6.1.2 Comparison of analytical and FE results

The analytical results obtained in this study for rotating FGM disc D1 (Table 3.1), having variable thickness, are also compared with the numerical results estimated for the same disc by using ANSYS, which is a commercial finite element package. The FGM disc (disc D1) is modeled in ANSYS using solid modeling approach by discretizing it into eighteen elementary discs having different radius and thickness. The inner radius of the first elementary disc and the outer radius of the last elementary disc are kept as 31.75 *mm* and 152.4 *mm*, respectively. However, the radial width of each elementary disc is kept equal (= 6.70 *mm*). The thickness profile of each elementary disc has been varied according to Eq. (3.1). Each of the elementary discs has been assigned different values of density (ρ), Young's modulus (E) and creep parameters, owing to radially varying content of reinforcement (SiC_p) in the functionally graded Al-SiC_p composite disc. However, the values of density, Young's modulus and creep parameters for a particular elementary disc have been kept the same. For each elementary disc, the density has been estimated from Eq. (3.3) and the Young's modulus has been estimated from the rule of mixture given by,

$$E(r) = E_d V_d + E_m (1 - V_d) \tag{3.22}$$

where V_d is the volume fraction of SiC_p reinforcement in the elementary disc at its mean radius (r), and E_d (= 410 *GPa*) and [Budinski (2000)] and E_m (= 70 *GPa*) [Clyne and Withers (1993)] are the Young's modulus of SiC_p reinforcement and Al matrix, respectively.

During the FEM analysis, the inbuilt Norton's creep law [Singh and Ray (2001)], as given below in Eq. (3.23), has been chosen to describe the steady state creep behavior of the disc material,

$$\dot{\bar{\varepsilon}} = B(r)\,\bar{\sigma}^{\,n(r)} \tag{3.23}$$

where $B(r)$ and $n(r)$ are the creep parameters of the disc material, *i.e.* Al-SiC_p composite. The values of creep parameters for Al-SiC_p depend on the size (P) and content, $V(r)$, of the SiC_p

reinforcement, and the operating temperature (T). The values of creep parameters $B(r)$ and $n(r)$ for different elementary discs are estimated from the following regression equations, as developed by Singh and Ray (2001) for Al-SiC_p,

$$\log B(r) = -29 + 1729.38 \log e - 274.71 \log T - 1.98 \log P - 15.88 \log V(r) \quad (3.24)$$

$$\log n(r) = -21.54 \log e + 3.80 \log T + 0.07 \log P + 0.07 \log V(r) \quad (3.25)$$

The content, $V(r)$, of SiC_p reinforcement at mean radius (r) of various elementary discs are estimated from Eq. (3.2). Knowing P (=1.7 μm), T (=623 K) and $V(r)$, the values of creep parameters $B(r)$ and $n(r)$ for various elementary discs are estimated, respectively, from Eqs. (3.24) and (3.25). The creep parameters, thus estimated, have been assigned to the corresponding elementary discs.

After assigning the properties to various elementary discs, they have been assembled to create a single FGM disc (D1). The interactions between the contacting surfaces of various elementary discs have been defined in such a way that no relative motion exists between the neighboring elementary discs. Following assembly, the FGM disc model was meshed using tetrahedral 3D elements with 10 nodes (SOLID92). The element has quadratic displacement behavior with three degrees of freedom at each node, translations in X, Y and Z directions. This element also has plasticity, creep, swelling, stress stiffening, large deflection and large strain capabilities. The disc model was then subjected to free-free boundary conditions and an inertia load corresponding to disc rpm of 15000. In addition, the entire disc model was also subjected to a uniform thermal load. The solutions were obtained for radial strain rate in the FGM disc until the stress distribution reaches to steady state condition.

The radial strain rate estimated using FE analysis in ANSYS have been compared with the analytically estimated values for the same FGM disc (*i.e.* disc D1), by following the analysis procedure described in Section 3.5. The analytical results are observed to be in excellent agreement with the FE results, as is evident from Fig. 3.4b, which further inspires confidence in the analysis carried out and the computer code developed in this study.

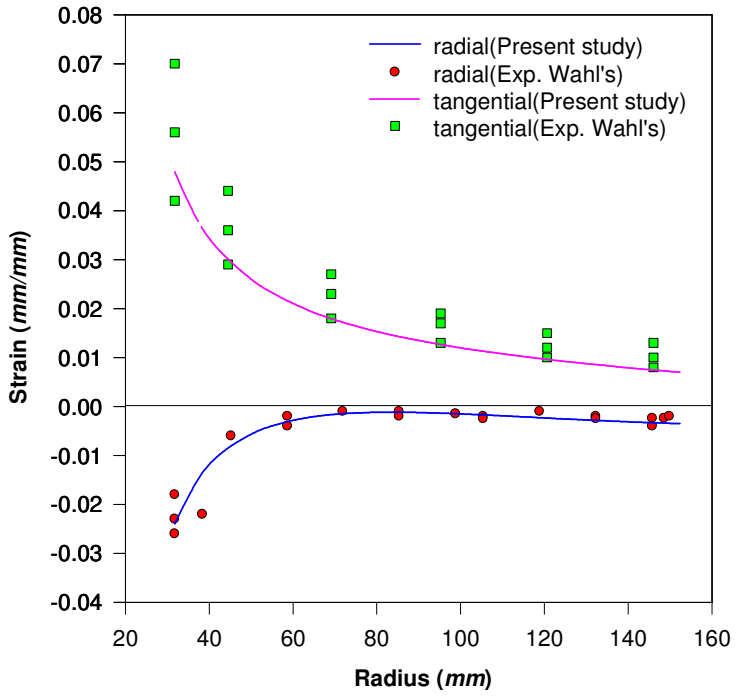

Fig. 3.4(a): Comparison of results of present study and experimental study on steel disc

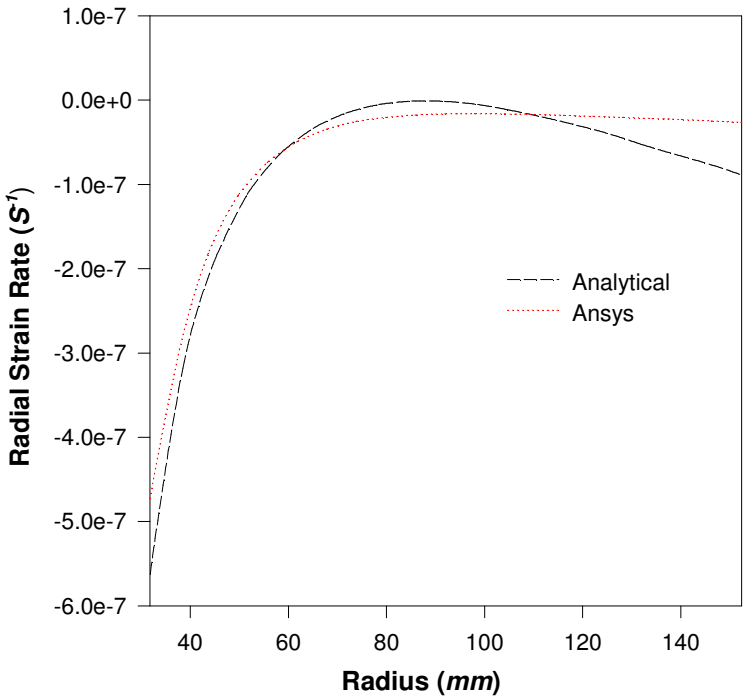

Fig. 3.4(b): Comparison of analytical and FE results for FGM disc D1

3.6.2 Comparison of Creep Response of Constant and Variable Thickness FGM Discs

The earlier studies [Bayat *et al.* (2009b, 2011), Zenkour and Mashat (2010)] reveal that the creep response of variable thickness disc is superior to uniform (constant) thickness

disc. In order to further verify this fact for the FGM disc, the creep performance of constant and variable thickness FGM discs have been compared in this study. The creep stresses and strain rates are estimated, following the analysis based on Tresca criterion (Section 3.5), for the FGM discs having linear and uniform thickness profiles but having similar type of linear SiC_p gradient, with V_{max} = 25%, as observed in disc D1. The thickness of the uniform thickness disc is estimated as 25.4 *mm*, obtained by averaging the thickness profile of the variable thickness (Fig. 3.1).

The tangential stress (Fig. 3.5) in variable thickness disc is significantly lower than the uniform thickness disc. The difference noticed decreases slightly with the increase in radius, with a maximum difference of 19 *MPa* observed at the inner radius. Similar to tangential stress, the variable thickness disc also exhibits lower radial stress throughout (Fig. 3.6), with a maximum decrease of 5.5 *MPa* noticed at a radius of 78.7 *mm*. The strain rates, tangential as well as radial, in variable thickness disc are also observed to reduce significantly (Figs. 3.7 - 3.8) when compared to those noticed in uniform thickness disc. The maximum reduction noticed in tangential and radial strain rates is 14.5 x 10^{-6} and 7.24 x 10^{-6} respectively, at the inner radius. Thus, it is evident that if one replaces uniform thickness FGM disc with variable thickness FGM disc, the magnitude of creep stresses and creep rates in the FGM disc are reduced significantly.

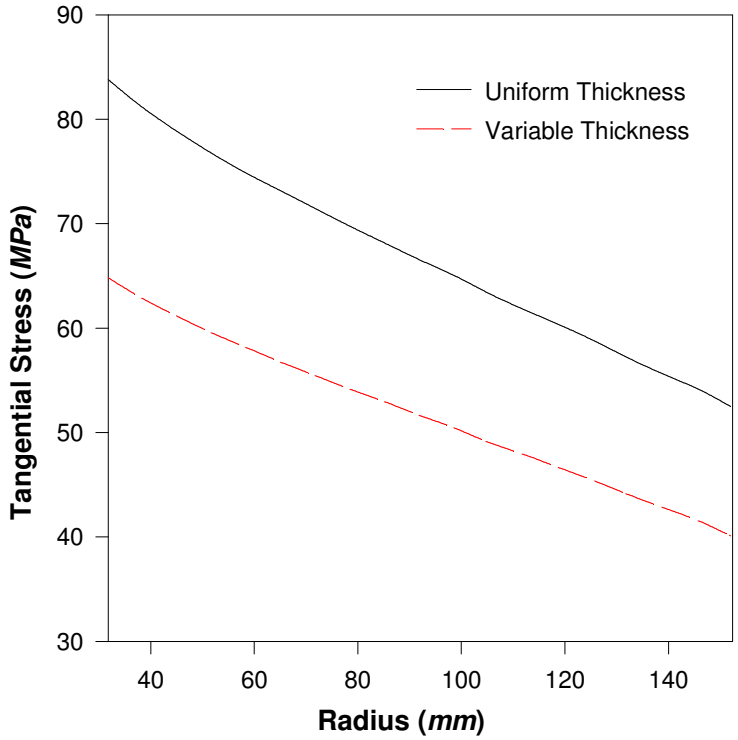

Fig. 3.5: Tangential stress in constant and variable thickness FGM discs

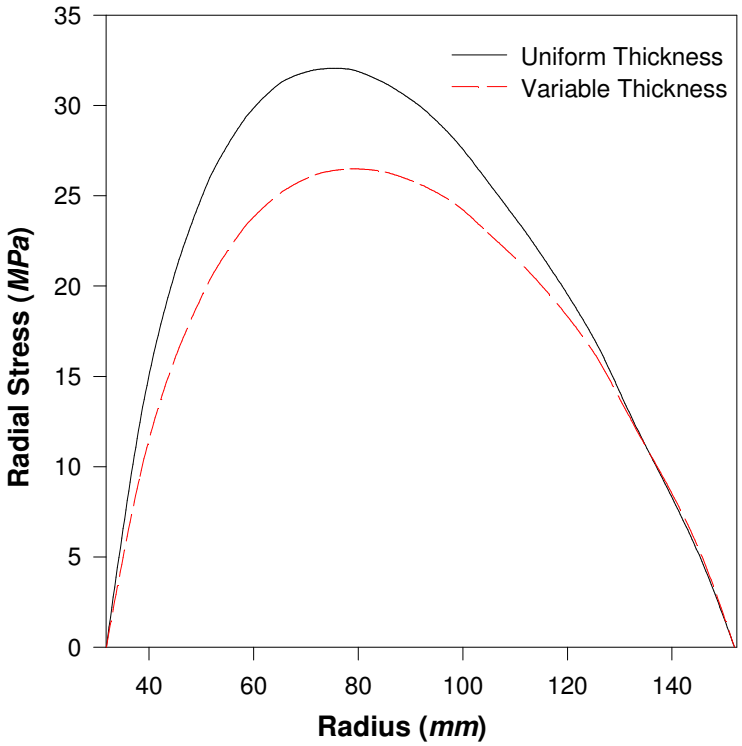

Fig. 3.6: Radial stress in constant and variable thickness FGM discs

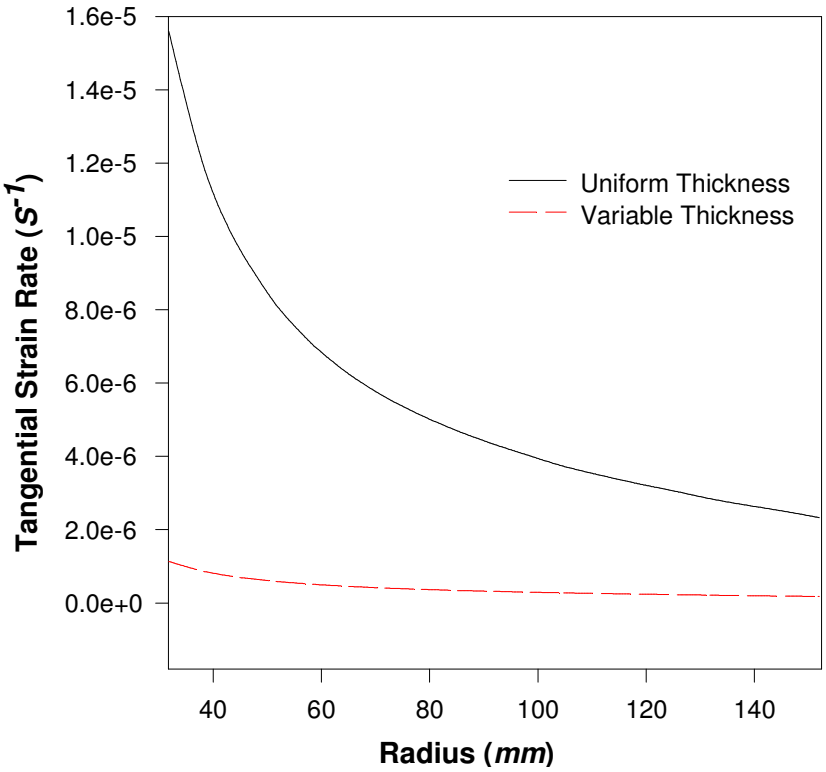

Fig. 3.7: Tangential strain rate in constant and variable thickness FGM discs

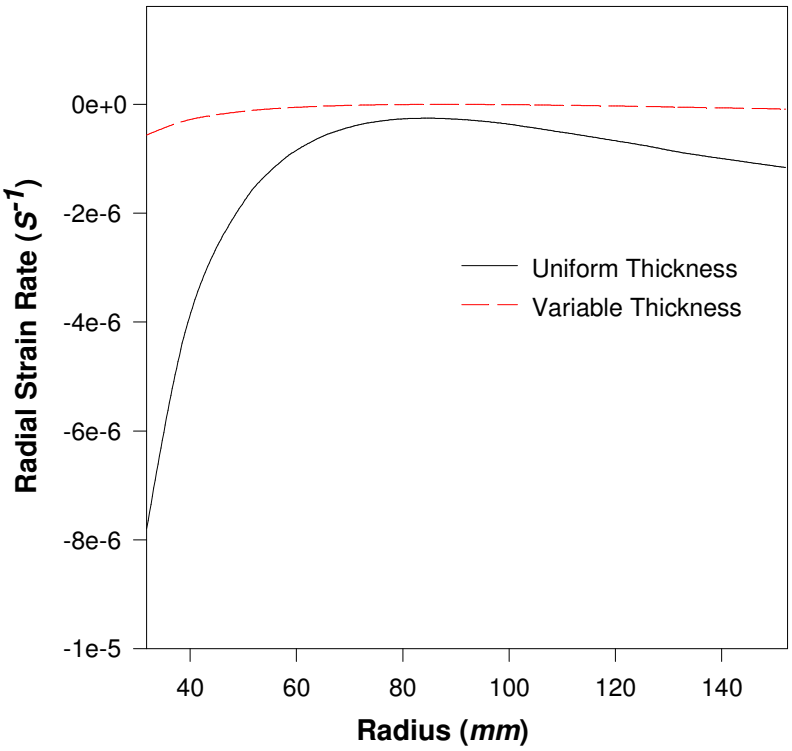

Fig. 3.8: Radial strain rate in constant and variable thickness FGM discs

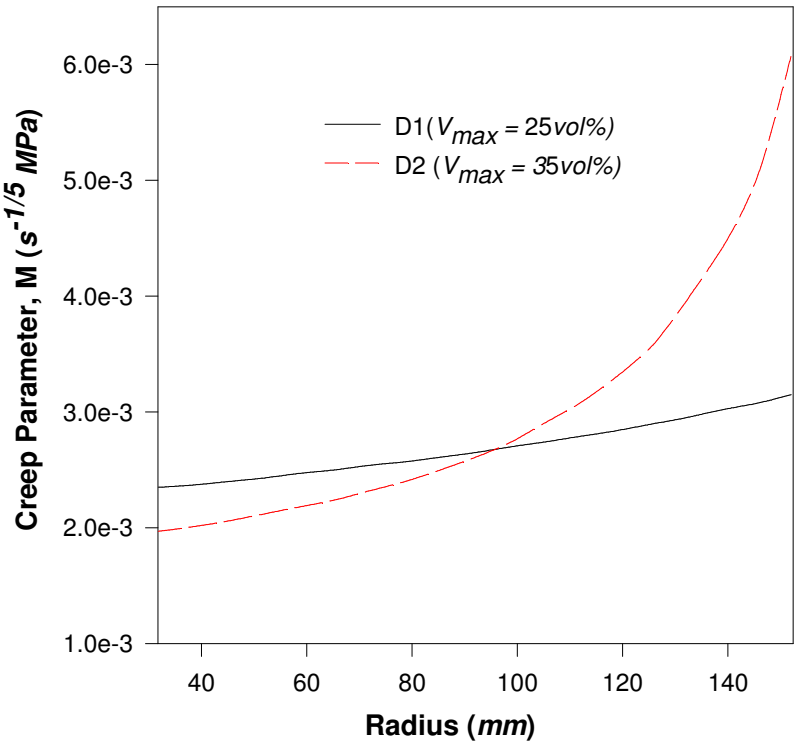

Fig. 3.9: Variation of creep parameter in FGM discs

3.6.3 Comparison of Creep Results using Tresca and von Mises Criteria

The results of previous section reveal that the creep response of a variable thickness FGM disc is superior to a constant thickness FGM disc. Therefore, in this section variable thickness FGM discs D1 and disc D2 (Table 3.1) are chosen for the purpose of comparing creep stresses and creep rates, estimated by using analysis schemes based on Tresca criterion (present study) and von Mises criterion [Deepak *et al.* (2010a)].

(*i*) *Variation of creep parameters in FGM discs*

The creep parameter *M* (Fig. 3.9) increases on moving from the inner to the outer radius of the disc. The FGM disc D2 has lower value of *M* near the inner radius but the higher value of *M* towards outer radius when compared to FGM disc D1. This is attributed to relatively higher and lower SiC_p content near the inner and outer radii, respectively, of the FGM disc D2 as compared to FGM disc D1, Fig. 3.2. However, the variation of threshold stress in FGM discs D1 and D2 (Fig. 3.10) is opposite to that observed for creep parameter *M* (Fig. 3.9). The σ_o is higher in both the FGM discs at locations having higher SiC_p gradient, as is evident from regression Eq. (3.6).

(*ii*) *Comparison of stresses in FGM discs*

The trend of variation of tangential stress, obtained by using Tresca and von Mises criteria, is slightly different (Fig. 3.11). The tangential stress estimated by using Tresca criteria is maximum at the inner radius whereas its maximum value is noticed at a radius of 38.5 mm when von Mises criterion is used. The tangential stress estimated using Tresca criterion is a little lower than obtained using von Mises criterion, except for some portion near the inner and outer radii where Tresca criterion estimates slightly higher stress value. Similar variations have been noticed in tangential stress, estimated using Tresca and von Mises criteria, for steel disc [Wahl *et al.* (1954)]. The maximum variation noticed in tangential stress, estimated using Tresca and von Mises criteria, is 7.20 *MPa* and 8.40 *MPa* in FGM discs D1 and D2, respectively, at the inner radius. In general, the difference noticed in tangential stress, estimated using both the criteria, is observed to reduce with the increase in SiC_p gradient (Table 3.1) in the FGM discs, as evident from the comparison of FGM discs D1 and D2, Fig. 3.11. The trend of variation of radial stress obtained using both the yield criteria is similar (Fig. 3.12), though Tresca criterion estimates slightly higher in the region of the disc between 31.75 *mm* to 110 *mm*. Beyond a radius of 110 *mm*, both the criteria estimates almost equal value of radial stress. The maximum variation noticed in radial stress using

Tresca and von Mises criteria is 1.1 *MPa* and 1.2 *MPa*, respectively, for FGM discs D1 and D2, at a radius of 45.2 *mm*. Like tangential stress, the difference in radial stress estimated using both the criteria slightly reduces with increasing SiC_p gradient. The trend of effective stress, using Tresca and von Mises yield criteria (Fig. 3.13), is also similar. Though, the Tresca criterion estimates higher values of effective stress throughout the disc. The difference observed in effective stress using both the criteria decreases with increasing radius. The difference noticed is also observed to decrease with the increase in SiC_p gradient in the disc. The maximum variation in effective stress using Tresca and von Mises criteria is 7.2 *MPa* and 8.40 *MPa* for FGM discs D1 and D2, respectively, at the inner disc radius.

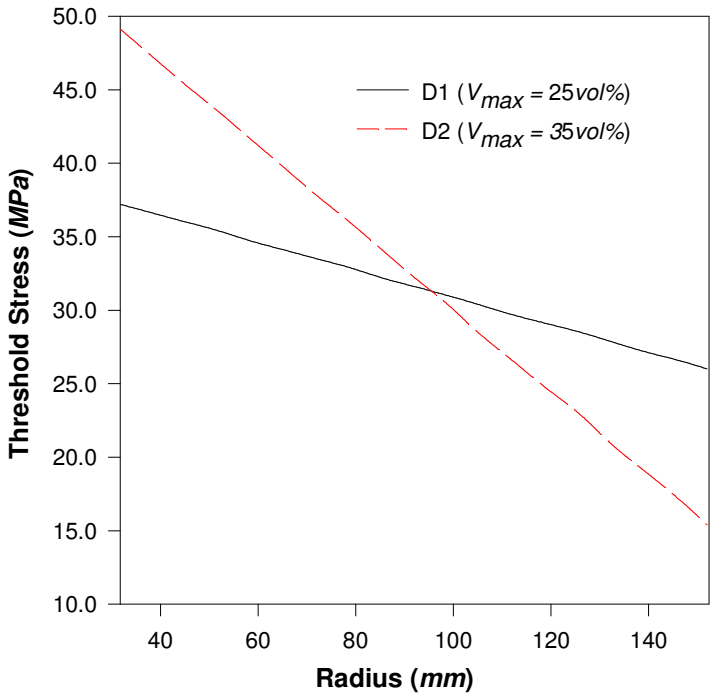

Fig. 3.10: Threshold stress in variable thickness FGM discs

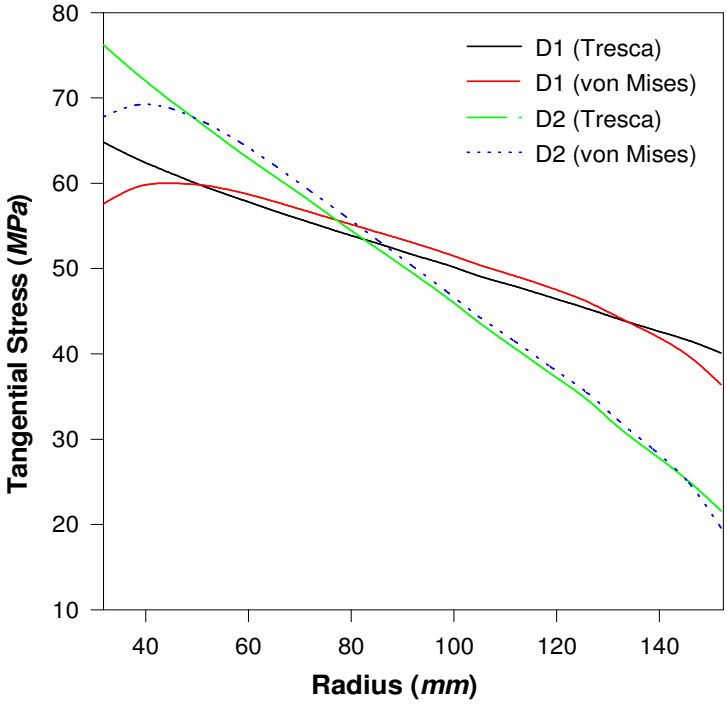

Fig. 3.11: Tangential stress in FGM discs using Tresca and von Mises criteria

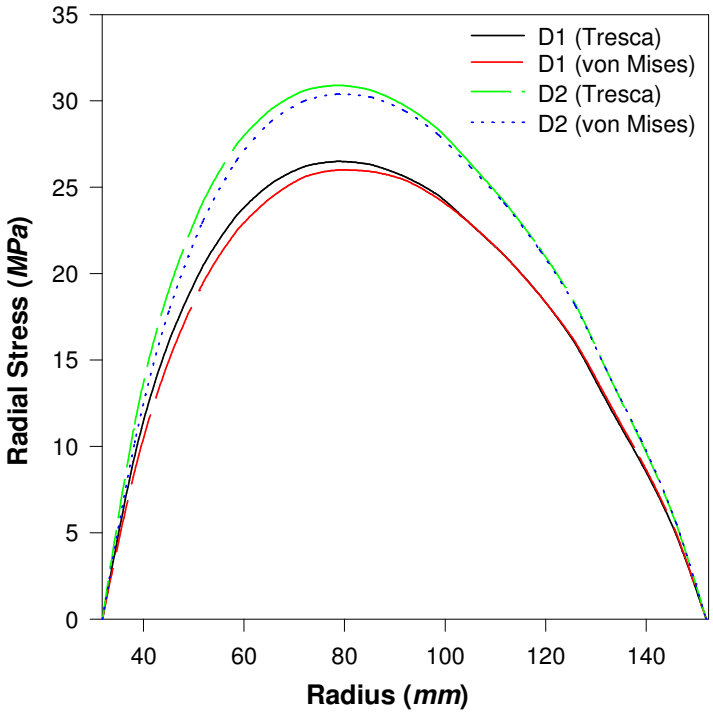

Fig. 3.12: Radial stress in FGM discs using Tresca and von Mises criteria

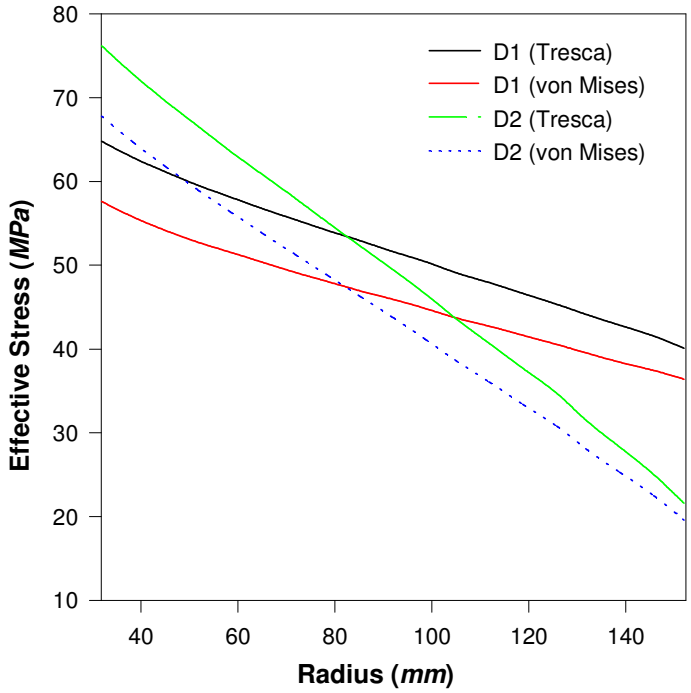

Fig. 3.13: Effective stress in FGM discs using Tresca and von Mises criteria

(iii) Comparison of strain rates in FGM discs

The trends of tangential and radial strain rates (Figs. 3.14-3.15), obtained using different yield criteria, are also similar. Tresca criterion estimates higher strain rates throughout the disc. The difference noticed in tangential strain rate estimated using different yield criteria is observed to decrease with increasing radius. The maximum relative difference noticed in tangential strain rate using both the criteria is 0.78 and 0.84 in FGM discs D1 and D2, respectively, at the inner radius. On the other hand, the difference noticed in radial strain rate (compressive) estimated using Tresca and von Mises criteria is maximum at the inner radius and its magnitude decreases with increasing radius, reaches a minimum in the middle and increases again on moving towards the outer radius. Similar to tangential strain rate, the maximum relative difference noticed in radial strain rate using both the criteria is also 0.78 and 0.84 in FGM discs D1 and D2, respectively, at the inner radius. Similar to stresses, the difference in strain rates estimated using Tresca and von Mises criteria is observed to reduce with the increase in SiC_p gradient in the FGM disc. The higher effective stress and higher strain rates estimated using Tresca criterion, as compared to those obtained using von Mises criterion, reveal that the FGM disc designed using Tresca criterion will also be safe in comparison to FGM disc designed using von Mises criterion. Thus, the results of the present

study also confirm the conservative nature of Tresca criterion, as reported in the standard texts.

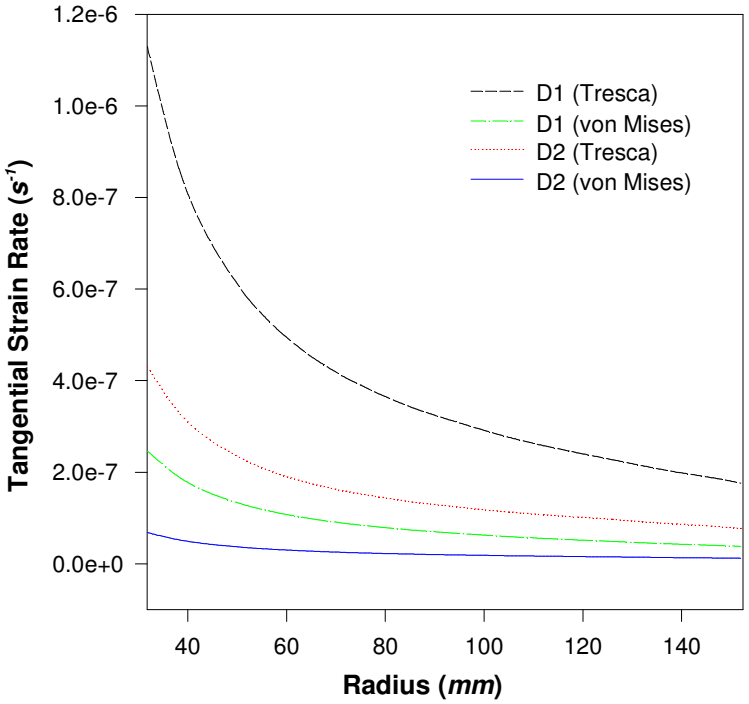

Fig. 3.14: Tangential strain rate in FGM discs using Tresca and von Mises criteria

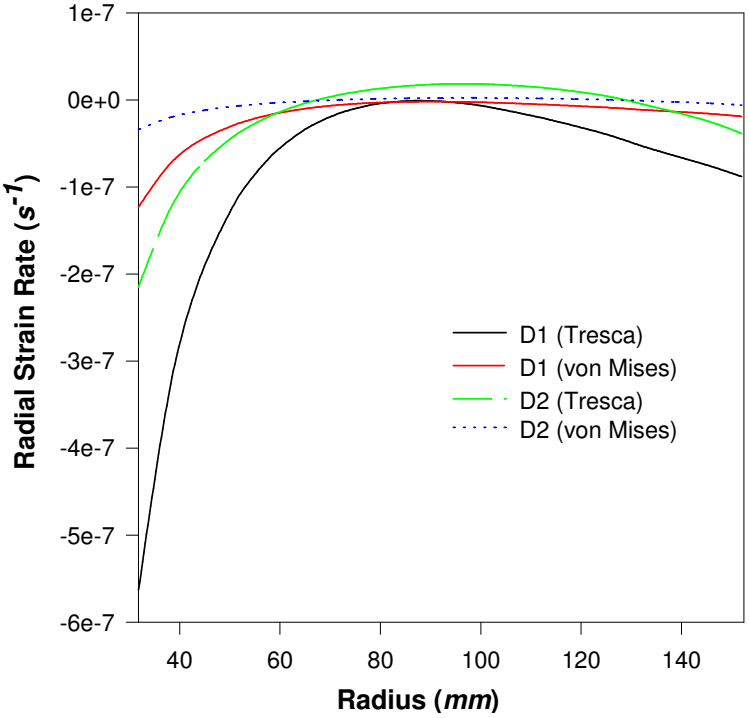

Fig. 3.15: Radial strain rate in FGM discs using Tresca and von Mises criteria

CHAPTER-4

EFFECT OF VARYING DISC PROFILE, REINFORCEMENT GRADIENT AND THERMAL GRADIENT ON CREEP PERFORMANCE OF A ROTATING FGM DISC

4.1 INTRODUCTION

The literature reported in Chapter 2 reveals that several studies have been carried out to investigate the elastic, elastic-plastic and creep stresses and deformations in variable thickness rotating disc. Bayat e*t al.* (2008) obtained exact elastic solutions for rotating FGM disc having constant, parabolic and hyperbolic convergent thickness profiles. They observed that the FGM disc with parabolic or hyperbolic convergent thickness profile has lower stresses and displacements. Bayat *et al.* (2009a) obtained thermo-elastic solutions for rotating FGM disc of variable thickness subjected to steady temperature field. It is observed that the FGM disc with concave thickness profile has smaller stresses and lesser weight than a uniform thickness FGM disc. Bayat *et al.* (2011) analyzed elastic stresses and displacement in metal-ceramic and ceramic-metal FGM discs for varying material grading index and different disc geometry. The results indicate that radial displacement in the disc is reduced when it is made of ceramic-metal FGM and has concave thickness profile. Most of the studies, as outlined above, deal with the analysis of elastic, elastic-plastic and thermo-elastic stresses and deformations in the FGM disc. However, in number of applications such as turbine rotor and disc brake etc., the disc operates under elevated temperature where creep becomes significant. The literature reveals that the studies have been conducted to analyze the steady state creep in a rotating FGM disc but by assuming uniform or constant thickness profile [Singh and Ray (2003a), Gupta *et al.* (2004a, 2005a), Singh (2008)]. In some of the studies [Deepak *et al.* (2010a), Garg *et al.* (2013a, 2013b)], the steady state creep has been analyzed in rotating FGM disc by considering linearly varying thickness profile and linear distribution of reinforcements along the disc radius. It is revealed that the creep stresses and strain rates in a rotating FGM disc having linearly varying thickness are lower than that in a constant thickness FGM disc.

In the light of above observation, it is imperative to investigate the steady state creep response of rotating disc having different kinds of non-linear thickness profiles and non-linear distributions of reinforcement along the disc radius. The present investigation has been carried out by assuming three different non-linear thickness profiles and four different non-linear distributions of reinforcement along the disc radius. The results have also been estimated for constant thickness and uniform composite (non-FGM) discs for the purpose of comparison. An attempt has further been made to investigate the effect of imposing different types of radial thermal gradients (*i.e.* linear, parabolic and exponential) on creep behavior of the FGM disc of variable thickness.

4.2 DISC THICKNESS PROFILE

The study assumes a composite disc rotating at 15000 *rpm* with inner and outer radii as $a(=31.75\ mm)$, $b(=152.4\ mm)$, respectively. The disc thickness, $h(r)$, is assumed to vary non-linearly, with radius (r) according to the following relation (Fig. 4.1),

$$h(r) = h_b \left(\frac{r}{b} \right)^k \tag{4.1}$$

where h_b and k denote disc thickness at the outer radius and disc thickness index, respectively. By varying k, the thickness profile of the disc gets modified, except for $k=0$, which corresponds to constant thickness disc. The disc dimensions, as mentioned above, are similar to those considered and shown in Fig. 3.1.

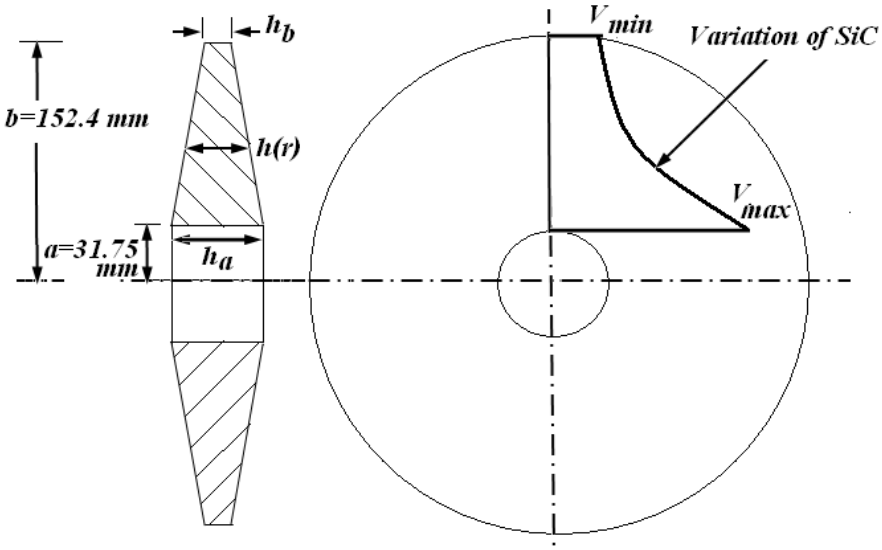

Fig. 4.1: Diagram showing disc dimensions and geometry

For comparison, the volume of variable thickness disc is kept equal to a similar composite disc but of uniform thickness *t (=25.4 mm), i.e.*

$$\int_a^b 2\pi r h(r) dr = \pi(b^2 - a^2)t \,.$$

The above equation can be simplified to yield,

$$h_b = \frac{[(2+k)b^k(b^2 - a^2)t]}{[2(b^{k+2} - a^{k+2})]} \tag{4.2}$$

4.3 DISTRIBUTION OF REINFORCEMENT

It is assumed that the FGM disc is made of Al-SiC_p composite with SiC_p content, $V(r)$, decreasing non-linearly from the inner to outer radius (Fig. 4.1) according to [Hassani *et al.* (2012)],

$$V(r) = V_{\min}\left(\frac{r}{b}\right)^m \tag{4.3}$$

where V_{min} is the SiC_p content at outer radius and m is the reinforcement gradation index. On varying m, the radial distribution of SiC_p in the FGM disc changes, except for $m = 0$, which corresponds to disc having uniform SiC_p content (non-FGM disc). If the total SiC_p content in variable thickness FGM disc and constant thickness uniform composite disc is considered equal, then,

$$\int_a^b 2\pi r V(r) h(r) dr = \pi(b^2 - a^2) t V_{avg} \tag{4.4}$$

where V_{avg} is the average SiC_p content in the FGM disc.

Substituting $h(r)$ and $V(r)$ from Eqs. (4.1) and (4.3), respectively, in to the above equation, one gets,

$$V_{\min} = \frac{[(2+m+k)b^m(b^{k+2} - a^{k+2})V_{avg}]}{[(2+k)(b^{2+m+k} - a^{2+m+k})]} \tag{4.5}$$

where V_{min} is the content of SiC_p at the outer disc radius.

Following the rule of mixture, the density of FGM disc at any radius (r) is given by [Gupta *et al.* (2005)],

$$\rho(r) = \rho_m + 0.01(\rho_d - \rho_m)V_{\min}\left(\frac{r}{b}\right)^m = A_\rho + B_\rho r^m \tag{4.6}$$

where,

$A_\rho = \rho_{m,}\, B_\rho = \dfrac{(\rho_d - \rho_m)V_{\min}}{(100b^m)}$, $\rho_m (= 2698.9\, kg/m^3)$ is the density of Al and $\rho_d\,(= 3210\, kg/m^3)$ is the density of SiC_p [Gupta *et al.* (2005a)].

4.4 ANALYSIS OF CREEP IN FGM DISC

Similar to analysis given in the previous chapter, the present analysis also assumes that the disc material is incompressible, subjected to plane stress condition and has negligible elastic deformations. The material of the disc is assumed to undergo steady state creep condition described by Eq. (3.4). Following the analysis scheme described in Section-3.5, but using Eq. (4.1) for disc thickness $h(r)$, and Eq. (4.3) for radial distribution of SiC_p, $V(r)$, in the FGM disc, one may obtain the average tangential stress, $\sigma_\theta(avg)$, in the FGM disc as,

$$\sigma_\theta(avg) = \frac{\omega^2 h_b}{A_0 b^k}\left[\frac{\{A_\rho(b^{3+k} - a^{3+k})}{(3+k)} + \frac{B_\rho(b^{3+k+m} - a^{3+k+m})}{(3+k+m)}\right] \tag{4.7}$$

where,

$$A_0 = \int_a^b h(r)dr$$

Similarly, one may obtain the tangential stress in the disc as,

$$\sigma_\theta(r) = \frac{\Psi_1(r)\left[A_0\sigma_\theta(avg) - \int_a^b h(r)\sigma_0(r)\,dr\right]}{M(r)\int_a^b \dfrac{h(r)\Psi_1(r)}{M(r)}dr} + \sigma_0(r) \tag{4.8}$$

where the symbols used are the same as described earlier in Chapter-3, but are reproduced below for ease of understanding,

$$\Psi_1(r) = \Psi(r)^{1/n};$$

$$\Psi(r) = 2/[r\{2 - x(r)\}]\exp\int_a^r \Phi(r)/r\,dr;$$

and,

$$\Phi(r) = \left[\frac{2\sigma(r)}{\sigma(\theta)} - 1\right] \Big/ \left[2 - \frac{\sigma(r)}{\sigma(\theta)}\right]$$

Integrating the force equilibrium equation of the FGM disc, Eq. (3.13), between limits a to r, under the imposed free-free boundary conditions (Eq. 3.14), the distribution of radial stress in the FGM disc may be obtained as,

$$\sigma_r(r) = \frac{1}{rh(r)}\left[\int_a^r h(r)\sigma_\theta dr - \frac{\omega^2 h_b}{b^k}\left\{\frac{A_\rho(r^{3+k} - a^{3+k})}{(3+k)} + \frac{B_\rho(r^{3+k+m} - a^{3+k+m})}{(3+k+m)}\right\}\right] \quad (4.9)$$

Knowing the distributions of $\sigma_\theta(r)$ and $\sigma_r(r)$ from Eqs. (4.8) and (4.9), respectively, the strain rates $\dot{\varepsilon}_\theta$ and $\dot{\varepsilon}_r$ in the FGM disc are estimated, respectively, from Eqs. (3.9) and (3.10).

4.5 RESULTS AND DISCUSSION

The stresses and strain rates in different types of discs are estimated from the analysis given in Section-4.4 by following an iterative numerical scheme described in Fig. 3.3. The analysis carried out has been firstly used to demonstrate the effect of varying disc thickness profile of a uniform composite disc (non-FGM), obtained by varying the value of disc thickness index (k). The literature reveals that the stresses and strain rates in rotating disc could be significantly reduced by radially varying the disc thickness, with higher thickness near the inner radius [Deepak *et al.* (2010a)]. In order to achieve this kind of disc thickness profile, the index 'k' is kept negative and its value is arbitrarily varied from 0 to -0.6.

After investigating the effect of varying disc thickness profile in uniform composite disc, the analysis has been used to investigate the effect of varying SiC_p gradient in variable thickness disc. To accomplish this task, the value of SiC_p gradation index 'm' is varied from 0 to -1.8295, since for 'm' = -1.8295, the content of SiC_p at the inner radius (V_{max}) becomes 100% (pure ceramic). The purpose of choosing negative values of 'm' is to achieve radially decreasing SiC_p distribution in the FGM disc, which helps in reducing creep deformations in the FGM disc as compared to uniform composite disc [Singh and Ray (2003a)].

A segment of the study also investigates the effect of imposing different types of radial thermal gradients, viz. linear, parabolic and exponential, on the creep performance of variable thickness rotating FGM disc.

4.5.1 Effect of Varying Disc Thickness Profile

The effect of varying disc thickness index (k) on the steady state creep behavior of uniform composite disc [$V(r)$ = 20%] with four different thickness profiles (Table 4.1) and shown in Fig. 4.2, is presented and discussed in this section. The average thickness (h_{avg} = 25.4 *mm*) is kept equal for all the composite discs. It is noticed that with the decrease in index 'k' from 0 to -0.6, the disc thickness gradient, *i.e.* the difference of maximum and minimum disc thickness, increases from 0 to 29.9 (Table 4.1).

Table 4.1: Uniform composite discs of variable thickness [$V(r)$ = 20%, h_{avg} = 25.4 mm]

Disc Notation	Thickness Index (k)	Disc Thickness (mm)		Thickness Gradient (mm) = (h_a-h_b)
		h_a	h_b	
D1	0	25.4	25.4	0.0
D2	-0.2	31.8	23.2	8.6
D3	-0.4	39.6	21.2	18.4
D4	-0.6	49.0	19.1	29.9

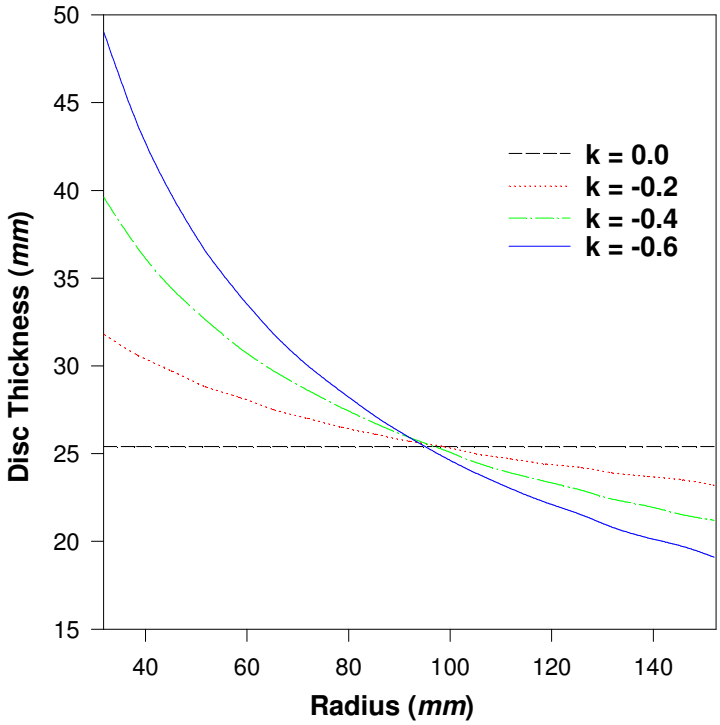

Fig. 4.2: Variation of disc thickness profile with varying thickness index

(i) Effect on stresses

As compared to uniform thickness disc D1, the radial stress in variable thickness discs (D2-D4) decreases towards the inner radius but increases towards the outer radius (Fig. 4.3). The amount of decrease and increase noticed in radial stress increases with the decrease in '*k*'. The decrease observed in radial stress towards the inner radius is relatively higher than the increase observed in radial stress towards the outer radius. It is important to mention that the maximum radial stress decreases slightly with the decrease in '*k*' and also the location of

maximum radial stress is marginally shifted towards the outer radius. For example, the maximum radial stress in disc D4 (k = -0.6) decreases by about 2% when compared to uniform thickness disc D1.Unlike radial stress, the tangential stress (Fig. 4.4) decreases over the entire radius with the decrease in thickness index 'k'. The decrease observed in tangential stress decreases slightly with the increasing radius. On increasing the thickness gradient, the disc thickness increases near the inner radius (Fig. 4.2), because of this the centrifugal force, caused by disc rotation, also increases due to increase in disc mass near the inner radius. As a result of increase in disc thickness near the inner radius, the cross-section area of the disc also increases, which is responsible for reducing the tangential stress near the inner radius. However, towards the outer radius, the reduced mass of the disc, caused by reduced disc thickness with decreasing 'k', tends to reduce the tangential stress, in spite of reduced cross-sectional area. The tangential stress in variable thickness disc D4 is lower by 19.44% and 13.93% at the inner and outer radii, respectively, as compared to those observed in uniform thickness disc D1.

(*ii*) *Effect on strain rates*

The radial strain rate (compressive) decreases with the decrease in index 'k', over the entire disc radius (Fig. 4.5). The decrease observed is significantly higher near the inner radius as compared to those noticed towards the outer radius. The radial strain rate in disc D4 is lower by 9.81×10^{-6} and 1.39×10^{-6} at the inner and outer radii, respectively, when compared to disc D1. The effect of varying the index 'k' on tangential strain rate (Fig. 4.6) is similar to that observed for radial strain rate in Fig. 4.5. However, the decrease noticed in tangential strain rate is much higher than that observed for radial strain rate (Fig. 4.5) in the corresponding disc. The tangential strain rate in disc D4 is lower by 19.62×10^{-6} and 2.78×10^{-6} at the inner and outer radii, respectively, as compared to disc D1. It is evident from Eqs. (3.9) and (3.10) that the reduction in strain rates with increasing disc thickness gradient (k) is attributed to reduction in effective stress ($\bar{\sigma} = \sigma_\theta$) with increasing disc thickness gradient (Fig. 4.4). Further, with the increase in disc thickness gradient (or decrease in thickness index k), the distribution of radial and tangential strain rates become relatively more uniform, and thereby reduces the chances of distortion in the disc.

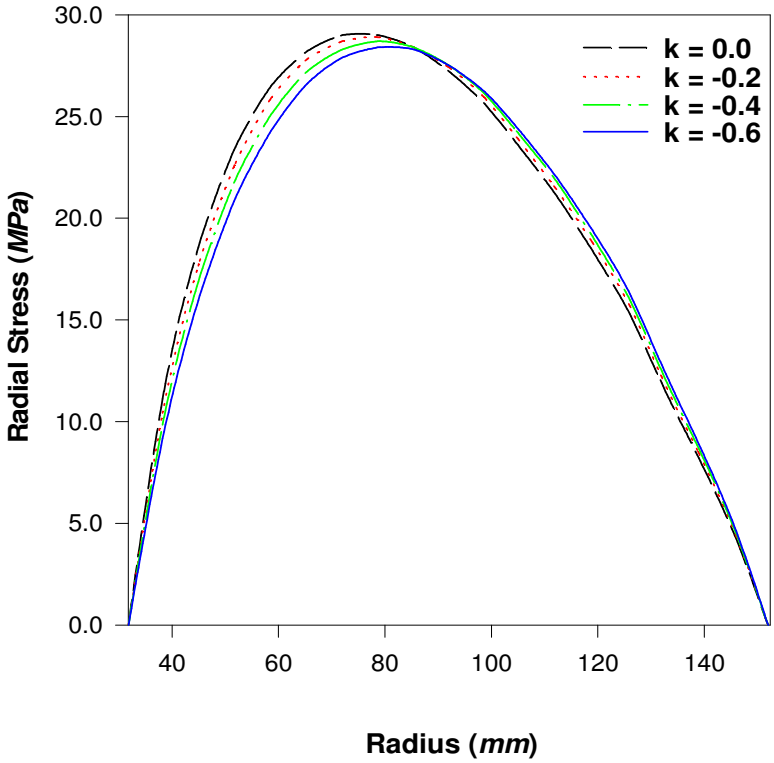

Fig. 4.3: Effect of thickness index on radial stress

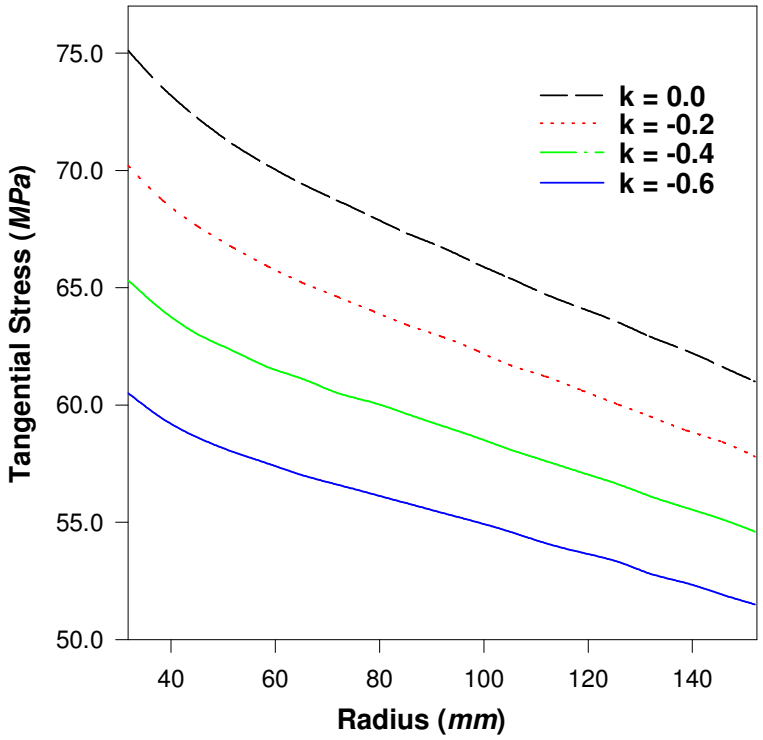

Fig. 4.4: Effect of thickness index on tangential stress

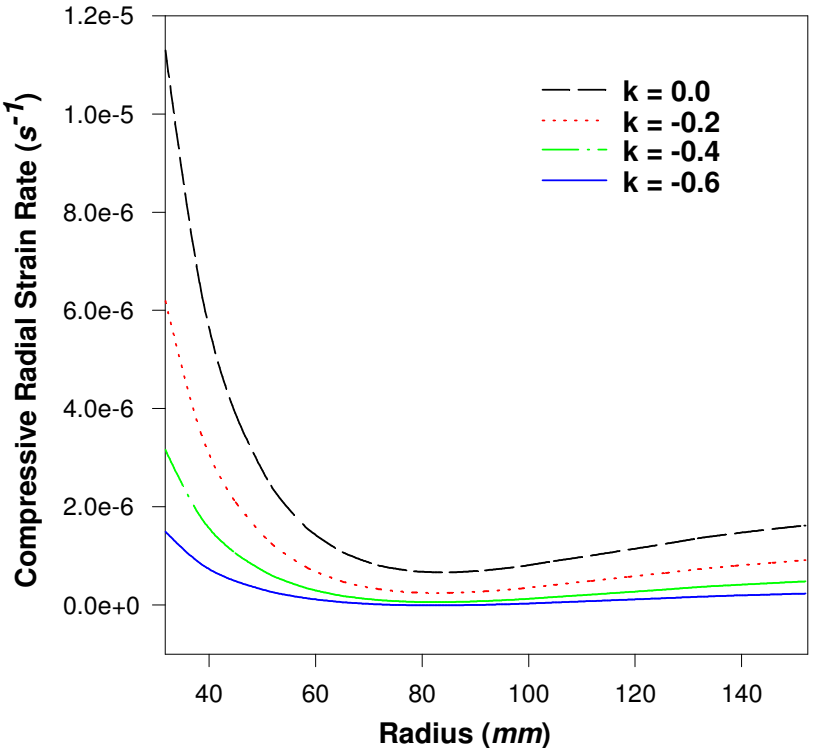

Fig.4.5: Influence of thickness index on radial strain rate

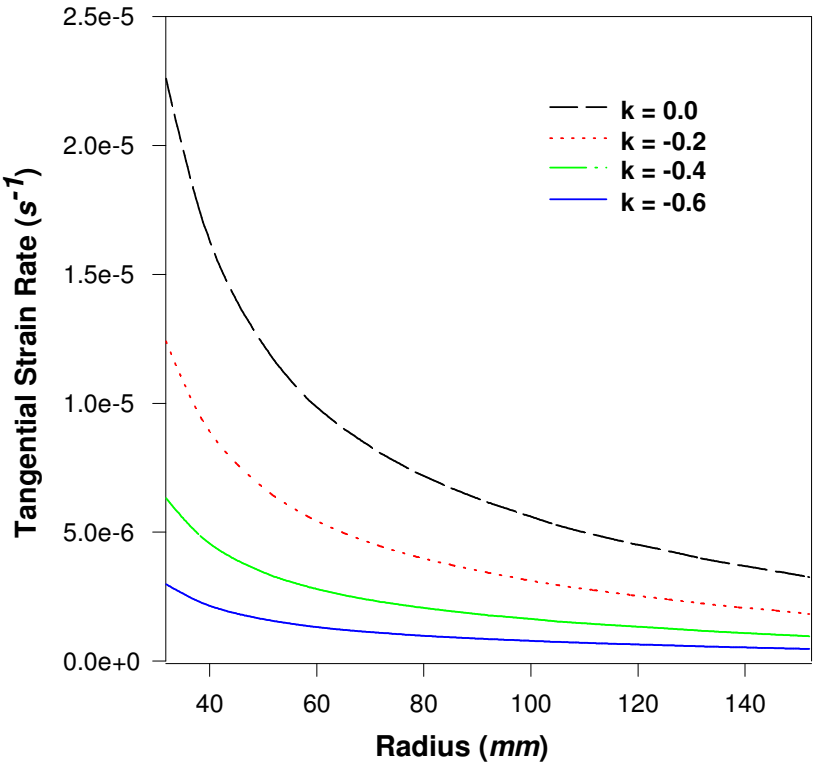

Fig.4.6: Influence of thickness index on tangential strain rate

4.5.2 Effect of Varying Reinforcement Gradient

To investigate the effect of varying particle gradation index (*m*) on the creep response of variable thickness disc with '*k*'= -0.6, the creep results are estimated for four different FGM discs DS2-DS5 (Table 4.2) and compared with a uniform composite disc DS1 (*m*=0.0000). On decreasing '*m*' from 0.0000 to -1.8295, the SiC_p content in the FGM discs (DS2-DS5) increases near the inner radius but decreases towards the outer radius, and as a result the particle gradient (referred as PG hereafter) increases, when compared to uniform composite disc DS1 (Table-4.2).

Table 4.2: Uniform composite and FGM discs of variable thickness (V_{avg} = 20%, k = -0.6)

Disc Notation	Gradation Index (*m*)	Particle Content (*vol%*)		Particle Gradient (PG) = (V_{max} - V_{min}) in *vol%*
		V_{max} (%)	V_{min} (%)	
DS1	0.000	20	20	0
DS2	-0.5000	33.1	15.1	18
DS3	-1.0000	52.3	10.9	41.4
DS4	-1.5000	78.6	7.48	71.12
DS5	-1.8295	100	5.67	94.33

(*i*) *Effect on stresses*

As compared to uniform composite disc DS1, the radial stress (Fig. 4.7) increases significantly throughout with the increase in PG in the FGM discs (DS2-DS5). The increase is more in the middle than that observed towards the inner and outer radii. Apart from increase in the magnitude of maximum radial stress, its location also shifts towards the inner radius as PG in the disc increases from 0 to 94.33 (Table 4.2).The maximum radial stress in the FGM disc DS5 is 18.6 *MPa* (65.5%) higher as compared to those observed in uniform composite disc DS1. The tangential stress (Fig. 4.8) increases towards the inner radius but decreases towards the outer radius when PG in the disc increases from 0 to 94.33, with a crossover noticed in tangential stress at a radius of around 65 *mm*. The increase observed in tangential stress towards the inner radius is significantly higher than the decrease noticed towards the outer radius. The increase observed in tangential stress near the inner radius, with increasing PG, is attributed to increase in disc density near the inner radius, owing to higher amount of SiC_p reinforcement, which leads to an increase in the centrifugal load near the inner disc radius. However, towards the outer radius, the tangential stress decreases due to reduction in

SiC_p content, which results in lesser centrifugal load. The increase and decrease observed in tangential stress in the FGM disc DS5, respectively, at the inner and outer radii, are 91.5 *MPa* (151.24%) and 32.5 *MPa* (63.11%) respectively, when compared to uniform composite disc.

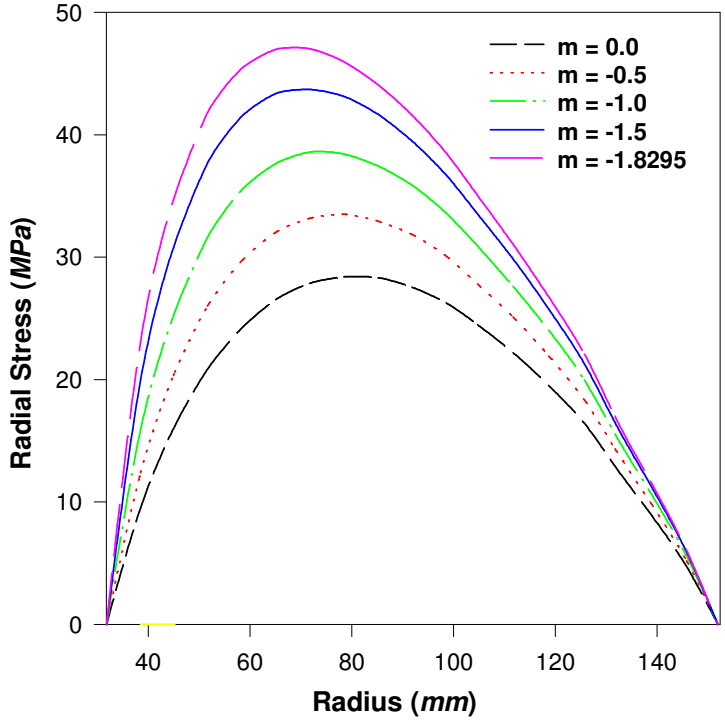

Fig.4.7: Effect of gradation index on radial stress in composite disc (k=-0.6)

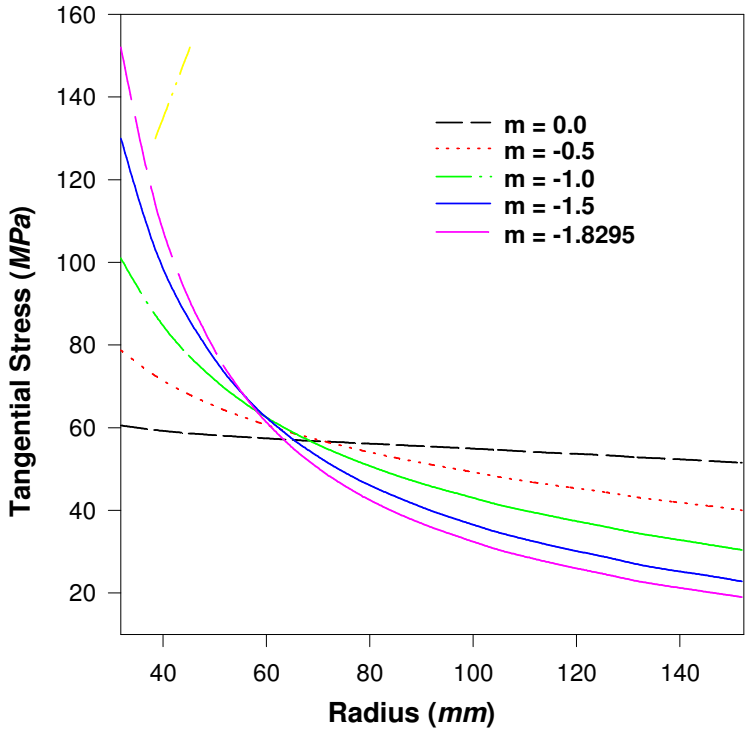

Fig.4.8: Effect of gradation index on tangential stress in composite disc (k=-0.6)

(*ii*) *Effect on strain rates*

The radial strain rate in the disc (Fig. 4.9) reduces over the entire disc with the increase in PG in the disc from 0 to 94.33. The decrease in radial strain rate reduces with the increasing radius, until one reaches near the middle of the disc, and thereafter the radial strain rate exhibits slight increase with further increase in radius. When PG in the disc increases beyond 18 (*vol%*), the radial strain rate changes its nature from compressive to small tensile for some region in the middle of the disc. The reduction observed in radial strain rate in the FGM disc DS5, as compared to uniform composite disc DS1, is 1.45×10^{-6} (97.7%) and 2.18×10^{-7} (93.4%) at the inner and the outer radii, respectively. The tangential strain rate, (Fig. 4.10), also decreases with the increase in PG in the disc. As compared to uniform composite disc DS1, the tangential strain rate in FGM disc DS5 reduces by 2.91×10^{-6} (97.7%) and 0.435×10^{-6} (93.4%), respectively at the inner and outer radii. The FGM disc having higher PG, in spite of higher tangential stress, exhibits lower strain rates near the inner radius. It may be attributed to higher value of threshold stress and lower value of creep parameter *M* (Figs. 4.11-4.12) near the inner radius of the FGM disc, due to higher SiC_p content, which dominates over higher value of effective stress $(\bar{\sigma} = \sigma_\theta)$ and causes reduction in strain rates near the inner disc radius. Towards the outer radius of the FGM disc, in spite of lower value of threshold stress and higher value of creep parameter *M* (Figs. 4.11-4.12), owing to lower SiC_p content, the strain rates are again observed to be lower in FGM disc with higher PG due to lower value of effective stress. The lower value of effective stress noticed towards the outer radius of the FGM disc having higher PG may be attributed to reduction in centrifugal load due to lower density of the disc, as a result of lesser SiC_p content.

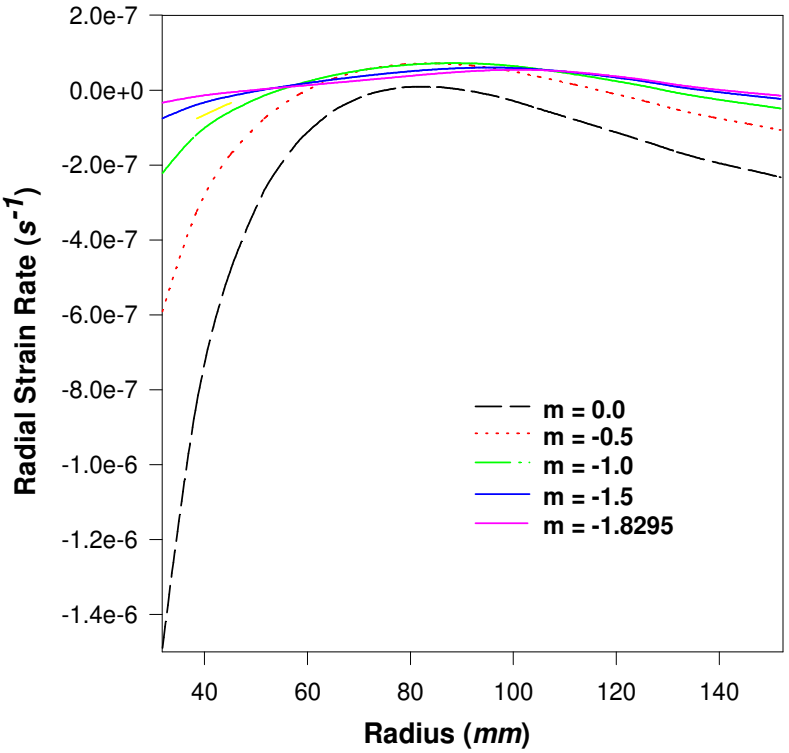

Fig.4.9: Influence of gradation index on radial strain rate in composite disc (k=-0.6)

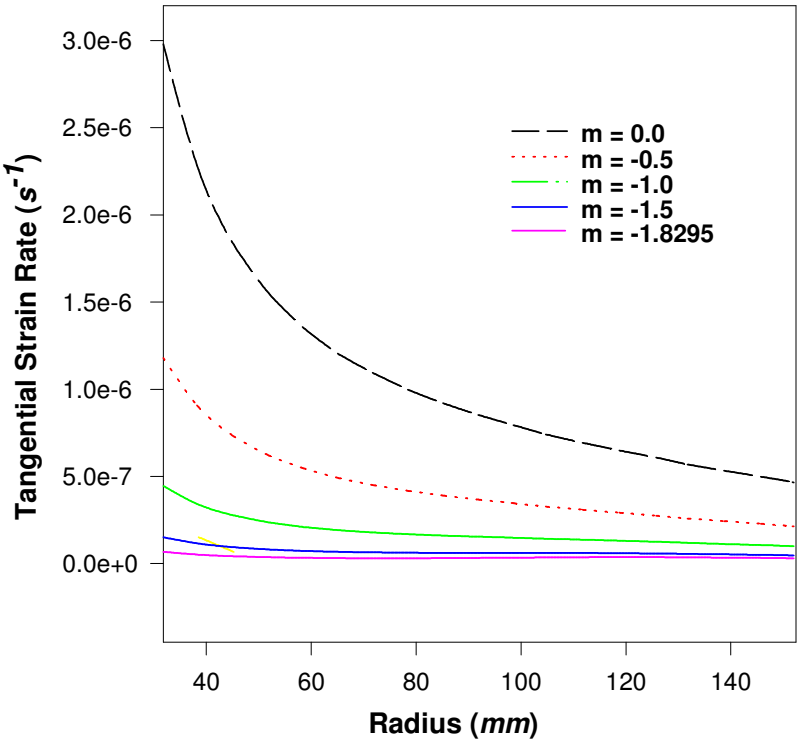

Fig. 4.10: Influence of gradation index on tangential strain rate in composite disc (k=-0.6)

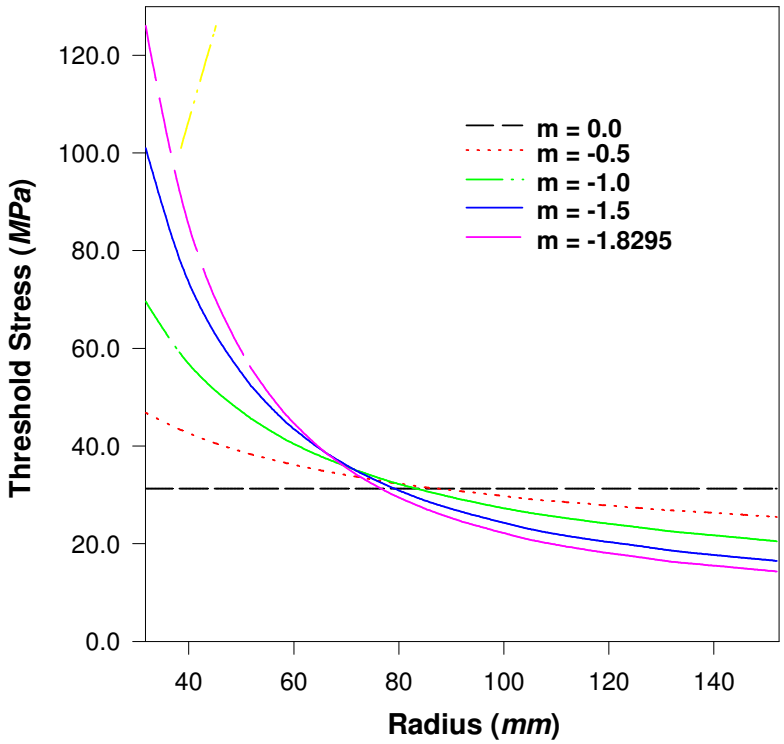

Fig. 4.11: Effect of gradation index on threshold stress in composite disc (k=-0.6)

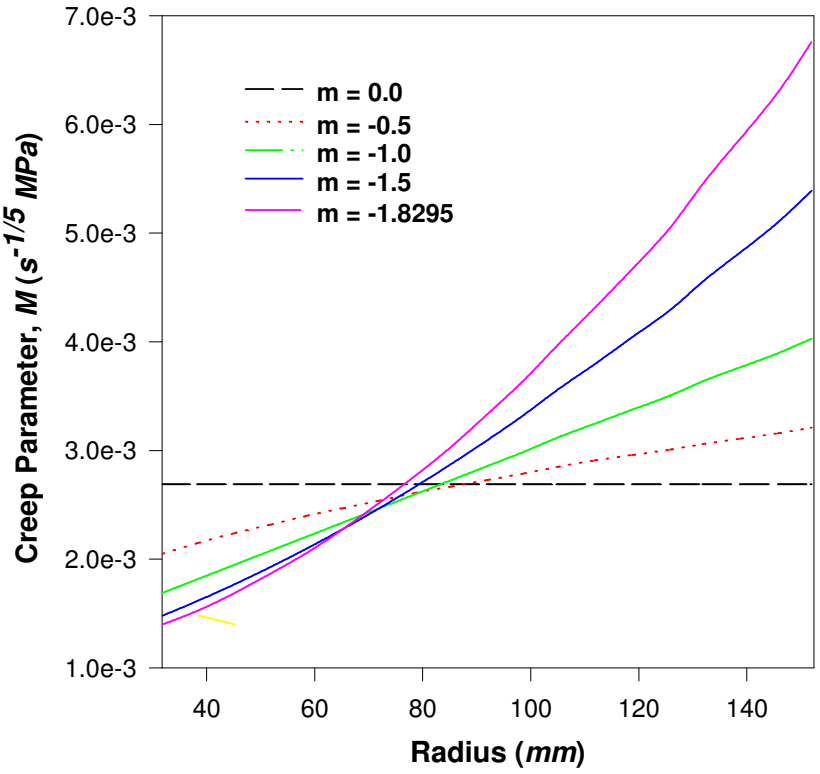

Fig. 4.12: Effect of gradation index on creep parameter 'M' in composite disc (k=-0.6)

4.6 EFFECT OF IMPOSING RADIAL THERMAL GRADIENTS

The investigation carried out in the previous section, assumes the disc to operate at constant temperature. However, in real life applications, such as turbine rotor and disc brake, the disc operates under a radial thermal gradient [Ali and Mostefa (2013)]. Gupta *et al.* (2005a) in their studies simulated the effect of imposing radial thermal gradient on the creep behavior of rotating FGM disc of constant thickness. Garg *et al.* (2013c) analyzed the effect of imposing radially varying linear thermal gradient on the creep performance of FGM disc with linearly varying thickness profile. The studies reveal that the creep response of FGM disc, either having uniform thickness [Gupta *et al.* (2005a) and Kordkheili and Livani (2013)] or having linearly varying thickness [Garg *et al.* (2013c)], is significantly affected by varying the radial thermal gradient. The study carried out in the previous sub section 4.5.1 and 4.5.2, pertaining to the effects of varying disc thickness profile and reinforcement gradient, it is revealed that the FGM disc having higher thickness (inner radius) and higher reinforcement gradients exhibits lower strain rates. In these studies the disc was assumed to operate at uniform temperature. This section investigates the effect of imposing different kinds of radial thermal gradients, viz. linear, parabolic and exponential, on the creep performance of rotating FGM disc of variable thickness.

The results are estimated for a variable thickness FGM disc DS5 (Table 4.2), which exhibits superior creep performance in terms of creep rates amongst all the discs DS1-DS5. The thickness at the inner and outer radii as h_a (=49.00 *mm*) and h_b (=19.1 *mm*), respectively, and its thickness, $h(r)$, at any radius r, varies according to Eq.(4.1). The content of SiC_p reinforcement in this disc at the inner and outer radii are V_{max} (=100%) and V_{min} (=5.67%), respectively, with content of SiC_p at any radius r, $V(r)$, is assumed to decrease radially from the inner to outer radius according to Eq. (4.3). The value of creep parameter $M(r)$ and $\sigma_0(r)$ required during the course of computation process are estimated from regression Eqs. (3.5) and (3.6), respectively, by assuming the size of SiC_p (P) = 1.7 μm. These equations are rewritten below by taking into account the radial variation of temperature, denoted by $T(r)$, in the FGM disc as,

$$M(r) = 0.0288 - \frac{0.0088}{P} - \frac{14.0267}{T(r)} + \frac{0.0322}{V(r)} \tag{4.10}$$

$$\sigma_0(r) = 22.207 - 0.084P - 0.023T(r) + 1.185V(r) \tag{4.11}$$

4.6.1. Distribution of Radial Temperature Profiles

As outlined earlier, in applications of rotating disc such as turbine rotor and disc brake, the disc is subjected to radial temperature gradient, with the temperature at the outer radius being higher than that at the inner radius. In case of disc brake, frictional heat generated due to braking action causes higher temperature at the contact area between the brake pad and the disc outer surface, and the temperature decreases radially on moving towards the inner disc radius. Similarly, in turbine rotor, due to the entrance of steam / gas at the outer radius, a radially decreasing temperature distribution is developed.

To impose such a radial temperature gradient in the disc, the following equation, as proposed by Hassani *et al.* (2011) in their study on elastic behavior of rotating FGM disc, has been used to estimate temperature, $T(r)$, at any radius r of the disc,

$$T(r) = (T_o - T_i)\left(\frac{r-a}{b-a}\right)^{n_T} + T_i \qquad (4.12)$$

where T_i (=623 K) and T_o (=723 K) are the temperatures at the inner and outer disc radii, respectively and n_T is the temperature exponent. To obtain different kinds of radial temperature profiles in the disc (Fig. 4.13), the value of exponent n_T is taken as 1, 2 and 10, which refer to linear, parabolic and exponential temperature profiles, respectively, in this study. For comparison, the study also considers an FGM disc operating at uniform temperature of 673 K, which is the mean of temperature at the inner and outer disc radii.

4.6.2 Effect of Varying Temperature Exponent on Creep Parameters

The stresses and strain rates in the FGM disc are estimated by assuming the disc to operate under four different kinds of radial temperature profiles (Fig. 4.13). It is evident from Eqs. (4.10) and (4.11) that the creep parameters $M(r)$ and $\sigma_0(r)$ also depend on the operating temperature, therefore, in the different discs considered in this segment of the study the value of these parameters will vary due to different kinds of radial temperature distributions (Fig. 4.13). The value of parameter M increases on moving from the inner to outer disc radius (Fig. 4.14). The FGM disc with exponential temperature profile shows the lowest value of M throughout, when compared to FGM discs with linear and parabolic temperature distributions. The variation observed in value of M is higher in the middle of the disc, although at the inner and outer radii the values of parameter M are the same in all the discs, operating under different kinds of radial temperature profiles. The uniform temperature disc exhibits higher M value towards the inner radius but lower M value towards the outer radius, when compared to FGM discs with radially varying temperature profiles. The effect of varying temperature

profile in the disc is not significant on the threshold stress (σ_0), Fig. 4.15, which may be attributed to low value (= 0.023) of the coefficient of $T(r)$ in Eq. (4.11).

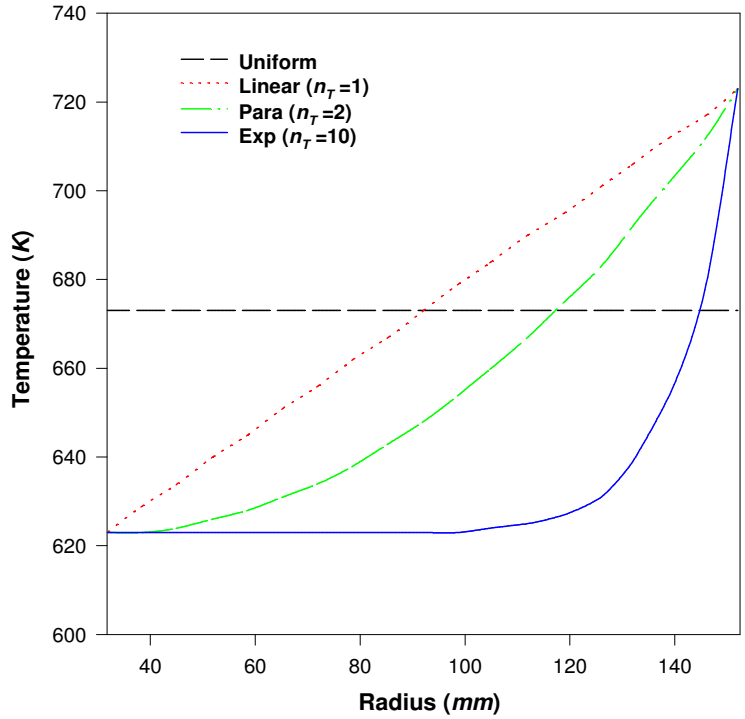

Fig. 4.13: Temperature profiles in FGM disc for varying temperature exponent

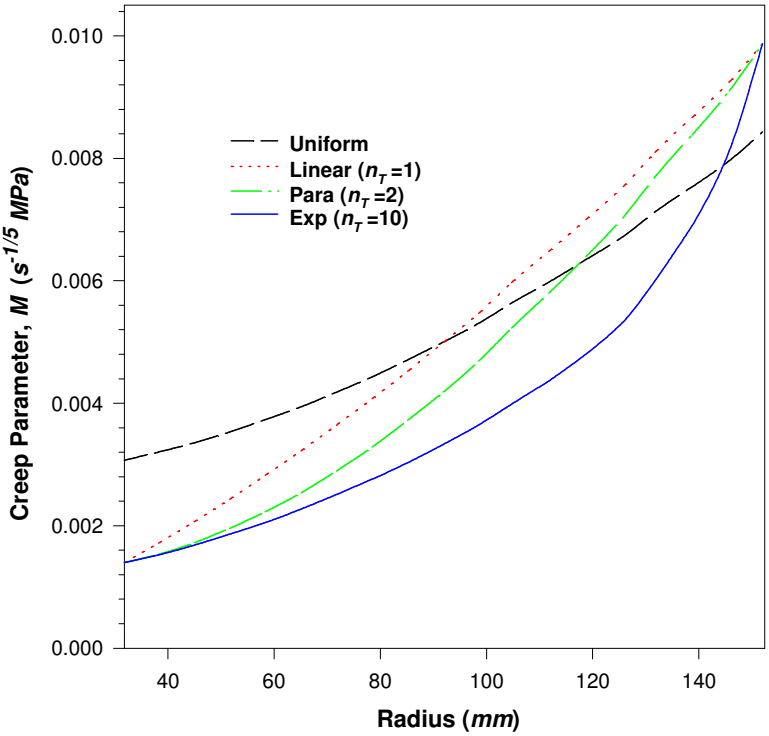

Fig. 4.14: Effect of temperature exponent on parameter M in FGM disc (m=-1.8295, k=-0.6)

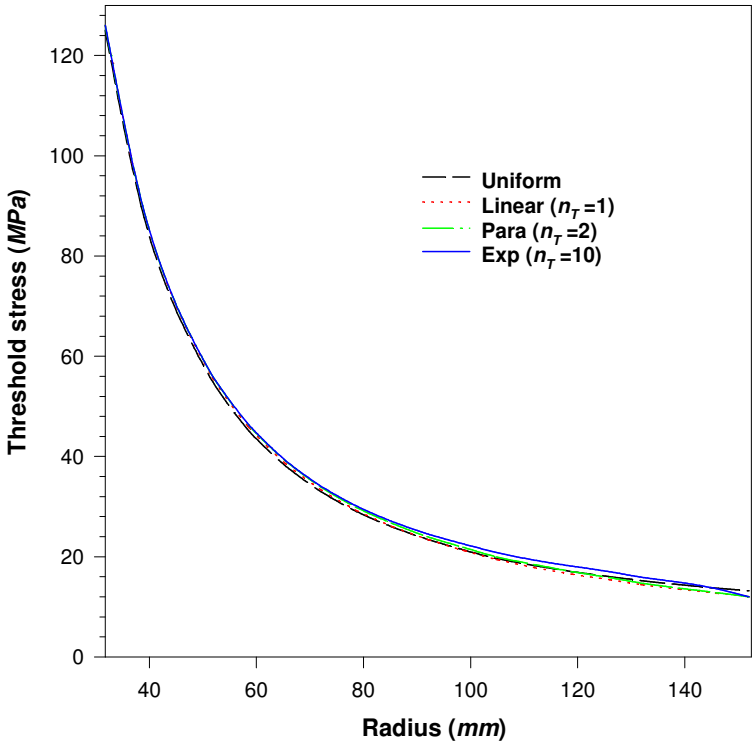

Fig. 4.15: Effect of temperature exponent on threshold stress in FGM disc (m=-1.8295, k=-0.6)

4.6.3 Effect of Varying Temperature Exponent on Stresses and Strain Rates

As compared to uniform temperature disc, the radial stress in FGM discs with radial temperature distributions is slightly higher throughout (Fig. 4.16). The maximum variation of 3 *MPa* is observed at a radius of 65.3 *mm* between the FGM discs subjected to linear temperature profile and uniform temperature. On imposing radial thermal gradient in the FGM disc, the tangential or effective stress ($\bar{\sigma} = \sigma_\theta$) increases towards the inner radius but decreases towards the outer radius (Fig. 4.17), when compared to uniform temperature FGM disc. The maximum variation of 15 *MPa* is noticed at the inner radius between the FGM discs with linear and uniform temperature profiles.

The radial strain rate in all the FGM discs is tensile near the ends but has compressive nature in the middle (Fig. 4.18). The magnitude of radial strain rate (tensile as well as compressive) is observed to decrease with the increase in temperature exponent (n_T) when compared to those observed in uniform temperature FGM disc. The decrease observed is maximum in the middle of the disc. Besides reduction in magnitude, the strain rate tends to become relatively uniform with the increase in exponent n_T. Similarly, the tangential strain rate in the FGM discs also decreases significantly with the increase in exponent n_T (Fig. 4.19). The decrease observed is more near the inner radius of the FGM disc. The reduction observed

in strain rates near the inner radius of the FGM disc having radially varying temperature, is attributed to significant reduction in creep parameter M in these discs (Fig. 4.14), which dominates over the effect caused by the slightly higher effective stress observed near the inner radius of these discs, as compared to those observed in uniform temperature FGM disc (Fig. 4.17). However, towards the outer radius, inspite of high M value observed in FGM discs having radially varying temperature (Fig. 4.14), the lower effective stress (Fig. 4.17) tends to reduce strain rates in these discs, as compared to uniform temperature FGM disc. Thus, for given values of temperatures at the inner (= 623 K) and outer (= 723 K) surface of the FGM disc, the FGM disc operating under exponentially varying temperature profile develops lower and relatively uniform distribution of strain rates and therefore have lesser tendency to distort.

4.6.4 Effect of Varying Temperature Exponent on Rupture Time

In this section, the effect of varying the value of temperature exponent (n_T) has been investigated on the creep rupture time of the FGM discs, when all the FGM discs operate under the same average temperature (T_{avg}) and at a fixed value of outer surface temperature (T_o = 723 K). As the FGM disc subjected to exponential thermal gradient (n_T =10) exhibits superior creep response. Therefore, the average temperature (T_{avg} = 632.09 K) has been calculated for this disc from the following equation, obtained by integrating Eq. (4.12) between limits a to b.

$$T_{avg} = \frac{(T_o - T_i)}{(n_T + 1)} + T_i \tag{4.13}$$

For given values of temperature T_o and T_{avg}, the temperature at the inner surface of the FGM disc (T_i) may be estimated from Eq. (4.13) for different values of n_T, that is varied in the range 2 to 15. The values of T_i, thus obtained, are substituted in Eq. (4.12) to obtain the radial variation of temperature in the FGM disc for different values of n_T (Fig. 4.20). It is important to mention that the value of temperature exponent (n_T) has not been reduced below 2, as it yields negative value of creep parameter M, which is practically impossible. It is observed that for given value of average temperature (T_{avg}) in the disc, the temperature decreases near the inner disc radius but increases towards the outer disc radius (Fig. 4.20). It is necessary to mention that the different temperature profiles shown in Fig. 4.20 have the fixed values of T_o (=723 K) and T_{avg} (=632.09 K). However, the temperature profiles, corresponding to different values of n_T, in Fig. 4.13 have been plotted by fixing the values of temperature at the inner (T_i) and outer (T_o) surface of the disc as 623 K and 723 K, respectively, without maintaining the same average value of temperature. Corresponding to different kinds of temperature profiles

shown in Fig. 4.20 for the FGM disc, the radial and tangential strain rates are estimated at the inner and outer disc radii. With the decrease in temperature exponent (n_T) from 15 to 2, both the strain rates are observed to reduce drastically by about 8 orders of magnitude (Fig. 4.21).

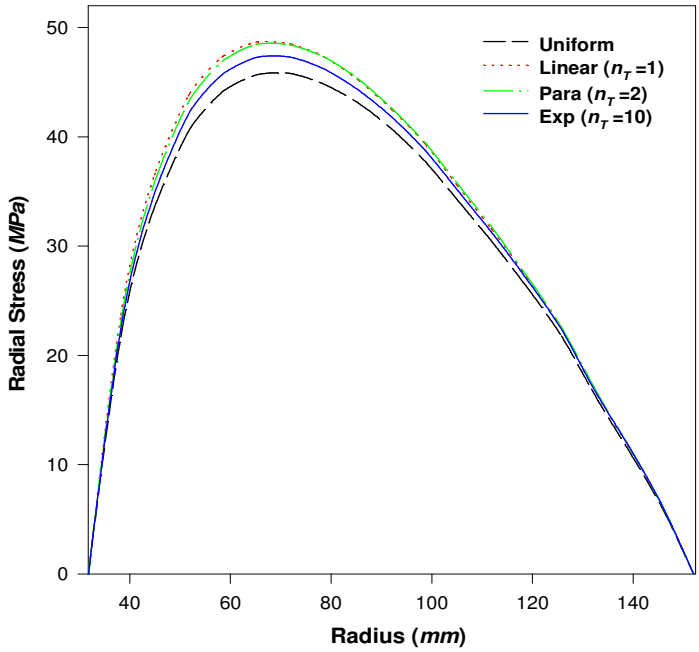

Fig. 4.16: Influence of temperature exponent on radial stress in FGM disc (m=-1.8295, k=-0.6)

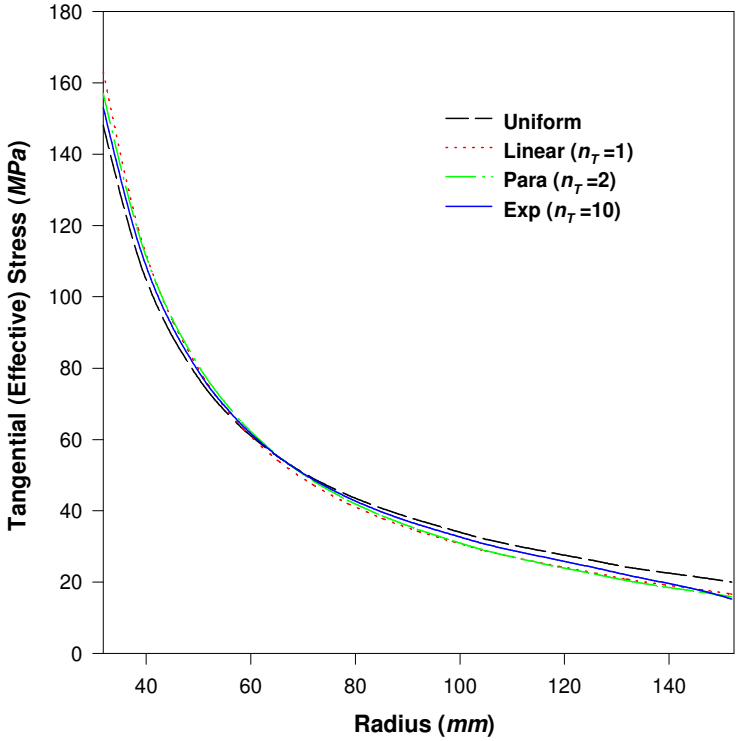

Fig. 4.17: Influence of temperature exponent on tangential (effective) stress in FGM disc (m=-1.8295, k=-0.6)

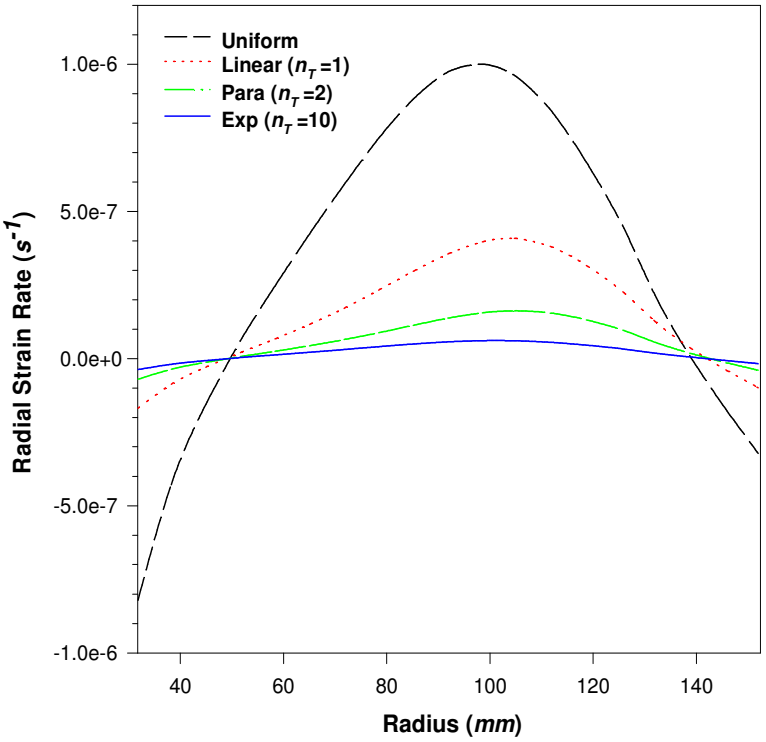

Fig. 4.18: Effect of temperature exponent on radial strain rate in FGM disc (*m*=-1.8295, *k*=-0.6)

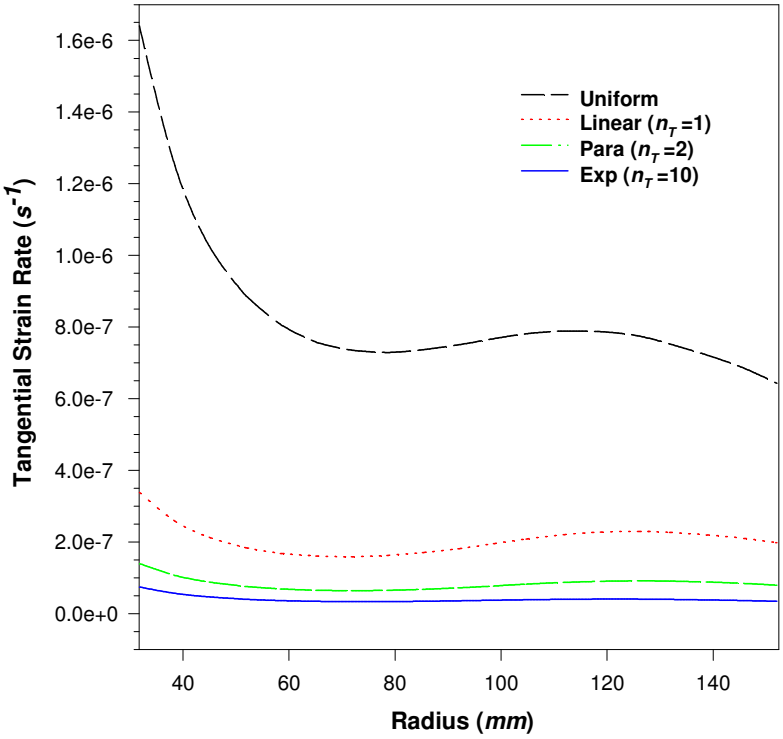

Fig. 4.19: Effect of temperature exponent on tangential strain rate in FGM disc (*m*=-1.8295, *k*=-0.6)

Based on the maximum strain rates (*i.e.* tangential strain rate), observed at the inner disc radius, the creep life (defined in terms of creep rupture time) of the FGM disc has been estimated for different values of n_T. The rupture strain for Al-SiC composites is observed in the range of 2% to 4% [Nieh (1984), Orlando and Filho (2004)]. Therefore, in this study, the rupture time (= rupture strain/maximum strain rate) has been estimated for different values of n_T by taking 2%, 3% and 4% (*i.e.* 0.02, 0.03 and 0.04) strain as the rupture strain. The rupture time is observed to increase slightly (by few hours) as the value of exponent n_T decreases from 15 to 5 (Fig. 4.22). On decreasing the value of exponent n_T below 5, the rupture time is observed to increase significantly (by several years). As an example, the rupture time increases by around nine orders of magnitude when the value of n_T decreases from 5 to 2. The increase in rupture time, with decreasing value of exponent n_T , is attributed to the reduction in temperature at the inner radius (Fig. 4.20), which leads to significant reduction in strain rate (Fig. 4.21). Thus, if one controls the rate of heat transfer along the radial direction of the FGM disc, which is possible by employing suitable thermal barrier coatings, heat sink [Padture *et al.* (2002), Lepeshkin (2012)] etc., the creep induced damage in the FGM disc could be reduced significantly. This will help in enhancing the creep life of rotating disc components.

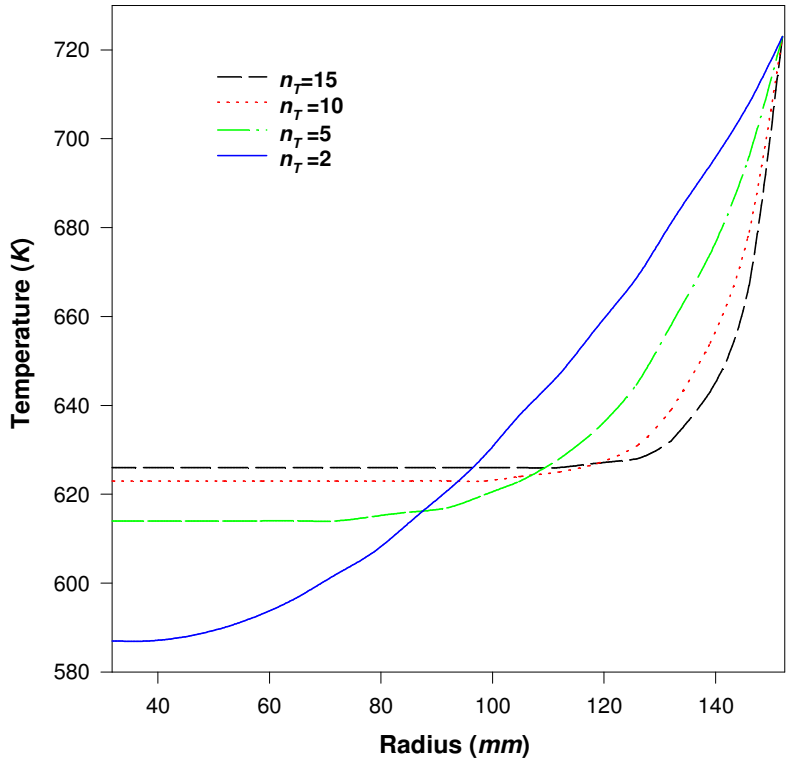

Fig. 4.20: Temperature profile in FGM disc for different n_T (T_{avg} = 632.09 *K*, T_o = 723 *K*)

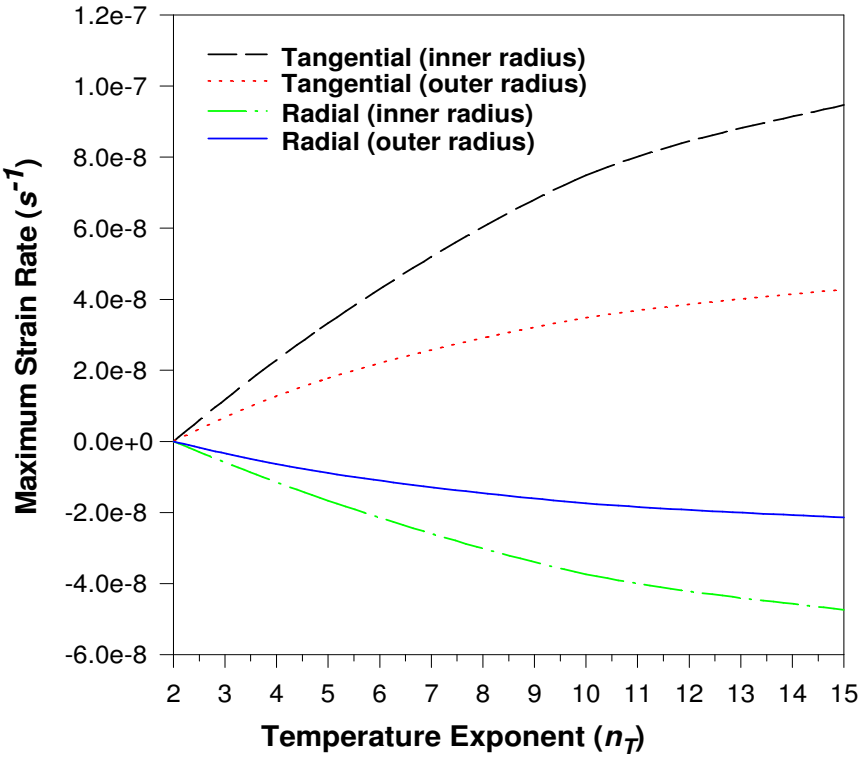

Fig. 4.21: Effect of varying n_T on strain rates in FGM disc (T_{avg} = 632.09 K, T_o = 723 K)

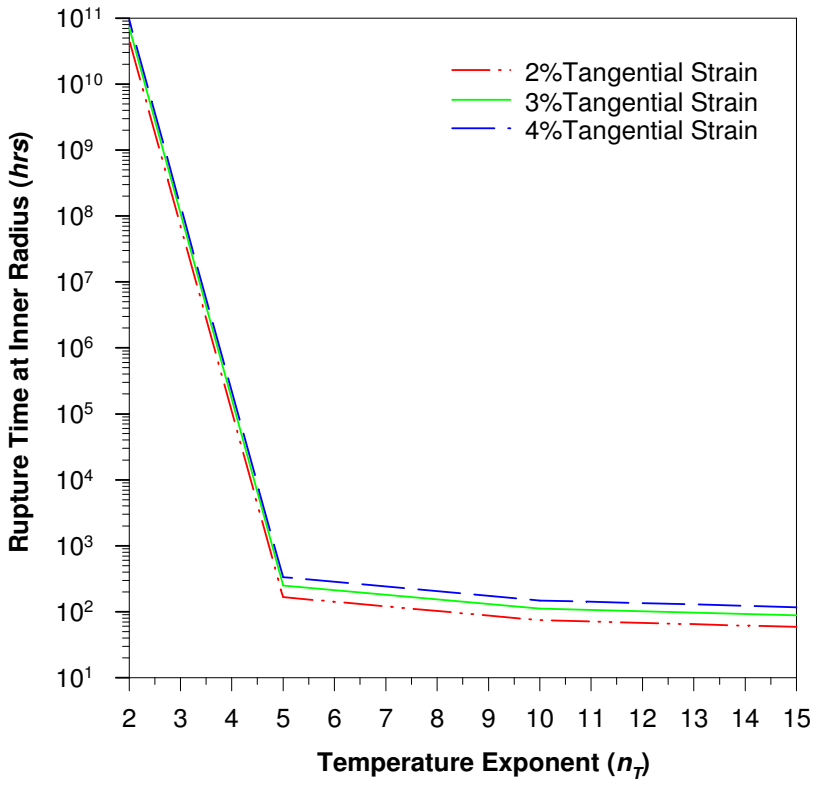

Fig. 4.22: Effect of varying n_T on rupture time in FGM disc (T_{avg} = 632.09 K, T_o = 723 K)

CHAPTER-5

EFFECT OF VARYING ANISOTROPY ON THE CREEP PERFORMANCE OF A VARIABLE THICKNESS ROTATING FGM DISC

5.1 INTRODUCTION

The literature survey outlined in the previous chapters indicates that during the last decade, the researchers have made attempts to analyze stresses and deformations in rotating FGM disc [Hassani *et al.* (2012), You *et al.* (2007), Bayat *et al.* (2008), Çallıoğlu *et al.* (2011a), Akbari and Ghanbari (2015)]. Most of the available analysis, pertaining to rotating FGM disc, assumes the disc to be made of isotropic material. However, in case of disc composed of short-fiber or whisker reinforced composite, the assumption of isotropy is no longer valid, as the material flows during the processing operations like forging, rolling and extrusion etc. The material flow leads to preferential alignment of whiskers or short-fibers and as a result of which material of the disc becomes anisotropic. Keeping this in view, some of the investigators have analyzed the effect of anisotropy on the stresses and deformations in rotating disc. Bhatnagar *et al*. (1986) used Norton's creep law to analyze creep behavior of orthotropic rotating disc with different thickness profiles. Tutuncu (1995) analyzed the effect of anisotropy on the stresses and deformations in orthotropic rotating circular plates. Jain *et al.* (1999) proposed a design procedure to achieve a constant thickness composite disc of uniform strength by radially tailoring the anisotropic elastic constants. Singh and Ray (2002) analyzed the effect of anisotropy on the creep behavior of rotating disc made of 6061Al-20 wt% SiC_w ('w' for whisker) composite by using Norton's power law. The study reveales that the presence of anisotropy significantly reduces the strain rates over the entire disc radius. Alexandrova and Alexandrov (2004) analyzed the effect of plastic anisotropy on the distribution of stresses in an anisotropic rotating disc using Hill's quadratic yield criterion. Chamoli *et al*. (2010) investigated the effect of anisotropy on the creep stresses and creep

rates in rotating disc made of uniform composite. Vandana and Singh (2011) investigated the steady state creep response of variable thickness rotating disc made of anisotropic Al-SiC_p composite. Nie *et al*. (2011) investigated the effect of using different types of radial distribution of elastic modulus of the disc material to identify the better design of rotating disc made of fiber-reinforced orthotropic composite.

The literature consulted so far reveals that no study has been undertaken to investigate the creep behavior of rotating disc made of anisotropic FGM and having variable thickness profile. The present study is an attempt to investigate the effect of varying the extent of anisotropy of the disc material on its creep response. The disc is assumed to be made of functionally graded 6061Al-SiC_w composite having non-linear distribution of SiC_w reinforcement along the radial direction. The thickness of the disc is assumed to decrease radially on moving from the inner towards the outer radius. The results are estimated for anisotropic FGM discs and are compared with those obtained for similar FGM disc but having isotropic properties.

5.2 DISC GEOMETRY AND REINFORCEMENT PROFILE

For the purpose of analysis, the disc dimensions and the distribution of SiC_w reinforcement in the FGM disc are taken similar to those depicted in Fig. 4.1. The disc thickness at the inner and outer radii are taken as h_a (=49.00 *mm*) and h_b (=19.1 *mm*) respectively. Similar to Chapter 4, the disc thickness, $h(r)$, at any radius (r), is assumed to vary according to the following power law relation,

$$h(r) = h_b \left(\frac{r}{b} \right)^k \tag{5.1}$$

where a, b and k (= -0.6) are the inner disc radius, the outer disc radius and the disc thickness gradient, respectively. The disc is assumed to rotate at 15000 *rpm* and made of 6061Al-SiC_w composite, wherein the content of SiC_w decreases radially with increasing radius. The content of SiC_w at any radius r, $V(r)$, is also assumed to vary according to power law given in Eq. (4.3), and reproduced below,

$$V(r) = V_{\min} \left(\frac{r}{b} \right)^m \tag{5.2}$$

where m (= -1.8295) is the reinforcement gradient.

The purpose of selecting the value of disc thickness gradient (k) = -0.6 (Eq. 5.1) and reinforcement gradient (m) = -1.8295 (Eq. 5.2) is due to the fact that corresponding to these

values of k and m the strain rates in the disc are the lowest, as revealed from the results reported in Sections 4.5.1 and 4.5.2.

5.3 DISTRIBUTION OF SiC_w REINFORCEMENT

It is revealed from Eq. (5.2) that in variable thickness FGM disc the content of SiC_w will decrease linearly from the inner (a) to the outer disc radius (b), similar to those assumed in Chapter 4 for functionally graded Al-SiC_p disc (Fig. 4.1). For the assumed disc dimensions (a = 31.75 *mm*, b = 152.4 *mm*), k = -0.6 and m = -1.8295, the values of V_{max} and V_{min} are 100% and 5.67%, respectively, which correspond to FGM disc DS5 (Table 4.2). Knowing V_{min} (= 5.67%), the content of SiC_w in the FGM disc, $V(r)$, may be estimated from Eq. (5.2).

5.4 ESTIMATION OF CREEP PARAMETERS

The values of creep parameters $M(r)$ and $\sigma_0(r)$ for the disc material (*i.e.*6061Al-SiC_w) are estimated from the following regression equations, as developed by Singh and Gupta (2011),

$$M(r) = 0.0288 - \frac{0.0088}{P} - \frac{14.0267}{T} + \frac{0.0322}{V(r)} + dM_1 + dM_2 \tag{5.3}$$

$$\sigma_0(r) = -0.084P - 0.023T + 1.185V(r) + 22.207 + d\sigma_{0_1} + d\sigma_{02} \tag{5.4}$$

The above equations have been developed by Singh and Gupta (2011) from the regression equations applicable for Al-SiC_p composite (Eqs. 3.5 and 3.6). The terms dM_1 (= 0.00411) and $d\sigma_{0_1}$ (= -8.71) appearing in Eqs. (5.3) and (5.4) compensate for the effect of changing the matrix from pure Al to 6061Al alloy. The values of these terms have been obtained by Singh and Gupta (2011) by comparing the experimental creep data of 6061Al-SiC_p composite [Nieh *et al*. (1988)] with those of Al-SiC_p composites, which can be estimated from Eqs. (3.5) and (3.6). On the other hand, the terms dM_2 (Eq. 5.3) and $d\sigma_{0_2}$ (Eq. 5.4) account for the effect of changing the shape of SiC reinforcement from particle (p) to whisker (w) on the creep parameters $M(r)$ and $\sigma_0(r)$, respectively. Singh and Gupta (2011) estimated the values of dM_2 and $d\sigma_{0_2}$ by comparing the creep parameters $M(r)$ and $\sigma_0(r)$ estimated using regression equations developed for 6061Al-20*vol*% SiC_p with those of 6061Al-20*vol*% SiC_w at an operating temperature of 561 *K*. The creep parameters for

6061Al-20*vol%* SiC_w were extracted from the experimental creep data reported by Nieh *et al.* (1988). The parameters dM_2 and $d\sigma_{0_2}$ will depend on the operating temperature, which has been taken constant by Singh and Gupta (2011). To develop the regression equations, describing the dependence of dM_2 and $d\sigma_{0_2}$ on the operating temperature. The creep parameters $M(r)$ and $\sigma_0(r)$ of 6061Al-20*vol%* SiC_p have been compared with those of 6061Al-20*vol%* SiC_w corresponding to three different operating temperatures (Table 5.1). The parameters $M(r)$ and $\sigma_0(r)$ of 6061Al-20*vol%* SiC_p have been estimated from the regression equations while those of 6061Al-20*vol%* SiC_w have been extracted from the experimental creep data reported by [Nieh *et al.* (1988)], by following the procedure described in Singh and Gupta (2011).

Table 5.1: Comparison of creep parameters of 6061Al-20*vol%* SiC_p and 6061Al-20*vol%* SiC_w ($P = 1.23\ \mu m$; $V = 20vol\%$)

$T(K)$	$M\ (s^{-1/5}/MPa)^{\blacklozenge}$		$dM_2 = M^W - M^P$	$\sigma_0\ (MPa)^{\blacklozenge}$		$d\sigma_{02} = \sigma_0^W - \sigma_0^P$
	M^P	M^W		σ_0^P	σ_0^W	
505	-4.393E-04	1.457 E-03	1.896 E-03	25.39	88.35	62.96
561	2.333E-03	2.710 E-03	3.768 E-04	24.09	61.91	37.82
616	4.566 E-03	3.938 E-03	-6.278 E-04	22.81	41.78	18.97

$^{\blacklozenge}$ Superscripts 'P' and 'W' refer to 6061Al-SiC_p and 6061Al-SiC_w composites, respectively

The values of dM_2 and $d\sigma_{0_2}$, as reported in Table 5.1, at different operating temperatures have been subjected to regression analysis to develop their mathematical correlations with the operating temperature. The developed regression equations are,

$$dM_2 = -5.837\times10^{-3} + \frac{1968.141}{T^2} \tag{5.5}$$

$$d\sigma_{0_2} = -80.53 + \frac{5.88\times10^6 \log_e T}{T^2} \tag{5.6}$$

Thus, the creep parameters M and σ_0 for 6061Al-SiC_w can now be estimated, from Eqs. (5.3) and (5.4), respectively, after substituting the values of dM_2 from Eq. (5.5) and

$d\sigma_{0_2}$ from Eq. (5.6) for the given operating temperature. In this study, the size (P) of SiC_w reinforcement and the operating temperature are assumed as 1.23 μm and 616 K, respectively.

5.5 ANALYSIS OF CREEP IN ANISOTROPIC FGM DISC

The analysis given in this section also assumes the material of the disc (6061Al-SiC_w) to be incompressible and under plane stress condition. The elastic deformations in the disc are neglected. The steady state creep of the disc material is again described by Eq. (3.4) and the disc is assumed to rotate at 15000 *rpm*.

However, unlike previous analysis, the present analysis assumes the material of the disc is orthotropic, and has different mechanical properties along the mutually perpendicular directions of the disc *i.e*. radial (r), tangential (θ) and axial directions. The anisotropy induced is assumed to originate due to the flow of disc material during its processing through forging, rolling or extrusion operations. The yielding of the disc material is described by the Hill's criterion [Dieter (1988)], which under plane stress condition can be given by,

$$\bar{\sigma} = \frac{1}{\sqrt{G+H}}\left[(G+H)\,\sigma_r{}^2 + (H+F)\,\sigma_\theta{}^2 - 2H\sigma_r\sigma_\theta\right]^{1/2} \tag{5.7}$$

where F, G and H are Hill's constants, and $\bar{\sigma}$ is the effective stress, which is the uniaxial state of stress equivalent to the general/multi-axial state of stress. The values of these constants depend on the yield strengths of the disc material along the radial, tangential and axial directions, denoted by σ_{r_y} σ_{θ_y} and σ_{z_y}, respectively. The values of constants F, G and H in terms of yield strengths are given by [Khan and Huang (1995)],

$$F = \frac{1}{2}\left[\frac{1}{\sigma_{\theta_y}{}^2} + \frac{1}{\sigma_{z_y}{}^2} - \frac{1}{\sigma_{r_y}{}^2}\right]$$

$$G = \frac{1}{2}\left[\frac{1}{\sigma_{z_y}{}^2} + \frac{1}{\sigma_{r_y}{}^2} - \frac{1}{\sigma_{\theta_y}{}^2}\right] \tag{5.8}$$

$$H = \frac{1}{2}\left[\frac{1}{\sigma_{r_y}{}^2} + \frac{1}{\sigma_{\theta_y}{}^2} - \frac{1}{\sigma_{z_y}{}^2}\right]$$

The constitutive equations for multi-axial creep in a composite disc made of orthotropic FGM under plane stress condition, when the reference frame is taken along the principal directions r, θ and z of the disc, are given by [Gupta *et al.*, 2004(a)],

$$\dot{\varepsilon}_r = \frac{\left[(G+H)\sigma_r - H\sigma_\theta\right]}{(G+H)}\left(\frac{\dot{\bar{\varepsilon}}}{\bar{\sigma}}\right)$$

$$\dot{\varepsilon}_\theta = \frac{\left[(H+F)\sigma_\theta - H\sigma_r\right]}{(G+H)}\left(\frac{\dot{\bar{\varepsilon}}}{\bar{\sigma}}\right) \tag{5.9}$$

$$\dot{\varepsilon}_z = \frac{-\left[F\sigma_\theta + G\sigma_r\right]}{(G+H)}\left(\frac{\dot{\bar{\varepsilon}}}{\bar{\sigma}}\right)$$

where $\dot{\bar{\varepsilon}}$ is the effective strain rate, and $\dot{\varepsilon}$ and σ denote strain rates and stresses, respectively, in the disc. The subscripts r, θ and z refer to the radial, tangential and axial directions.

The set of Eqs. (5.9) may alternatively be written as,

$$\dot{\varepsilon}_r = \frac{\left[(\alpha+\beta)\sigma_r - \beta\sigma_\theta\right]}{(\alpha+\beta)}\left(\frac{\dot{\bar{\varepsilon}}}{\bar{\sigma}}\right)$$

$$\dot{\varepsilon}_\theta = \frac{\left[(1+\beta)\sigma_\theta - \beta\sigma_r\right]}{(\alpha+\beta)}\left(\frac{\dot{\bar{\varepsilon}}}{\bar{\sigma}}\right) \tag{5.10}$$

$$\dot{\varepsilon}_z = \frac{-\alpha\sigma_r - \sigma_\theta}{(\alpha+\beta)}\left(\frac{\dot{\bar{\varepsilon}}}{\bar{\sigma}}\right)$$

where $\alpha\left(=G/F\right)$ and $\beta\left(=H/F\right)$ are the ratios of Hill's constants. The constants α and β are referred as anisotropic constants in this study and their values will depend on the yield strengths of the disc material.

Substituting the values of $\dot{\bar{\varepsilon}}$ and $\bar{\sigma}$ from Eqs. (3.4) and (5.7), respectively, into the first equation amongst the set of Eqs. (5.10), one gets,

$$\dot{\varepsilon}_r = \frac{d\dot{u}_r}{dr} = \frac{(\alpha+\beta)x(r) - \beta\left[M(r)\{\bar{\sigma} - \sigma_0(r)\}\right]^n}{\sqrt{\alpha+\beta}\ \left[(\alpha+\beta)\{x(r)\}^2 + (1+\beta) - 2\beta x(r)\right]^{1/2}} \tag{5.11}$$

where $x(=\sigma_r(r)/\sigma_\theta(r))$ is the ratio of radial and tangential stresses, $\dot{u}_r(=du/dt)$ is the radial deformation rate, *u* is the radial deformation in the FGM disc, *M(r)* is the creep parameter and $\sigma_0(r)$ is the threshold stress.

Similarly, one gets from the second equation amongst the set of constitutive Eqs. (5.10),

$$\dot{\varepsilon}_\theta = \frac{\dot{u}_r}{r} = \frac{[(1+\beta)-\beta x(r)]\left[M(r)\{\bar{\sigma}-\sigma_0(r)\}\right]^n}{\sqrt{\alpha+\beta}\left[(\alpha+\beta)\{x(r)\}^2+(1+\beta)-2\beta x(r)\right]^{1/2}} \tag{5.12}$$

The effective stress given in Eq. (5.7) may also be expressed as,

$$\bar{\sigma} = \frac{\sigma_\theta}{\sqrt{\alpha+\beta}}\left[(\alpha+\beta)\{x(r)\}^2+(1+\beta)-2\beta x(r)\right]^{1/2} \tag{5.13a}$$

The above Eq. (5.13) may alternatively be written as,

$$\bar{\sigma} = \sigma_\theta\left[\{x(r)\}^2+\frac{1+\beta-2\beta x(r)}{(\alpha+\beta)}\right]^{1/2} \tag{5.13b}$$

On dividing Eq. (5.11) by Eq. (5.12) and integrating the resulting equation between limits *a* to *r*, one obtains,

$$\dot{u}_r = \dot{u}_a \exp\left[\int_a^r \frac{\phi(r)}{r}dr\right] \tag{5.14}$$

where $\dot{u}_a$ is the radial deformation rate at the inner disc radius and the value of function $\phi(r)$ is given by,

$$\phi(r) = \frac{[(\alpha+\beta)x(r)-\beta]}{[(1+\beta)-\beta x(r)]}$$

Using Eq. (5.14) into Eq. (5.12), one gets,

$$\frac{\dot{u}_a}{r}\left[\exp\int_a^r \frac{\phi(r)}{r}dr\right] = \frac{[(1+\beta)-\beta x(r)]\left[M(r)\{\bar{\sigma}-\sigma_0(r)\}\right]^n}{\sqrt{\alpha+\beta}\left[(\alpha+\beta)\{x(r)\}^2+(1+\beta)-2\beta x(r)\right]^{1/2}}$$

or,

$$\left[M(r)\{\bar{\sigma}-\sigma_0(r)\}\right] = (\dot{u}_a)^{1/n}\,\psi^{1/n}(r)$$

where,

$$\psi(r)=\left[\frac{1}{r}\exp\int_a^r\frac{\phi(r)}{r}dr\frac{\sqrt{\alpha+\beta}\left[(\alpha+\beta)\{x(r)\}^2+(1+\beta)-2\beta x(r)\right]^{1/2}}{\left[(1+\beta)-\beta x(r)\right]}\right]$$

The above equation may be simplified to obtain $\bar{\sigma}$ as,

$$\bar{\sigma}=\frac{(\dot{u}_a)^{1/n}\psi^{1/n}(r)}{M(r)}+\sigma_0(r) \tag{5.15}$$

Substituting $\bar{\sigma}$ from Eq. (5.13a) into Eq. (5.15) and simplifying, one obtains the tangential stress in the FGM disc as,

$$\sigma_\theta(r)=\frac{(\dot{u}_a)^{1/n}}{M(r)}\psi_1(r)+\psi_2(r) \tag{5.16}$$

where,

$$\psi_1(r)=\frac{\psi^{1/n}(r)\sqrt{\alpha+\beta}}{\left[(\alpha+\beta)\{x(r)\}^2+(1+\beta)-2\beta x(r)\right]^{1/2}}$$

and,

$$\psi_2(r)=\frac{\sigma_0(r)\sqrt{\alpha+\beta}}{\left[(\alpha+\beta)\{x(r)\}^2+(1+\beta)-2\beta x(r)\right]^{1/2}}$$

Multiplying both sides of Eq. (5.16) by $h(r)dr$ and integrating the resulting equation between limits a to b, one gets,

$$\dot{u}_a^{1/n}=\frac{A_0\sigma_{\theta(avg)}-\int_a^b h(r)\psi_2(r)dr}{\int_a^b\frac{h(r)\psi_1(r)}{M(r)}dr} \tag{5.17}$$

where $A_0=\int_a^b h(r)dr$ and $\sigma_{\theta(avg)}$ is the average tangential stress in the FGM disc, as given by,

$$\sigma_{\theta(avg)}=\frac{\int_a^b h(r)\sigma_\theta dr}{\int_a^b h(r)dr} \tag{5.18}$$

Substituting $\dot{u}_a^{1/n}$ from Eq. (5.17) into Eq. (5.16), one gets,

$$\sigma_\theta(r) = \frac{\psi_1(r)}{M(r)}\left[\frac{A_0\,\sigma_{\theta(avg)} - \int_a^b h(r)\psi_2(r)\,dr}{\int_a^b \frac{h(r)\psi_1(r)}{M(r)}\,dr}\right] + \psi_2(r) \tag{5.19}$$

The force equilibrium equation for a variable thickness rotating FGM disc, as given by Eq. 3.12 in Chapter 3, is rewritten as,

$$\frac{d}{dr}[h(r)r\sigma_r(r)] - h(r)\sigma_\theta(r) + \rho(r)\omega^2 r^2 h(r) = 0 \tag{5.20}$$

where $\rho(r)$ is the density of 6061Al-SiC_w composite at any radius *r*. The density of the disc can be estimated by using the rule of mixture, as given in Eq. (4.6), where, in the present case $\rho_m\,(=2680\,kg/m^3)$ and $\rho_d\,(=3210\,kg/m^3)$ are the densities of 6061Al matrix and SiC_w reinforcement, respectively.

The equilibrium Eq. (5.20) may be integrated under the free-free boundary conditions (Eq. 3.14), following the procedure given in Section-4.4, to obtain,

$$\sigma_{\theta(avg)} = \frac{\omega^2 h_b}{A_0 b^k}\left[A_\rho \frac{(b^{3+k} - a^{3+k})}{3+k} + B_\rho \frac{(b^{3+k+m} - a^{3+k+m})}{3+k+m}\right] \tag{5.21}$$

where $A_\rho = \rho_m$ and $B_\rho = \frac{(\rho_d - \rho_m)V_{\min}}{b^m(100)}$, as described earlier in Section- 4.3.

Once the value of average tangential stress, $\sigma_{\theta(avg)}$, in the FGM disc is estimated from Eq. (5.21), the tangential stress, $\sigma_\theta(r)$, in the FGM disc may be estimated from Eq. (5.19).

Following the analysis scheme reported in Section- 4.4, the equilibrium Eq. (5.20) is integrated between limits *a* to *r* under the boundary condition at the inner disc radius (*i.e.* $\sigma_r = 0$ at $r = a$), to obtain radial stress in the FGM disc as,

$$\sigma_r(r) = \frac{1}{rh(r)}\left[\int_a^r h(r)\sigma_\theta(r)dr - \frac{\omega^2 h_b}{b^k}\left\{A_\rho \frac{(r^{3+k} - a^{3+k})}{3+k} + B_\rho \frac{(r^{3+k+m} - a^{3+k+m})}{3+k+m}\right\}\right] \tag{5.22}$$

Knowing the distribution of stresses, $\sigma_\theta(r)$ from Eq. (5.19) and $\sigma_r(r)$ from Eq. (5.22), in the FGM disc, the distribution of strain rates, $\dot{\varepsilon}_r$ from Eq. (5.11) and $\dot{\varepsilon}_\theta$ from Eq. (5.12), in the disc are estimated.

5.6 RESULTS AND DISCUSSION

Corresponding to the analysis reported in the previous section, a computer code has been developed. The computations have been carried out from the developed code to investigate the effect of varying the extent of anisotropy on the steady state creep behavior of variable thickness rotating FGM disc. The stresses and strain rates have been estimated for different FGM discs reported in Table-5.2, which corresponds to different values of anisotropic constants α and β, ranging from 0.5 to 1.5, except for disc5 and disc7. The yield strengths of different discs considered are estimated by solving the set of Eqs. (5.8), by substituting the values of constants G and H in terms of constant F corresponding to different combinations of anisotropic constants α and β (Table 5.2) and keeping the value of σ_{zy} at a constant level. It is important to mention that the values of constants α and β for disc5 are estimated from Eq. (5.8) by inverting the ratio of yield strengths $\sigma_{ry}/\sigma_{\theta y}$ calculated for disc4 but keeping the same value of σ_{zy}. The values of constants α and β for disc7 are also derived in a similar way from the ratio of yield strengths $\sigma_{ry} : \sigma_{\theta y} : \sigma_{zy}$ reported for disc6. Thus, the results are estimated for four different orthotropic discs (disc4-disc7), two transversely isotropic discs (disc2 and disc3) and an isotropic disc (disc1), which acts as a reference disc.

Table 5.2: Details of FGM discs considered

Disc Notation	**Disc Material**	**Anisotropic Constants**			**Ratio of Yield Strengths**
		α **= G/F**	β **= H/F**	$(\alpha+\beta)$	$(\sigma_{ry} : \sigma_{\theta y} : \sigma_{zy})$
Disc1	Isotropic	1.0	1.0	2.0	1 : 1 : 1
Disc2	Transversely Isotropic	1.5	1.0	2.5	1 : 1.12 : 1
Disc3		1.0	1.5	2.5	0.89 : 0.89 : 1
Disc4	Orthotropic	1.5	0.5	2.0	1.12 : 1.29 : 1
Disc5		0.67	0.33	1.0	1.29 : 1.12 : 1
Disc6		0.5	1.5	2.0	0.87 : 0.77 : 1
Disc7		1.92	2.89	4.81	0.77 : 0.87 : 1

5.6.1 Effect of Varying Anisotropy on Stresses

(*i*) *Effect on radial stress*

The radial stress in all the FGM discs (Fig. 5.1) increases from zero at the inner radius to reach a maximum value somewhere in the middle and thereafter decreases to become zero at the outer radius, under the imposed free-free boundary condition given in Eq. (3.14). The effect of varying the extent of anisotropy on the radial stress distribution in the FGM disc is observed to be significant, especially in the middle region of the disc. It is observed to be the highest for orthotropic disc4 but the lowest for orthotropic disc6. Thus, in terms of radial stress, disc6 seems to be superior wherein yield strength of the material along the radial and tangential directions are lower by 13% and 23%, respectively, as compared to yield strength of the material along the axial direction. The maximum difference in radial stress of around 6 *MPa* is observed between disc4 and disc6 at a radius of around 65 *mm*. The comparison of radial stress within the different transversally isotropic discs (disc2 and disc3) and different orthotropic discs (disc4-disc7) reveals that the radial stress is lower in discs having weaker yield strength along the radial and tangential directions, as compared to yield strength along the axial direction. Further, the comparison of orthotropic disc6 and disc7 reveals that the disc6, having the lowest yield strength along the tangential direction, is better than disc7, which is the weakest along the radial direction.

(*ii*) *Effect on tangential stress*

The tangential stress in the FGM discs is observed to decrease with the increasing radial distance (Fig. 5.2). The effect of varying anisotropy on the distribution of tangential stress near the inner and the outer radii is similar to those observed for radial stress in Fig 5.1, with relatively larger variation noticed towards the inner disc region. However, in the middle portion of the disc, the effect of varying anisotropy is just opposite to those observed near the inner and the outer radii. At the inner radius, the tangential stress in disc4 is higher by about 30 *MPa* than that observed in disc6, whereas in the middle region (around a radius of 85 *mm*) the tangential stress in disc4 is lower by about 15 *MPa* than that observed in disc6.

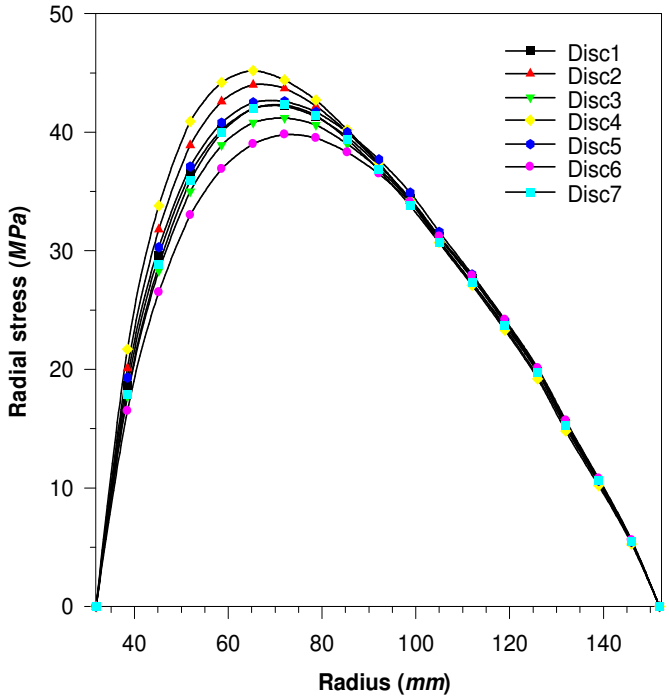

Fig. 5.1: Effect of varying anisotropy on radial stresses in FGM discs (k = -0.6, m = -1.8295, Disc RPM = 15000)

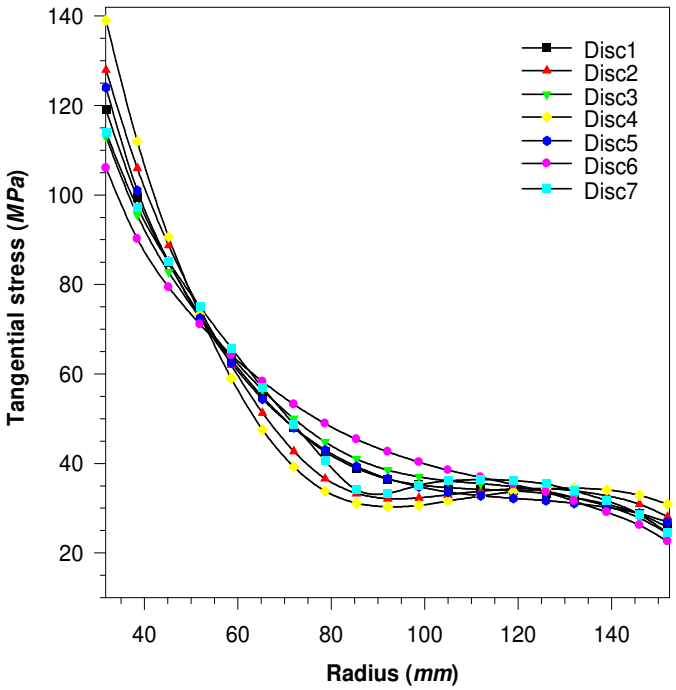

Fig. 5.2: Effect of varying anisotropy on tangential stresses in FGM discs (k = -0.6, m = -1.8295, Disc RPM = 15000)

(*iii*) ***Effect on effective stress***

The trend of radial variation of effective stress in the FGM discs (Fig. 5.3) is similar to those observed for tangential stress in Fig. 5.2. The effective stress, shown in Fig 5.3, is observed to be the lowest in disc7 and the highest in disc5, over the entire disc radius. Though, the values of σ_r and σ_θ in these discs are observed in between those noticed in disc4 and disc6. The difference in the magnitude of effective stress in various FGM discs is observed to decrease with increasing radius. It is evident from Eq. (5.13b) that the effective stress is inversely proportional to the square root of sum of anisotropic constants α and β (*i.e.* $\sqrt{(\alpha+\beta)}$) apart from the values of σ_r and σ_θ in the FGM disc. Table-5.2 reveals that the value of sum ($\alpha + \beta$) is the highest (= 4.81) for disc7, therefore, disc7 exhibits the lowest effective stress whereas disc5 shows the highest value of effective stress owing to the lowest value (=1) of sum ($\alpha + \beta$).

The above discussion indicates that the anisotropic disc with weaker yield strengths along the radial and tangential directions, as compared to axial direction, develops lower effective stress. The effective stress in such type of anisotropic disc could be further reduced if the yield strength along the radial direction is lower than the yield strength along the tangential direction, as evident from the comparison of distribution of effective stress in disc6 and disc7 (Fig. 5.3).

(*iv*) ***Effect on stress difference*** $(\bar{\sigma}-\sigma_0)$

While designing the disc for applications involving creep, the creep rate is an important design consideration. Thus, it is imperative to investigate the effect of varying the extent of anisotropy on creep rates in the FGM disc. It is observed that the radial and tangential strain rates, as given by Eqs. (5.11) and (5.12), respectively, depend on the difference of $\bar{\sigma}$ and σ_0 *i.e.* $(\bar{\sigma}-\sigma_0)$.Therefore, before discussing the effect of varying anisotropy on the strain rates, it is important to discuss the variation of stress difference $(\bar{\sigma}-\sigma_0)$ in different FGM discs. The effect of varying anisotropy on $(\bar{\sigma}-\sigma_0)$ in different FGM discs (Fig. 5.4) is similar to those observed for $\bar{\sigma}$ in Fig. 5.3. The difference $(\bar{\sigma}-\sigma_0)$ is positive in disc1-disc6, with the highest value observed in disc5. However, in disc7 the value of $(\bar{\sigma}-\sigma_0)$ is negative over the entire disc, which signifies that the effective stress $(\bar{\sigma})$

remains below the threshold stress (σ_0) in disc7 and thereby no creep deformation will occur in this disc.

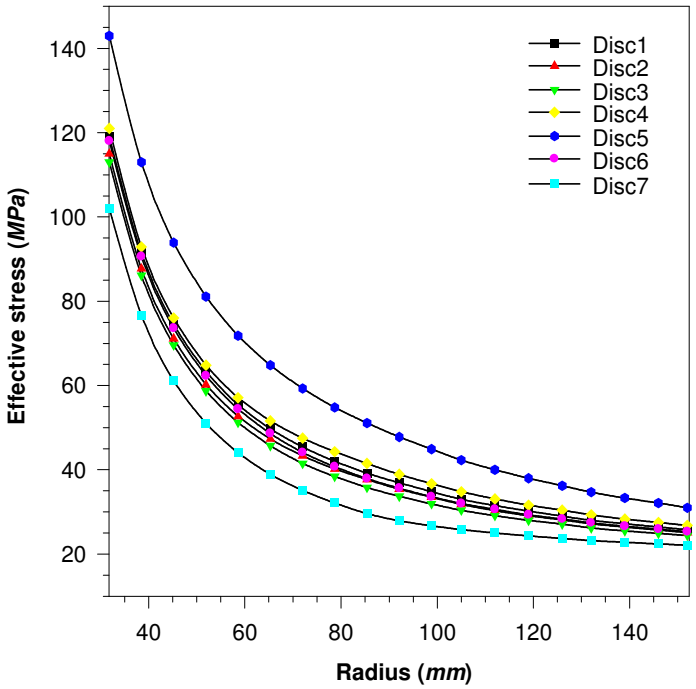

Fig. 5.3: Effect of varying anisotropy on effective stress in FGM discs (k = -0.6, m = -1.8295, Disc RPM = 15000)

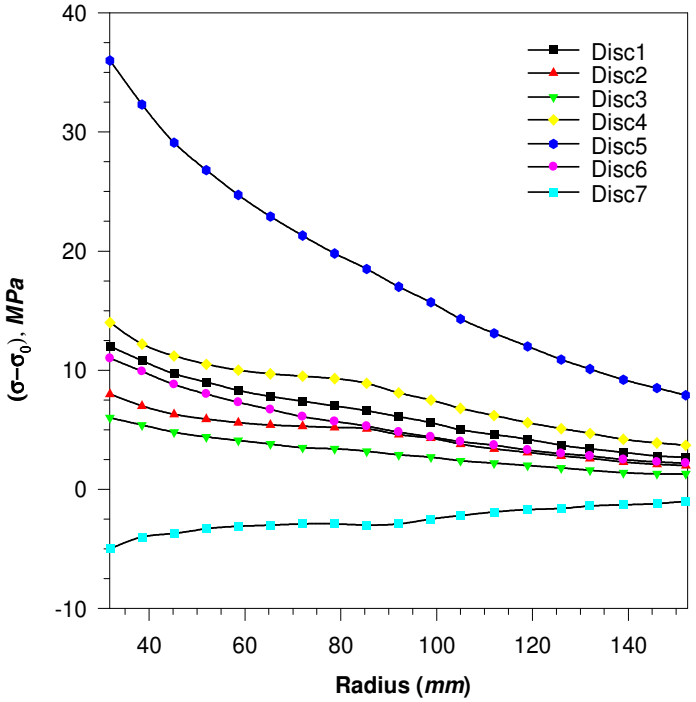

Fig. 5.4: Effect of varying anisotropy on stress difference $(\bar{\sigma} - \sigma_0)$ in FGM discs (k = -0.6, m = -1.8295, Disc RPM = 15000)

5.6.2 Effect of Varying Anisotropy on Strain Rates

The impact of varying the extent of anisotropy on the effective strain rate (Fig 5.5), as estimated from creep law given in Eq. (3.4), in different FGM discs is similar to those observed for stress difference $(\bar{\sigma} - \sigma_0)$ in Fig. 5.4. The anisotropic disc7 is observed to be superior as compared to any other discs, as in this disc the creep rates remain zero over the entire disc, owing to $\bar{\sigma} < \sigma_0$. The orthotropic disc5, with the lowest $\alpha + \beta$ value (= 1), exhibits the highest strain rates. If one excludes disc7, the transversely isotropic disc3 is observed to exhibit the lowest effective strain rates amongst the other discs (*i.e.* disc1-disc6). The effective strain rate in transversely isotropic disc3 is lower by about 4 orders of magnitude than that observed in orthotropic disc5, exhibiting the highest effective strain rate.

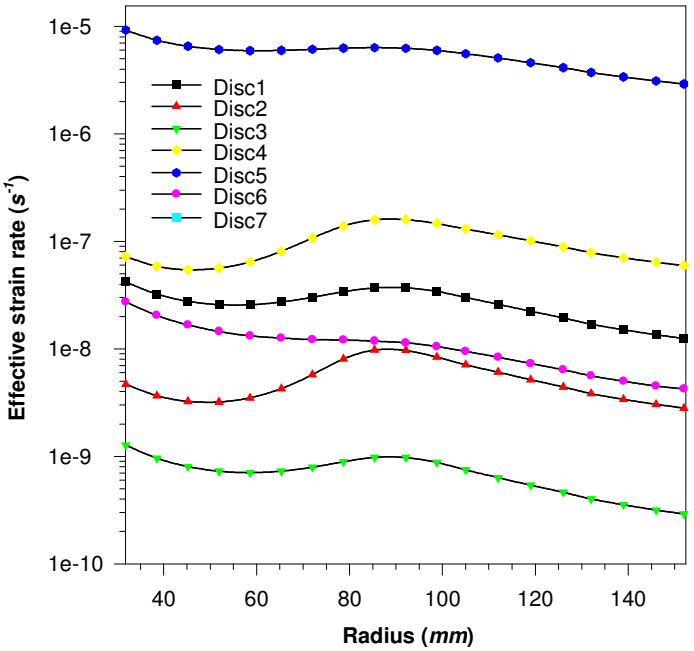

Fig. 5.5 : Effect of varying anisotropy on effective strain rate in FGM discs (k = -0.6, m = -1.8295, Disc RPM = 15000)

The effect of varying anisotropy on the tangential strain rates (Fig. 5.6) is similar to those observed in Fig. 5.5 for the effective strain rate. The impact of varying anisotropy on the radial strain rate (Fig. 5.7) also seems to be governed by the distribution of $(\bar{\sigma} - \sigma_0)$ in the FGM discs (Fig. 5.4). The radial strain rate is the highest in disc5, with tensile nature in the middle region and compressive nature near the inner and the outer radii. The radial strain rate is zero in disc7, though in other discs the order of radial strain rate is quite low as

compared to those observed in disc5 and hence could not be clearly revealed in Fig. 5.7. It is clearly evident from the distribution of strain rates in different FGM discs that the anisotropic disc with $\sigma_{ry} < \sigma_{\theta y} < \sigma_{zy}$ (*i.e.* disc7) appears to be superior amongst all the discs.

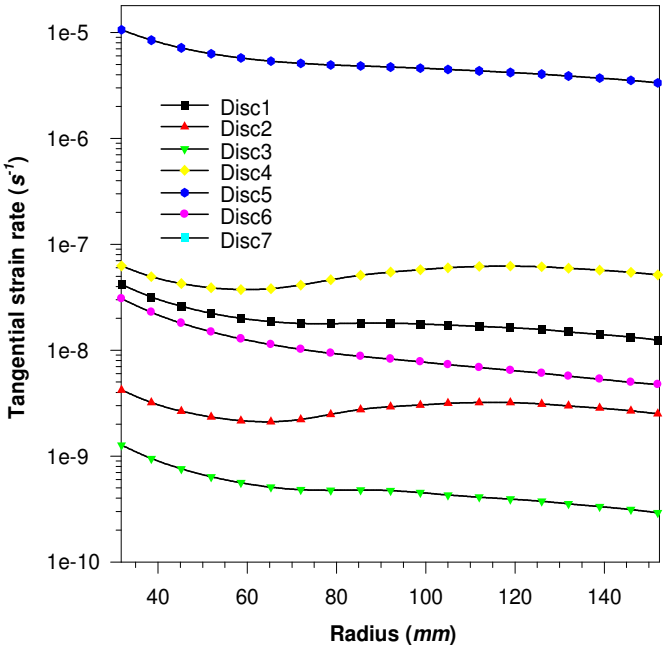

Fig. 5.6: Effect of varying anisotropy on tangential strain rate in FGM discs (k = -0.6, m = -1.8295, Disc RPM = 15000)

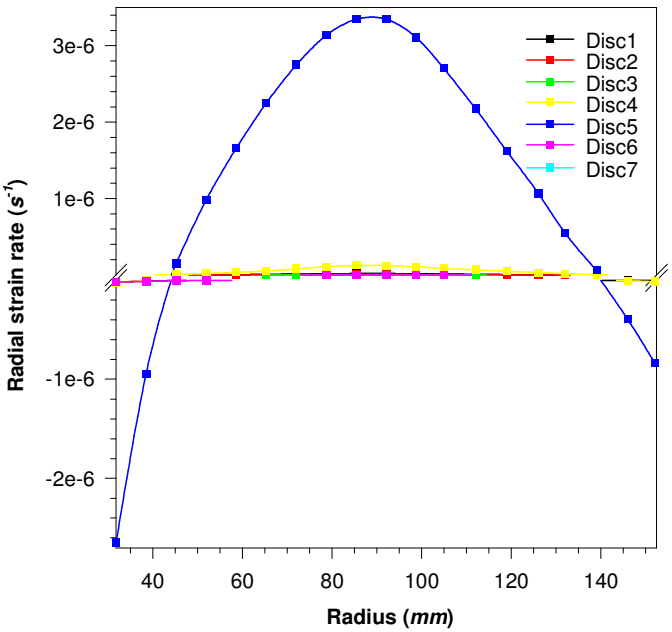

Fig. 5.7: Effect of varying anisotropy on radial strain rate in FGM discs (k = -0.6, m = -1.8295, Disc RPM = 15000)

5.6.3 Effect of Varying the Ratios of Yield Strengths on Strain Rates

As revealed from the above discussion that in orthotropic disc7, the strain rates remain zero owing to the condition $\bar{\sigma} < \sigma_0$. In the light of this fact, it would be worthwhile to investigate the influence of increasing $\sigma_{ry}/\sigma_{\theta y}$ ratio in orthotropic disc wherein the yield strengths increase in the order $\sigma_{ry} < \sigma_{\theta y} < \sigma_{zy}$ (as in disc7). The purpose of increasing $\sigma_{ry}/\sigma_{\theta y}$ ratio is to determine the threshold value of $\sigma_{ry}/\sigma_{\theta y}$ beyond which the creep will begin in the selected type of orthotropic FGM disc. After a few trials, it was observed that in orthotropic disc (with $\sigma_{ry} < \sigma_{\theta y} < \sigma_{zy}$) when the ratios σ_{ry}/σ_{zy}, $\sigma_{\theta y}/\sigma_{zy}$ and $\sigma_{ry}/\sigma_{\theta y}$ are 0.8246, 0.8700 and 0.9478, respectively, the creep rates are noticed to be zero throughout the disc. Taking this disc as a reference (referred to as disc of typeI) and fixing the σ_{ry}/σ_{zy} ratio as 0.8246, the ratio of yield strengths $\sigma_{\theta y}/\sigma_{zy}$ was decreased, which resulted simultaneous increase in $\sigma_{ry}/\sigma_{\theta y}$ ratio. Four different types of such discs (discI-discIV), with increasing $\sigma_{ry}/\sigma_{\theta y}$ ratio, have been considered (Table-5.3) and the tangential and radial strain rates have been estimated and compared in these discs, to investigate the role of increasing $\sigma_{ry}/\sigma_{\theta y}$ ratio on strain rates in the orthotropic FGM disc with $\sigma_{ry} < \sigma_{\theta y} < \sigma_{zy}$.

Table 5.3: Effect of varying $\sigma_{\theta y}$ in orthotropic disc $(\sigma_{zy} = 1)$

Disc Type	σ_{ry}/σ_{zy}	$\sigma_{\theta y}/\sigma_{zy}$	$\sigma_{ry}/\sigma_{\theta y}$
I	0.8246	0.8700	0.9478
II	0.8246	0.8699	0.9479
III	0.8246	0.8643	0.9540
IV	0.8246	0.8440	0.9770

It is observed that on increasing the ratio $\sigma_{ry}/\sigma_{\theta y}$, the FGM disc starts to creep along the radial as well as tangential directions (Figs. 5.8-5.9). The order of strain rates increase with further increase in $\sigma_{ry}/\sigma_{\theta y}$ ratio. In orthotropic disc of type-II, a very low magnitude of radial creep rate (of the order of 10^{-30}) with tensile nature is observed somewhere in the middle, though no creep appears in rest of the disc (Fig. 5.8). If the ratio $\sigma_{ry}/\sigma_{\theta y}$ is further increased (as in discs of type-III and IV), the radial creep is observed to occur throughout the

disc besides increase in the order of radial creep rate, with compressive nature near the inner and the outer disc radii but tensile nature in some portion in the middle of the disc. However, the magnitude of radial strain rate in type-III disc is quite small (of the order of 10^{-18}) when compared to those observed in type-IV disc (order of radial strain rate $\cong 10^{-15}$), which has $\sigma_{ry}/\sigma_{\theta y}$ close to unity (=0.9770). The tangential strain rate, which remains tensile throughout, is also observed to increase with the increase in $\sigma_{ry}/\sigma_{\theta y}$ ratio (Fig. 5.9). Some significant tangential strain rate is noticed in orthotropic discs of type-III and type-IV. Similar to radial strain rate, the tangential strain rate is also observed to be the highest in type-IV disc. The tangential strain rate in type-IV orthotropic disc is higher by about three orders of magnitude than that noticed in type-III orthotropic disc. Thus, in order to keep both the radial and tangential strain rates in the orthotropic FGM disc at zero level, the ratio of yield strength $\sigma_{ry}/\sigma_{\theta y}$ must be kept ≤ 0.9478.

In order to assess the role of simultaneously varying the yield strengths σ_{ry} and $\sigma_{\theta y}$, but keeping the constant value of $\sigma_{ry}/\sigma_{\theta y}$ $(=0.9770)$, on creep rates in orthotropic FGM disc of type-IV, two different cases of type-IV disc have been considered: Case(a): σ_{ry} = 0.8246 and $\sigma_{\theta y}$ =0.8440, and Case(b): σ_{ry} = 0.85 and $\sigma_{\theta y}$ =0.87. The radial and tangential strain rates corresponding to both the cases have been estimated and compared in Figs. 5.10 and 5.11 respectively. The strain rates in type-IV orthotropic FGM disc corresponding to case(a) is lower by about two orders magnitude than that observed in similar type of disc but corresponding to case(b). Thus, in order to reduce the creep rates in orthotropic FGM disc of type-IV ($\sigma_{ry} < \sigma_{\theta y} < \sigma_{zy}$), the disc having lower yield strengths along the radial and tangential directions performs better, provided the ratio of $\sigma_{ry}/\sigma_{\theta y}$ is kept constant.

The study concludes that the steady state creep behavior of a rotating FGM disc is significantly affected by varying the anisotropy of the disc material, which depends on the ratios of yield strengths. If during the processing of the disc, the alignment of reinforcement is controlled in such a way that the yield strength is maximum along the axial direction and minimum along the radial direction, the creep deformations in the FGM disc could reduced appreciably.

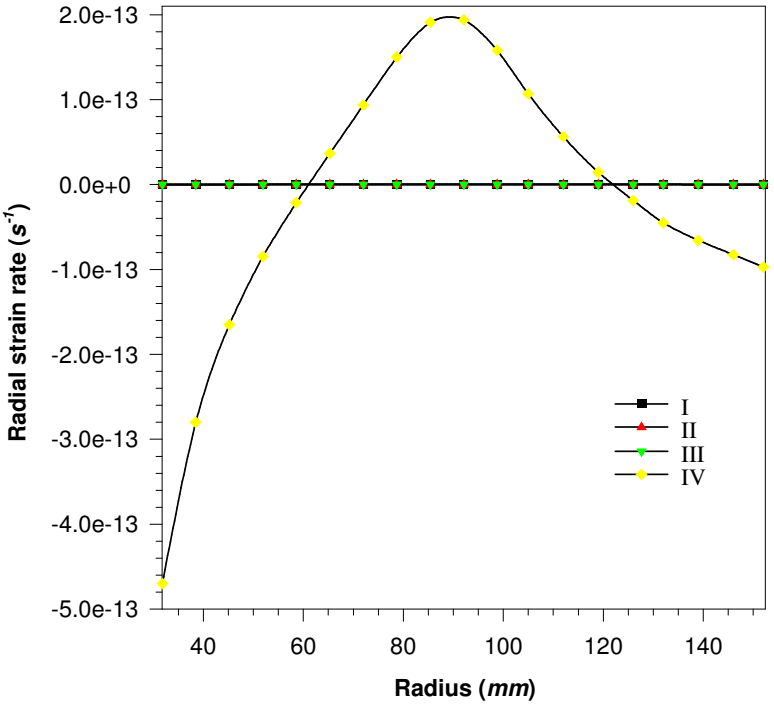

Fig. 5.8: Effect of varying $\sigma_{ry}/\sigma_{\theta y}$ ratio on radial strain rate in FGM discs (k = -0.6, m = -1.8295, Disc RPM = 15000)

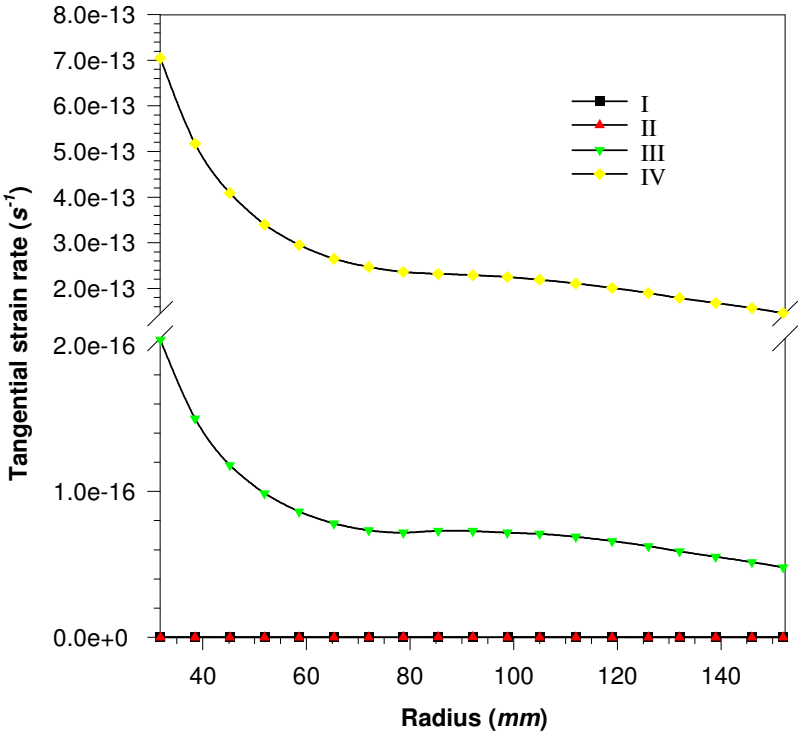

Fig. 5.9: Effect of varying $\sigma_{ry}/\sigma_{\theta y}$ ratio on tangential strain rate in FGM discs (k = -0.6, m = -1.8295, Disc RPM = 15000)

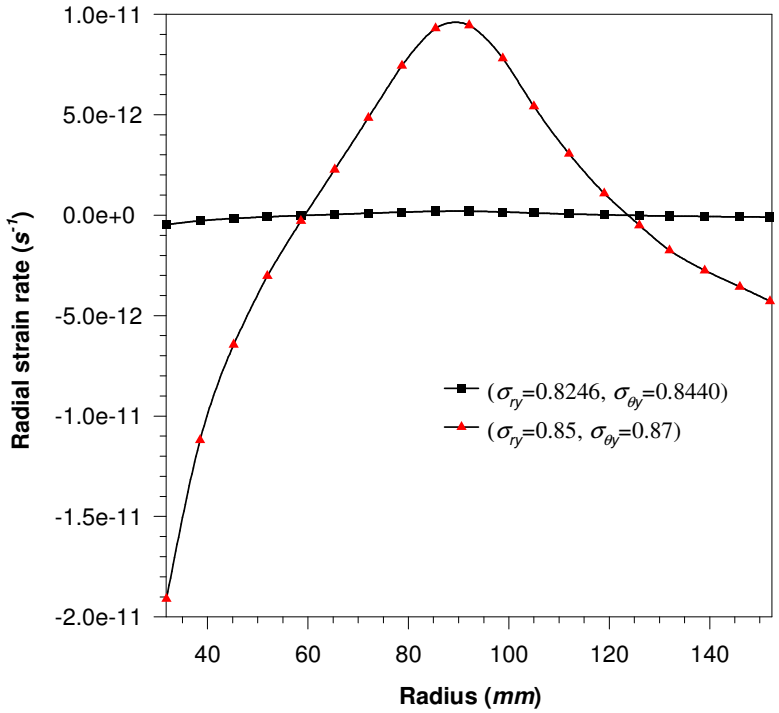

Fig. 5.10: Effect of varying the extent of anisotropy for constant $\sigma_{ry}/\sigma_{\theta y}$ ratio (=0.9770) on radial strain rate in type-IV orthotropic FGM disc (k = -0.6, m = -1.8295)

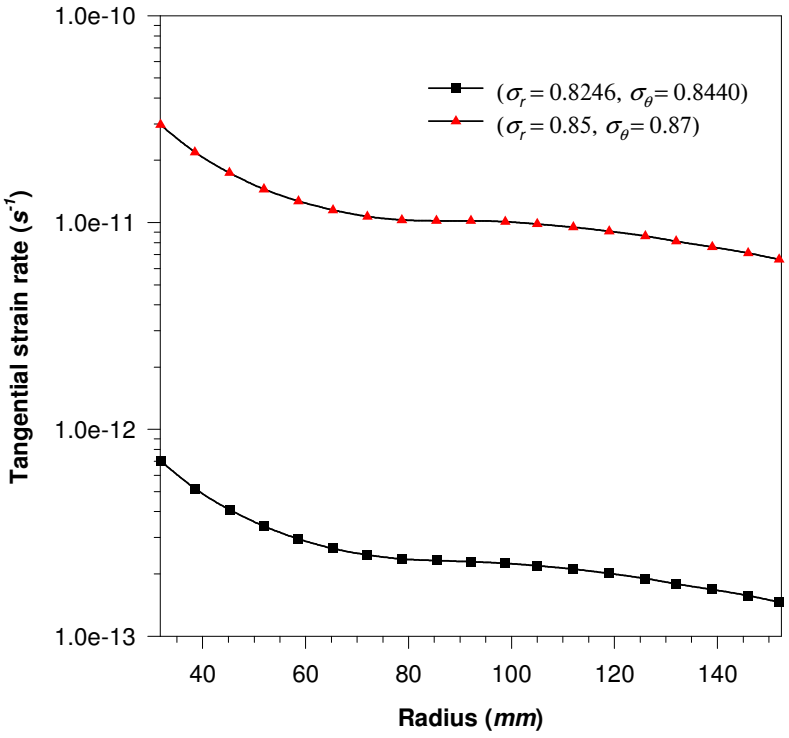

Fig. 5.11: Effect of varying the extent of anisotropy for constant $\sigma_{ry}/\sigma_{\theta y}$ ratio (=0.9770) on tangential strain rate in type-IV orthotropic FGM disc(k = -0.6, m = -1.8295)

CHAPTER-6

CREEP ANALYSIS IN VARIABLE THICKNESS ROTATING FGM DISC USING SETH's TRANSITION THEORY

6.1 INTRODUCTION

The problem of creep in a rotating FGM disc using classical theory has been addressed in Chapters 3-5. The literature review reveals that a few researchers have analyzed stresses and deformations (elastic-plastic / creep) in a rotating disc using Seth's transition theory [Shukla (1996), Gupta *et al*. (2000a, 2000b), Gupta and Pankaj (2007a), Pankaj and Bansal (2008b), Sharma and Sahni (2008), Thakur (2010a), Sharma *et al*. (2013)].

Seth's transition theory does not require a number of assumptions like yield criterion, incompressibility condition etc., as made during the analysis of creep in rotating disc based on classical approach. This theory uses the concept of generalized strain measure and asymptotic solution at turning (transition) points of the governing differential equations describing the deformed field. The theory has been successfully applied to a large number of problems in plasticity and creep [Gupta and Shukla (1994)]. An attempt, therefore, has been made in this chapter to implement Seth's transition theory for analyzing steady state creep in a variable thickness rotating disc made of functionally graded composite. The thickness of the disc and variation of reinforcement (SiC_p) in composite disc are assumed to vary radially according to a power law functions. The results are estimated for FGM disc having different types of reinforcement gradation and are compared with similar disc having radially uniform distribution of reinforcement.

6.2 DISC PROFILE AND DISTRIBUTION OF REINFORCEMENT

For the purpose of analysis, the disc dimensions and the distribution of SiC_p reinforcement in the FGM disc are taken similar to those given in Chapter 4. Thus, the inner (a) and outer (b) radii are taken, respectively, as 31.75 *mm* and 152.4 *mm*. Similar to Eq. (4.1), the disc thickness, $h(r)$, at any radius, (r), is assumed to vary according to the following power law relation,

$$h(r) = h_b \left(\frac{r}{b} \right)^k \tag{6.1}$$

where k is the thickness gradation index and h_b is the disc thickness at the outer radius.

As in Chapter-4, the disc is assumed to rotate at 15000 *rpm* and its material is taken as Al-SiC_p composite wherein the content of SiC_p is assumed to decrease radially from V_{max} to V_{min}, as one moves from the inner to outer radius. The content of SiC_p, $V(r)$, at any radius, r, is assumed to vary according to power law given in Eq. (4.3), and reproduced below,

$$V(r) = V_{\min} \left(\frac{r}{b} \right)^m \tag{6.2}$$

where m is the reinforcement gradation index.

It is evident from above equation that as the index m changes, the radial distribution of SiC_p in the FGM disc will also change. But for $m = 0$, the content of SiC_p remains uniform (V_{avg}) over the entire disc radius. The content V_{avg} is the average content of SiC_p in the FGM disc. Following the procedure given in Section 4.3, one gets the following relation between V_{min} and V_{avg}, and reproduced below,

$$V_{\min} = \frac{[(2+m+k)b^m(b^{k+2} - a^{k+2})V_{avg}]}{[(2+k)(b^{2+m+k} - a^{2+m+k})]} \tag{6.3}$$

where V_{min} is the content of SiC_p at the outer disc radius.

In the FGM disc, the properties like density (ρ) and Young's modulus (E), will vary due to radially varying SiC_p content. The density and Young's modulus are assumed to vary radially according to following power relation,

$$\rho(r) = \rho_0 \left(\frac{r}{b} \right)^{n_1} \tag{6.4}$$

$$E(r) = E_0 \left(\frac{r}{b} \right)^{n_2} \tag{6.5}$$

where ρ_0 and E_0 are the density and Young's modulus, respectively, at the outer radius of the FGM disc and exponents n_1 and n_2 are the gradation indices for density and Young's modulus, respectively.

6.3 MATHEMATICAL FORMULATION

Assuming the thickness of the disc to be very small compared to its diameter, the axial stress (σ_z) is taken as zero in the disc [(Gupta *et al*. (2005a), Deepak *et al*. (2010a)].

According to Seth (1966), the generalized principal strain measure is given by,

$$e_{ii} = \int_0^{e_{ii}^A} \left[1-2e_{ii}^A\right]^{\frac{n_m}{2}-1} de_{ii}^A = \frac{1}{n_m}\left[1-(1-2e_{ii}^A)^{\frac{n_m}{2}}\right], \qquad (i=1,2,3) \tag{6.6}$$

where e_{ii}^A are the principle Almansi finite strain components and n_m is the measure.

The components of generalized strain in cylindrical polar co-ordinate system are [Gupta and Shukla (1994)],

$$\begin{aligned} e_r &= \frac{1}{n_m^{m_I}}\left[1-(r\beta^{'}+\beta)^{n_m}\right]^{m_I} \\ e_\theta &= \frac{1}{n_m^{m_I}}\left[1-\beta^{n_m}\right]^{m_I} \\ e_z &= \frac{1}{n_m^{m_I}}\left[1-(1-d)^{n_m}\right]^{m_I} \\ \gamma_{r\theta} &= \gamma_{\theta z} = \gamma_{zr} = 0 \end{aligned} \tag{6.7}$$

where e is the normal strain, γ is the shear strain, β is the function of radius, *r, d* is a constant, m_I is the irreversibility index and $\beta^{'} = d\beta/dr$. The value of $m_I = 1$, for steady state creep [Gupta and Dharmani (1979)].

The stress-strain relations for an isotropic material in cylindrical polar-coordinate system are given by [Dieter (1988)],

$$\sigma_r = \frac{E(r)}{(1-v^2)}\left[e_r + v\, e_\theta\right] \tag{6.8}$$

$$\sigma_\theta = \frac{E(r)}{(1-v^2)}\left[e_\theta + v\, e_r\right] \tag{6.9}$$

where v is the Poisson's ratio, and σ_r and σ_θ are the radial and tangential stresses, respectively.

The Poisson's ratio (v) for the FGM disc can be taken constant since its variation is practically insignificant as compared to variation in other material properties, like Young's modulus and density.

Substituting the values of strain components from set of Eqs. (6.7) into Eqs. (6.8) and (6.9), one gets,

$$\sigma_r = \frac{E(r)}{n_m(1-v^2)}\left[(1+v)-\beta^{n_m}\{(1+P)^{n_m}+v\}\right] \tag{6.10}$$

$$\sigma_\theta = \frac{E(r)}{n_m(1-v^2)}\left[(1+v)-\beta^{n_m}\{1+v(1+P)^{n_m}\}\right] \tag{6.11}$$

where $P = r\beta'/\beta$ is a function of β.

The force equilibrium equation for a variable thickness FGM disc rotating with angular velocity ω, is given by [Deepak *et al.* (2010a)],

$$\frac{d}{dr}[rh(r)\sigma_r]-h(r)\sigma_\theta+\rho(r)\omega^2 r^2 h(r)=0 \tag{6.12}$$

As given in the previous Chapters 3-5, the present study also assumes that the disc is free-free conditions, given by,

$$\sigma_r = 0 \text{ at } r=a \text{ and } \sigma_r = 0 \text{ at } r=b \tag{6.13}$$

Substituting Eqs. (6.1), (6.4), (6.10) and (6.11) into Eq. (6.12), one gets the following non-linear differential equation in β,

$$\begin{aligned} n_m\beta^{n_m+1}(1+P)^{n_m-1}P\frac{dP}{d\beta} &= \beta^{n_m}(1-v)[1-(1+P)^{n_m}]+k[(1+v)-\beta^{n_m}(1-v)\{(1+P)^{n_m}+v\}] \\ &\quad -n_m\beta^{n_m}P\{v+(1+P)^{n_m}\}+n_2[(1+v)-\beta^{n_m}\{v+(1+P)^{n_m}\}] \\ &\quad +\frac{\rho_0\omega^2 n_m(1-v^2)b^{n_2-n_1}r^{2+n_1-n_2}}{E_0} \end{aligned} \tag{6.14}$$

The transition points of β in the above equation are P = -1, 0 and $\pm\infty$ [Shukla (1996)].

6.3.1 Solution for Estimating Stresses

Transitional creep stresses for steady state of creep in rotating disc are obtained by taking the asymptotic solution through the stress difference ($\sigma_r-\sigma_\theta$) at the transition point

$P \to -1$ [Shukla (1997)]. Subtracting Eq. (6.11) from Eq. (6.10) and putting P = -1, the transition function (f) is obtained as,

$$f = \sigma_r - \sigma_\theta = \frac{E\beta^{n_m}}{n_m(1+v)}[1-(1+P)^{n_m}] \tag{6.15}$$

Taking log of Eq. (6.15) and differentiating with respect to r, one gets,

$$\frac{d(\log f)}{dr} = \frac{(n_m P + n_2)[1-(1+P)^{n_m}] - n_m(1+P)^{n_m-1}\beta P\frac{dP}{d\beta}}{r[1-(1+P)^{n_m}]} \tag{6.16}$$

Substituting the value $\frac{dP}{d\beta}$ from Eq. (6.14) into Eq. (6.16) corresponding to the transition points $P \to -1$ [Pankaj and Sonia (2008)], one obtains,

$$\frac{d(\log f)}{dr} = \frac{1}{r}\left[\begin{array}{l}(n_2 - n_m - n_m v - 1 + v) - \dfrac{k[(1+v)-v\beta^{n_m}]}{\beta^{n_m}} - \dfrac{n_2[(1+v)-v\beta^{n_m}]}{\beta^{n_m}} \\ -\dfrac{\rho_0\omega^2 n_m(1-v^2)b^{n_2-n_1}\, r^{2+n_1-n_2}}{E_0\beta^{n_m}}\end{array}\right] \tag{6.17}$$

As $P \to -1$, $\beta \to D/r$, where D is a constant and its value is 1.0, as reported by Pankaj and Bansal (2008a). Therefore, at transition point $P \to -1$, Eq. (6.17) becomes,

$$\frac{d(\log f)}{dr} = \frac{1}{r}\left[\alpha_1 + \alpha_2 r^{n_m} + \alpha_3 r^{2+n_m+n_1-n_2}\right] \tag{6.18}$$

where,

$$\alpha_1 = (n_2 - n_m - 1) + v(1 - n_m + k + n_2), \qquad \alpha_2 = -\frac{(1+v)(n_2+k)}{D^{n_m}},$$

and,

$$\alpha_3 = \frac{-\rho_0\omega^2 n_m(1-v^2)b^{n_2-n_1}}{E_0 D^{n_m}}$$

Integrating Eq. (6.18) with respect to r,

$$f = \sigma_r - \sigma_\theta = A r^{\alpha_1}\exp(\chi) \tag{6.19}$$

where A is a constant of integration and $\chi = (\alpha_4 r^{n_m} + \alpha_5 r^{2+n_m+n_1-n_2})$ wherein $\alpha_4 = \frac{\alpha_2}{n_m}$ and $\alpha_5 = \frac{\alpha_3}{(2+n_m+n_1-n_2)}$

The equilibrium Eq. (6.12) is simplified as,

$$\frac{d}{dr}\left[h(r)\sigma_r\right] + \frac{h(r)}{r}(\sigma_r - \sigma_\theta) + \rho(r)\omega^2 r h(r) = 0 \tag{6.20}$$

Substituting Eqs. (6.1), (6.4) and (6.19) into the equilibrium Eq. (6.20) and integrating the resulting equation yields,

$$h(r)\sigma_r = -\frac{Ah_b}{b^k}\int r^{k+\alpha_1-1}\exp(\chi)\,dr - \frac{\rho_0\omega^2 h_b r^{2+n_1+k}}{b^{n_1+k}(2+n_1+k)} + B \tag{6.21}$$

where B is a constant of integration.

Substituting the free-free boundary conditions [Eq. (6.13)] into Eq. (6.21), the constants of integration A and B are obtained as,

$$A = \frac{\rho_0\omega^2 (a^{2+n_1+k} - b^{2+n_1+k})}{b^{n_1}(2+n_1+k)\int_a^b r^{k+\alpha_1-1}\exp(\chi)\,dr}$$

$$B = \frac{Ah_b}{b^k}\int_{r=b} r^{k+\alpha_1-1}\exp(\chi)\,dr + \frac{\rho_0\omega^2 h_b b^{2+n_1+k}}{b^{n_1+k}(2+n_1+k)}$$

Putting the above values A and B in Eq. (6.21), the radial stress (σ_r) stress in the disc is obtained as,

$$\sigma_r = \frac{\rho_0\omega^2 (a^{2+n_1+k} - b^{2+n_1+k})\int_r^b r^{k+\alpha_1-1}\exp(\chi)\,dr}{r^k b^{n_1}(2+n_1+k)\int_a^b r^{k+\alpha_1-1}\exp(\chi)\,dr} + \frac{\rho_0\omega^2 (b^{2+n_1+k} - r^{2+n_1+k})}{b^{n_1} r^k (2+n_1+k)} \tag{6.22}$$

Substituting the value of constant A, in Eq. (6.19), the tangential (σ_θ) stress is obtained as,

$$\sigma_\theta = \sigma_r - \frac{\rho_0\omega^2 (a^{2+n_1+k} - b^{2+n_1+k}) r^{\alpha_1}\exp(\chi)}{b^{n_1}(2+n_1+k)\int_a^b r^{k+\alpha_1-1}\exp(\chi)\,dr} \tag{6.23}$$

In order to convert stresses in non-dimensional form, the following non-dimensional terms are introduced,

$$R_0 = \frac{a}{b},\ R = \frac{r}{b},\ \bar{\sigma}_r = \frac{\sigma_r}{E_0},\ \bar{\sigma}_\theta = \frac{\sigma_\theta}{E_0},\ \Omega^2 = \frac{\rho_0 \omega^2 b^2}{E_0}$$

Using the above mentioned non-dimensional terms in Eqs. (6.22) and (6.23), the non-dimensional radial ($\bar{\sigma}_r$) and tangential ($\bar{\sigma}_\theta$) stresses are obtained as below,

$$\bar{\sigma}_r = \frac{\Omega^2 (R_0^{\,2+n_1+k} - 1)\int_R^1 R^{k+\alpha_1-1} \exp(\psi)\, dR}{R^k (2+n_1+k)\int_{R_0}^1 R^{k+\alpha_1-1} \exp(\psi)\, dR} + \frac{\Omega^2 (1 - R^{2+n_1+k})}{R^k (2+n_1+k)} \tag{6.24}$$

$$\bar{\sigma}_\theta = \bar{\sigma}_r - \frac{\Omega^2 (R_0^{\,2+n_1+k} - 1) R^{\alpha_1} \exp(\psi)}{(2+n_1+k)\int_{R_0}^1 R^{k+\alpha_1-1} \exp(\psi)\, dR} \tag{6.25}$$

where $\psi = \alpha_6 R^{n_m} + \alpha_7 R^{2+n_m+n_1-n_2}$, $\alpha_6 = \alpha_4 b^{n_m}$ and $\alpha_7 = \alpha_5 b^{2+n_m+n_1-n_2}$.

6.3.2 Estimation of Strain Rates

As the creep sets in, the strains are replaced by the strain rates. Therefore, the generalized stress-strain relation is given by [Gupta *et al*. (2000a)],

$$\dot{e}_{ij} = \frac{1+v}{E}\sigma_{ij} - \frac{v}{E}\delta_{ij}\Theta \tag{6.26}$$

where $\dot{e}_{ij}$ is the strain rate tensor and $\Theta = \sigma_r + \sigma_\theta$ (for plane stress condition *i.e.* $\sigma_z = 0$).

In order to estimate tangential strain rate in the disc, differentiating Eq. (6.7) with respect to time and substituting, $m_I = 1$, for steady state creep),

$$\dot{\varepsilon}_\theta = -\beta^{n_m - 1}\dot{\beta} \tag{6.27}$$

For Swainger's measure ($n_m = 1$), Eq. (6.27) becomes,

$$\dot{\varepsilon}_\theta = -\dot{\beta} \tag{6.28}$$

Corresponding to transition point $P \to -1$, Eq. (6.15) leads to,

$$\beta = \left[\frac{n_m (1+v)}{E}\right]^{1/n_m} (\sigma_r - \sigma_\theta)^{1/n_m} \tag{6.29}$$

Substituting Eqs. (6.27), (6.28) and (6.29) into Eq. (6.26), the radial ($\dot{\varepsilon}_r$) and tangential ($\dot{\varepsilon}_\theta$) strain rates in the disc are obtained as,

$$\dot{\varepsilon}_r = [n_m(\bar{\sigma}_r - \bar{\sigma}_\theta)(1+v)]^{\frac{1}{n_m}-1}(\bar{\sigma}_r - v\bar{\sigma}_\theta) \tag{6.30}$$

$$\dot{\varepsilon}_\theta = [n_m(\bar{\sigma}_r - \bar{\sigma}_\theta)(1+v)]^{\frac{1}{n_m}-1}(\bar{\sigma}_\theta - v\bar{\sigma}_r) \tag{6.31}$$

The distributions of non-dimensional radial ($\bar{\sigma}_r$), and tangential ($\bar{\sigma}_\theta$) stresses in the FGM disc can be estimated from Eqs. (6.24) and (6.25), respectively. Using these values of stresses, the strain rates $\dot{\varepsilon}_r$ and $\dot{\varepsilon}_\theta$ in the FGM disc, are obtained, respectively, from Eqs. (6.30) and (6.31).

6.4 RESULTS AND DISCUSSION

Based on the analysis given in Section 6.3, a computer code has been developed to estimate the distributions of steady-state creep stresses and strain rates in variable thickness FGM disc for different values of reinforcement gradation index (*m*), as given in Eq. (6.2). But, before discussing the results obtained, it is necessary to establish the validity of the analysis carried out and the computer code developed.

6.4.1 Validation

For the purpose of validation, the distribution of non-dimensional tangential stress ($\bar{\sigma}_\theta$) has been estimated for a variable thickness disc having uniform distribution of reinforcement. The results estimated are compared with those published by Gupta *et al.* (2000a) based on Seth's transition theory for similar type of disc. The values of various parameters used during the course of validation process are taken from the published work [Gupta *et al.* (2000a)] and are given in Table 6.1.

Table 6.1: Parameters used for validation

Radius (Non-dimensional): $R_i = 0.5,\ R_0 = 1$ Measure: n_m = 1/3, 1/5 Non-dimensional angular speed: $\Omega^2 = 5$	Poisson's ratio: $v = 0.5$ Density Index: $n_1 = 0$ Index for Young's modulus: $n_2 = 0$ Disc thickness index: $k = -1$

It is observed from Fig. 6.1 that the trend as well as the values of non-dimensional tangential stress, estimated by using the present analysis and those reported by Gupta *et al.* (2000a) are in close agreement for both the values of measure n_m. The variation noticed between the tangential stress estimated from the present study and the earlier study of Gupta *et al.* (2000a) is noticed to be less than 3.8%, which establishes the validity of the analysis scheme carried out and computer code developed in this study.

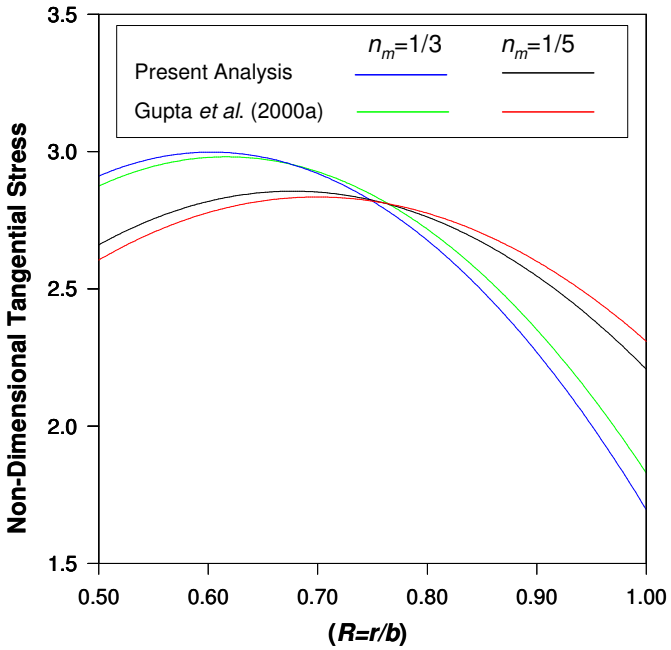

Fig. 6.1: Comparison of non-dimensional tangential stress estimated from the present analysis and reported by Gupta *et al*. (2000a)

6.4.2 Effect of Varying Reinforcement Gradient on Creep Response

In order to investigate the effect of varying SiC_p gradient on creep response of the composite disc, the results are estimated for four types of discs having different radial distributions of SiC_p reinforcement (Table 6.2), which is obtained by varying the value of reinforcement gradation index (m). However, all the discs are assumed to have the same thickness profile (Fig. 6.2), which corresponds to thickness index (k) = -0.6 and h_b = 19.1 *mm* (Eq. 6.1). The thickness of the disc decreases non-linearly on moving from the inner to outer radius. The purpose of selecting k = -0.6 is because minimum creep rate is observed for this value of k, as mentioned in Section 4.5.1. The distribution of SiC_p reinforcement in the disc becomes steeper as the value of reinforcement gradation index (m) increases from 0 to -1.5 (Fig. 6.3). The composite disc D1 with m = 0, has uniform distribution of SiC_p over the entire radius. Thus in order to keep the same average content of SiC_p (V_{avg}=20 *vol%*), the content of SiC_p increases near the inner radius but decreases towards outer radius of the FGM discs D2-

D4, as the value of reinforcement gradation index (m) increases. Further, the SiC_p gradient (PG), defined as the difference of maximum (V_{max}) and minimum (V_{min}) content of SiC_p reinforcement in the discs, increases from 0 to 71.12 (*vol %*) as the value of reinforcement gradation index (m) increases from 0 to -1.5 (Table 6.2).

The values of density (ρ) and Young's modulus (E), required during the estimation of stresses and strain rates in various composite discs D1-D4, are calculated from rule of mixture, as given in Eq. 4.6. For this purpose, the density of Al and SiC_p are taken respectively as $2698.9\,kg/m^3$ and $3210\,kg/m^3$ [Gupta *et al.* (2005a)] whereas the value of Young's modulus for Al and SiC_p are taken as 70 *GPa* [Clyne and Withers (1993)] and 410 *GPa* [Budinski (2000)], respectively. As during the computation process, the density $\rho(r)$ and Young's modulus $E(r)$ are to be expressed in the form of power law Eqs. (6.4) and (6.5), respectively. Therefore, the values of $\rho(r)$ and $E(r)$, estimated from the rule of mixture, at different radius of the disc are fitted in the form of Eqs. (6.4)-(6.5) using regression analysis in DATAFIT software. The developed regression equations yielded the values of constants ρ_0, E_0, n_1 and n_2 for different discs, as given in Table 6.2. As a result of radially decreasing SiC_p content in the FGM discs D2-D4, the density (ρ) and Young's modulus (E) are also observed to decrease with increasing radius, Figs. (6.4-6.5). Unlike FGM discs D2-D4, the uniform composite disc D1 has the same value of density and Young's modulus due to constant amount of SiC_p reinforcement (20 *vol%*) throughout.

Table 6.2: Detail of FGM discs with varying reinforcement particle gradient (PG)

[Disc RPM =15000, Disc outer radius (b) = 152.4 *mm*]

Disc Notation	**Gradation Index** (m)	**Particle Gradient (PG) = (V_{max}-V_{min}) (*vol %*)**	ρ_0 (***kg/m^3***)	**Density Index** (n_1)	E_0 (***GPa***)	**Index for Young's Modulus** (n_2)	$\Omega^2 = \frac{\rho_0 \omega^2 b^2}{E_0}$
D1	0.0	0	2801.12	0	138.0	0	1.162×10^{-3}
D2	-0.5	18.0	2772.16	-0.02011	119.95	-0.2598	0.899×10^{-3}
D3	-1.0	41.4	2738.59	-0.0439	101.35	-0.5471	0.681×10^{-3}
D4	-1.5	71.12	2700.96	-0.0711	82.49	-0.8608	0.526×10^{-3}

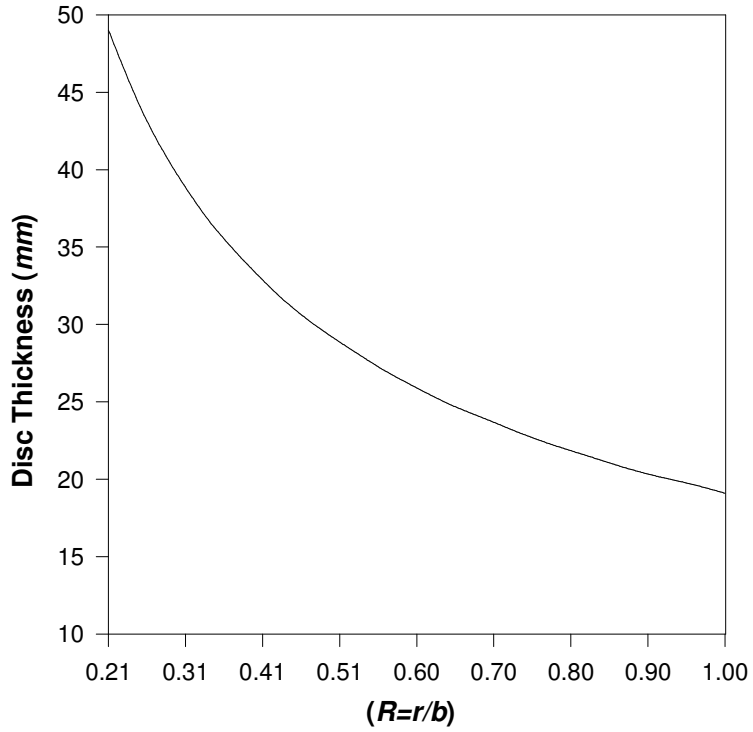

Fig. 6.2: Thickness profile of composite discs (k = -0.6)

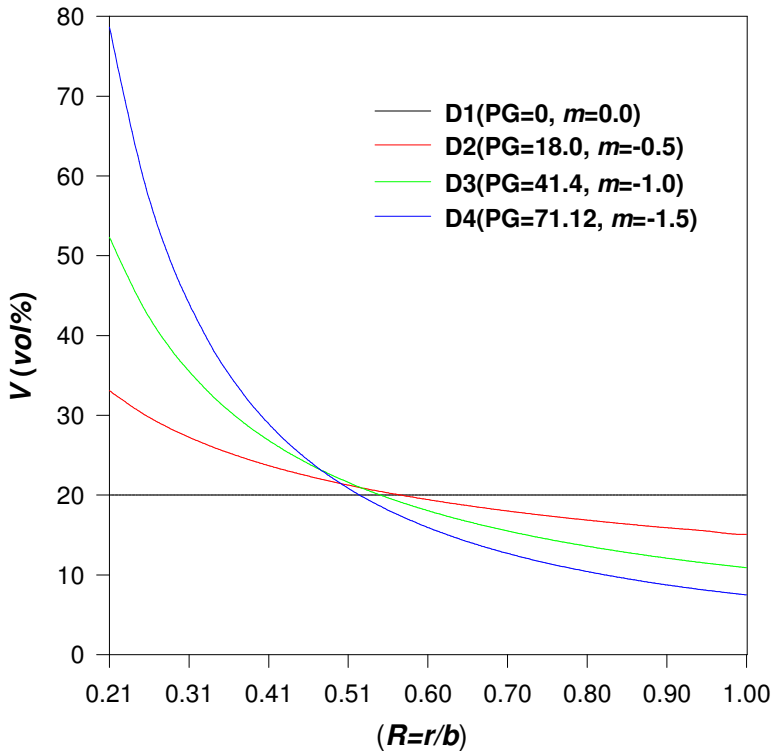

Fig. 6.3: Variation of SiC_p reinforcement in composite discs

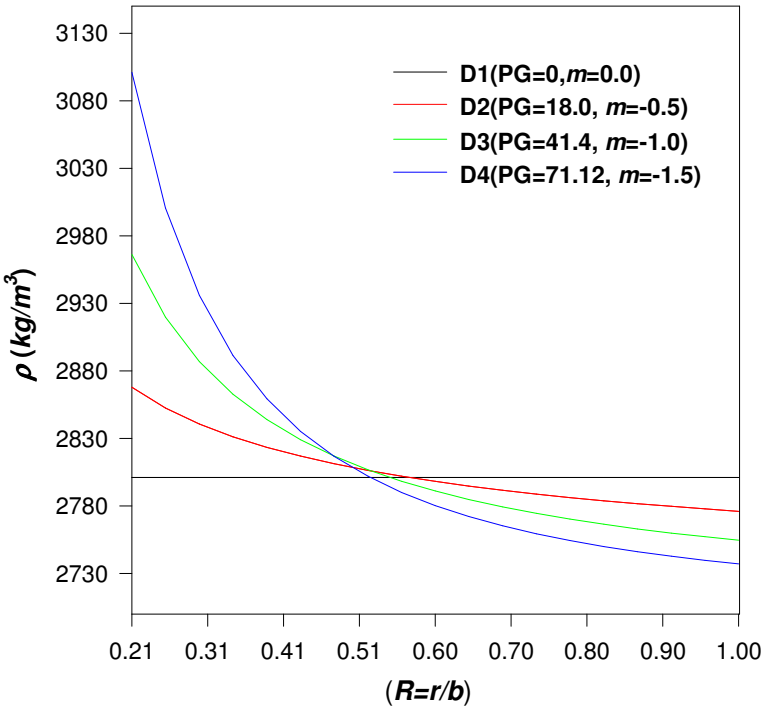

Fig. 6.4: Variation of density (ρ) in composite discs

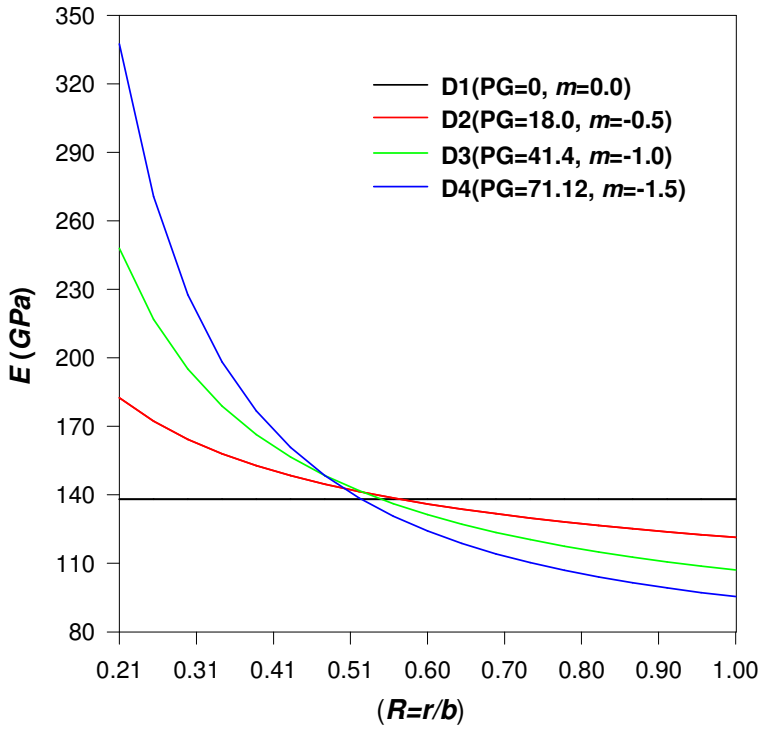

Fig. 6.5: Variation of Young's modulus (E) in composite discs

6.4.2.1 Effect of Varying Reinforcement Gradient on Stresses

The effect of varying SiC_p gradient on the distribution of non-dimensional radial stress ($\bar{\sigma}_r$) is depicted in Fig. 6.6. In all the discs, the radial stress increases from zero at the inner radius to become maximum somewhere in the middle of the disc and thereafter decreases to become zero again at the outer radius, under the imposed boundary conditions given in Eq. (6.13). The radial stress is observed to decrease with the increase in SiC_p gradient in the disc, with the maximum decrease noticed in the middle region of the disc. The maximum value of non-dimensional radial stress in the FGM disc D4 is approximately half the maximum value of non-dimensional radial stress in uniform composite disc D1.

The non-dimensional tangential stress ($\bar{\sigma}_\theta$) in discs D1-D2 increases with increasing radius, reaches a maximum value and thereafter decreases with further increase in radius (Fig 6.7). However, in the FGM discs D3-D4, the non-dimensional tangential stress is observed to reduce on moving from the inner to outer radius. The effect of varying particle gradient on the non-dimensional tangential stress is similar to those observed for non-dimensional radial stress (Fig. 6.6). The decrease observed in non-dimensional tangential stress with increasing particle gradient is less near the outer radius as compared to those observed in other region of the disc. The maximum value of non-dimensional tangential stress in FGM disc D4 is approximately half the maximum value of non-dimensional tangential stress in uniform composite disc D1.

It is evident that the radial and tangential strain rates, given by Eqs. (6.30) and (6.31) respectively, in the disc depend on the non-dimensional stress difference $(\bar{\sigma}_r - \bar{\sigma}_\theta)$. Therefore, it is important to study the effect of varying particle gradient on the non-dimensional stress difference $(\bar{\sigma}_r - \bar{\sigma}_\theta)$. As $\bar{\sigma}_r < \bar{\sigma}_\theta$ in all the discs (Figs. 6.6-6.7), thus, the stress difference $(\bar{\sigma}_r - \bar{\sigma}_\theta)$ is negative throughout in all the discs. The stress difference $(\bar{\sigma}_r - \bar{\sigma}_\theta)$ is observed to decrease with increase in radius for all the discs D1-D4 (Fig 6.8). Similar to the effect of varying particle gradient on $\bar{\sigma}_r$ and $\bar{\sigma}_\theta$, the stress difference $(\bar{\sigma}_r - \bar{\sigma}_\theta)$ also decreases with increase in particle gradient in the composite discs D1-D4. The decrease observed is almost uniform over the entire disc radius.

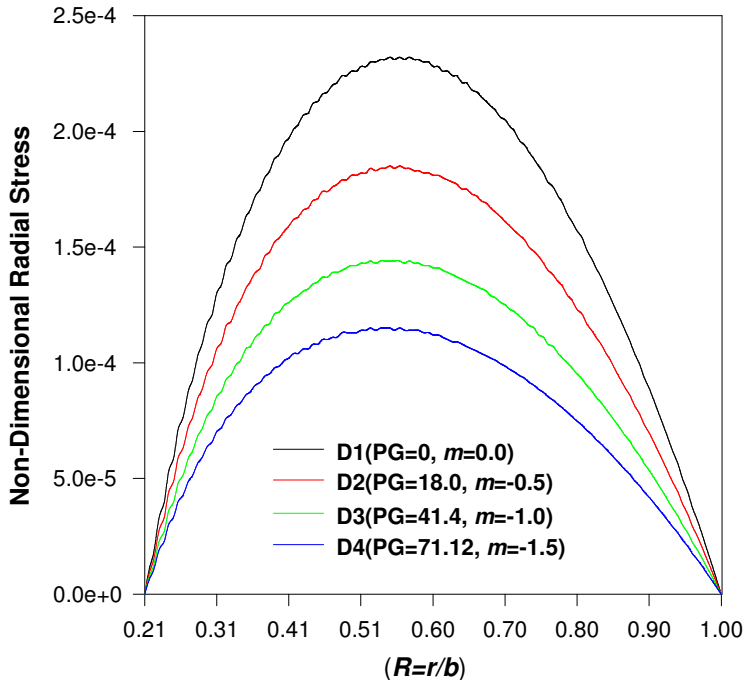

Fig. 6.6: Effect of varying SiC_p gradient (PG) on non-dimensional radial stress ($\overline{\sigma}_r$) in composite discs

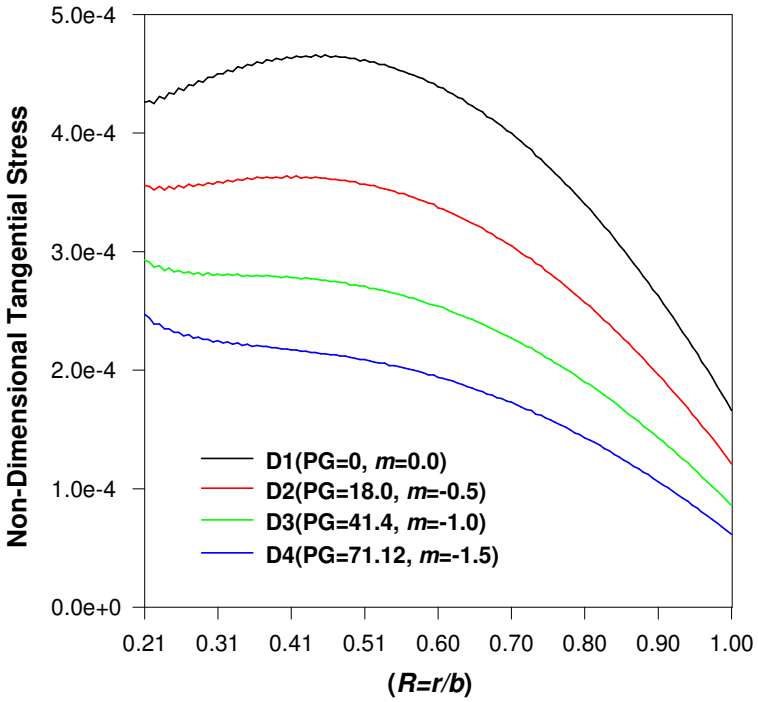

Fig. 6.7: Effect of varying SiC_p gradient (PG) on non-dimensional tangential stress ($\overline{\sigma}_\theta$) in composite discs

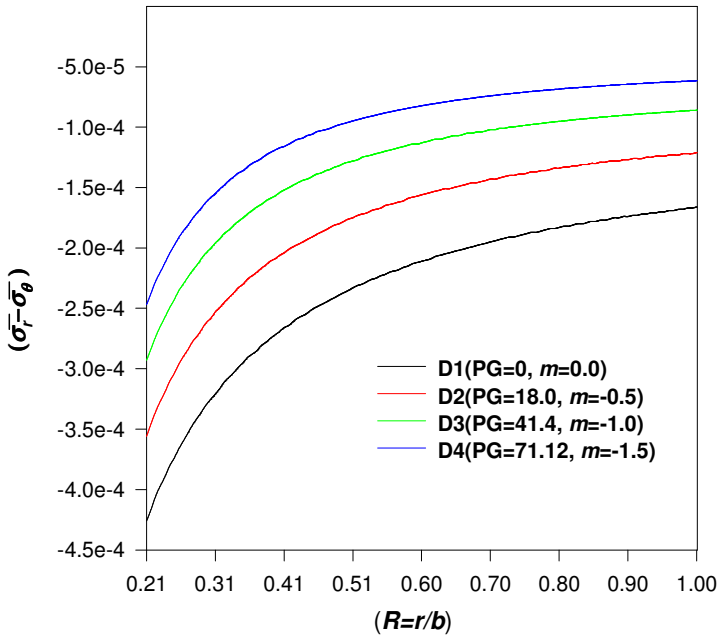

Fig. 6.8: Effect of varying SiC_p gradient (PG) on stress difference ($\bar{\sigma}_r - \bar{\sigma}_\theta$) in composite discs

6.4.2.2 Effect of Varying Reinforcement Gradient on Strain Rates

The radial strain rate (Fig. 6.9) in all the discs (D1-D4), decreases on moving from the inner to the outer radius. The radial strain rate in all the discs is maximum at the inner radius and decreases on moving towards the outer radius, reaches a minimum value (of the order of about 10^{-15} to 10^{-18}) somewhere in the middle of the disc and thereafter increases slightly on moving further towards the outer radius. It is important to mention that the nature of the radial strain rate becomes tensile in some portion in the middle of the composite discs D1-D4. Similar to the effect of varying particle gradient on stress difference ($\bar{\sigma}_r - \bar{\sigma}_\theta$), the radial strain rate is also observed to decrease with increasing SiC_p gradient in the composite disc, with a higher decrease observed at the inner radius.

The tangential strain rate (Fig. 6.10) decreases on moving from inner to outer radius in all the composite discs D1-D4. Similar to the effect of varying particle gradient on the radial strain rate (Fig. 6.9), the tangential strain rate in the composite disc also decreases with increase in SiC_p gradient in the disc. The decrease observed in tangential strain rate is more at the inner radius. The tangential strain rate in FGM disc D4 at the inner radius is lower by about one order of magnitude when compared to those observed at the inner radius of uniform composite disc D1. The decrease observed in both the strain rates (radial and

tangential) with increasing particle gradient in the composite disc, as mentioned above, is similar to those noticed in Section 4.5.2, wherein the creep analysis has been carried out using classical approach based on Tresca's yield criterion. Thus, both the approaches confirm that in order to reduce creep deformations in the composite disc it is advised to use higher reinforcement gradient while maintaining the same total amount of reinforcement.

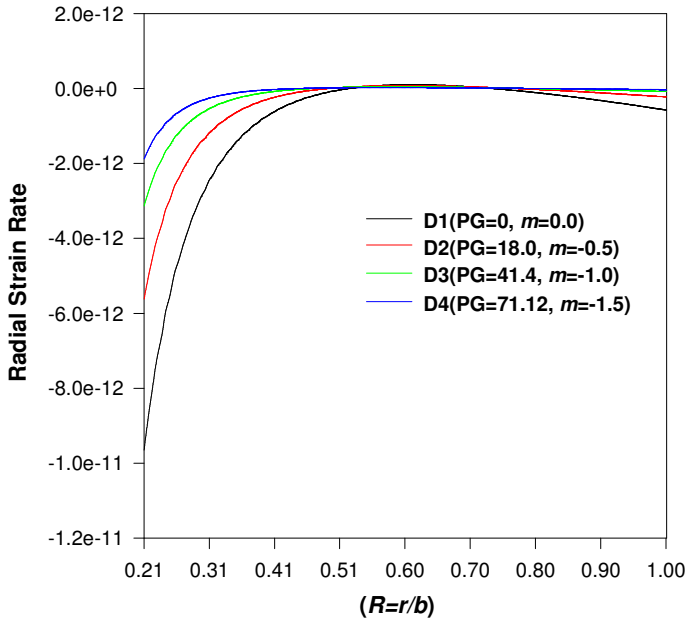

Fig. 6.9: Effect of varying SiC_p gradient (PG) on radial strain rates ($\dot{\varepsilon}_r$) in composite discs

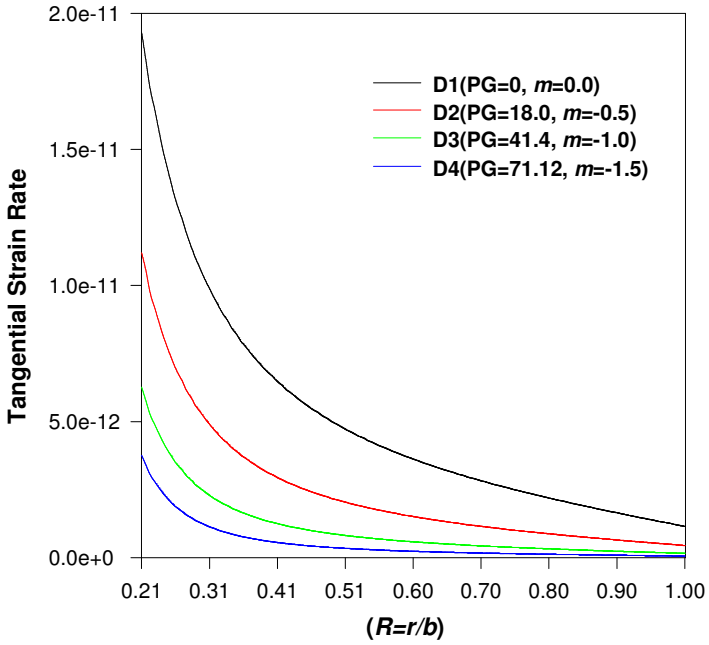

Fig. 6.10: Effect of varying SiC_p gradient on tangential strain rates ($\dot{\varepsilon}_\theta$) in composite discs

CHAPTER-7

CONCLUSIONS AND SCOPE OF FUTURE WORK

7.1 CONCLUSIONS

In the present study, the steady state creep response of a variable thickness rotating disc made of functionally graded Al-SiC_p/6061Al-SiC_w composite has been analyzed under free-free boundary conditions. The analysis given in Chapters 3-5 has been carried out using classical approach involving the use of yield criterion, creep law and incompressibilty assumption. The creep analysis has also been carried out using Seth's Transition theory (Chapter 6), which does not involve the use of semi-empirical laws, such as yield criterion and creep law, and the assumption of incompressibility condition. The conclusions drawn from the study are presented in the following sub-sections.

(A) Conclusions Based on Classical Approach

(i). The stresses and strain rates in a variables thickness FGM (Al-SiC_p) disc, with linearly decreasing SiC_p content from the inner to the outer radius, are lower than that observed in a similar FGM disc but of constant thickness. The variation observed in strain rates is maximum at the inner disc radius.

(ii). The comparison of creep results estimated using Tresca and von Mises yield criteria for a FGM disc of linearly varying thickness, indicates that:

- The tangential stress estimated using Tresca criterion is observed to decrease with increasing radius. However, the maximum tangential stress is noticed at a radius little away from the inner disc radius when the yielding is described by von Mises criterion.
- Tresca yield criterion estimates slightly lower values of tangential stress than those obtained using von Mises criterion, except for some portion near the inner and outer radii of the disc.

- The use of Tresca criteria results in slightly higher values of radial stresses than those estimated using von Mises criterion, except for some portion towards the outer radius where both the criteria estimate almost equal values of radial stress.
- The effective stress estimated using Tresca criterion is higher throughout the FGM disc when compared to those obtained using von Mises criterion. The increase observed in effective stress is higher near the inner radius than that noticed towards the outer radius.
- The tangential and radial strain rates obtained using Tresca criterion are higher over the entire disc radius than those estimated using von Mises criteria. The maximum increase in strain rates is noticed at the inner disc radius.
- The difference observed in the values of stresses and strain rates estimated using Tresca and von Mises criteria reduces with the increase in SiC_p gradient in FGM disc.
- The FGM disc designed on the basis of Tresca criterion is safer in comparison to the FGM disc designed using von Mises criterion.

(iii). The study pertaining to the effects of varying disc thickness and reinforcement (SiC_P) gradients on the steady state creep behavior of a rotating disc, yielding according to Tresca criterion, reveals that:

- On increasing the disc thickness gradient, the radial stress decreases towards the inner radius but increases towards the outer radius, with relatively higher decrease noticed towards the inner radius.
- The tangential stress decreases over the entire radius with the increase in disc thickness gradient, though the decrease observed reduces with the increasing disc radius.
- The strain rates decrease throughout with the increase in disc thickness gradient, with a significantly higher decrease observed near the inner radius. On increasing the disc thickness gradient from 0 to 29.9 *mm*, the radial and tangential strain rates are noticed to reduce by more than one order of magnitude.
- With the increase in SiC_p gradient in the FGM disc, the radial stress increases significantly throughout, with relatively higher increase in the middle.

- The tangential stress increases towards the inner radius but decreases towards the outer radius, with the increase in SiC_p gradient in the disc. The increase in tangential stress is more towards the inner radius.
- The maximum increase observed in the radial and tangential stresses is 65.5% and 151.25%, respectively, when SiC_p gradient in the disc increases from 0 to 94.33 (*vol.%*).
- With increasing SiC_p gradient in the disc, the strain rates reduce throughout, with significantly higher decrease noticed near the inner radius.
- The order of strain rates in the disc reduce by around two orders of magnitude, when SiC_p gradient in the disc increases from 0 to 94.33 (*vol.%*). On increasing SiC_p gradient in the FGM disc beyond 18*vol.%*., the nature of radial strain rate changes from compressive to small tensile in the middle of the disc.
- On increasing the thickness or reinforcement gradient in the disc, the distribution of strain rates become relatively more uniform, which reduces the chances of distortion in the disc.
- For given operating conditions, the uniform composite disc, with thickness gradient 29.9 *mm*, shows the lowest creep rates, which can be further reduced by increasing SiC_p gradient in the disc, till the disc material at the inner radius becomes pure ceramic (*i.e.* 100% SiC_p).

(iv). The study undertaken to investigate the imposition of different types of radial thermal gradients (*i.e.* linear, parabolic and exponential) on the steady state creep behavior of a variable thickness FGM disc, following Tresca yield criterion concludes that:

- In comparison to uniform temperature FGM disc, the FGM disc subjected to radial temperature profile has higher radial stress throughout and higher tangential stress near the inner radius, with the maximum stress noticed for FGM disc subjected to linear temperature gradient. However, near the outer radius, the tangential stress is minimum in the FGM disc subjected to radial thermal gradient, with the lowest stress noticed for FGM disc operating under exponential thermal gradient.

- The radial as well as tangential strain rates in the FGM disc operating under radial thermal gradient are significantly lower as compared to uniform temperature FGM disc. The maximum reduction in strain rates is observed for FGM disc operating under exponential thermal gradient.
- The imposition of exponential thermal gradient leads to relatively more uniform distribution of strain rates in the FGM disc and hence reduces the possibility of disc distortion.
- If a given FGM disc operates under different kinds of radial thermal gradients (corresponding to different values of temperature exponent, n_T), but having the same average and the fixed value of outer surface temperatures, the FGM disc with lower value of n_T exhibits the maximum creep life. On decreasing n_T from 15 to 2, the estimated creep life of the FGM disc is observed to increase from few hours to several years.

(v). The investigation dealing with the effect of varying the extent of materials' anisotropy, on the creep response of a variable thickness rotating functionally graded disc made of 6061Al-SiC_w, which yields according to Hill's yield criterion, indicates that:

- The magnitude of stresses in the FGM disc changes considerably, especially in the middle, on varying the extent of anisotropy of the disc.
- The radial stress (throughout the disc) and the tangential stress (barring some potion in the middle of the disc) are the lowest in orthotropic disc having the maximum and minimum yield strengths along the axial (z) and the tangential (θ) directions, respectively (*i.e.* yield strengths decreasing in the order $\sigma_{zy} > \sigma_{ry} > \sigma_{\theta y}$). However, in the middle region, the tangential stress is lowest in an orthotropic disc having the order of decreasing yield strength as $\sigma_{\theta y} > \sigma_{ry} > \sigma_{zy}$.
- The effective stress as well as the strain rates is the lowest in an orthotropic disc having the highest yield strength along the axial direction and the lowest yield strength along the radial direction.

- In an orthotropic disc, having the yield strengths decreasing in the order $\sigma_{zy} > \sigma_{ry} > \sigma_{\theta y}$, the strain rates are reduced to zero when the ratio of yield strengths $\sigma_{ry} / \sigma_{\theta y}$ is ≤ 0.9478.

- In an orthotropic FGM disc, with the ratio of yield strengths decreasing in the order $\sigma_{zy} > \sigma_{ry} > \sigma_{\theta y}$, the strain rates are noticed to be lower for disc having lesser yield strengths along the radial and tangential directions, although the ratio $\sigma_{ry} / \sigma_{\theta y}$ is maintained at the same level.

(B) Conclusions Based on Seth's Transition Theory

(i). The radial and tangential stresses in a variable thickness rotating Al-SiC_p disc reduce with the increase in SiC_p gradient, with maximum decrease observed somewhere in the middle region of the disc.

(ii). The radial and tangential stresses reduce by 50% as the value of SiC_p gradient increases from 0 to 71.12.

(iii). The radial as well as tangential strain rates reduce with increasing SiC_p gradient in the disc, with a higher decrease observed at the inner radius of the disc.

(iv). The radial as well as tangential strain rate in the FGM disc at the inner radius reduce by about one order of magnitude when SiC_p gradient in the disc increases from 0 to 71.12.

A better understanding of the effects of geometrical, material and operating parameters (viz. disc thickness profile, reinforcement distribution, presence of anisotropy and radial thermal gradient) on the creep response of a rotating FGM disc has evolved from the present study. The study highlights the advantage of using Tresca yield criterion for the design of rotating FGM disc. The study also demonstrates the application of Seth's transition theory for analyzing the creep problems in a rotating FGM disc. The present study emphasizes on systematically optimizing the disc design based on solid mathematical foundation rather than following ad-hoc approach. It is expected that the results obtained in the present work would help the designers in making decisions regarding the choice of disc profile and reinforcement distribution in a rotating composite disc subjected to specified thermo-mechanical loading.

7.2 SCOPE OF FUTURE WORK

The research work carried out in the present study may be extended in future on the following lines:

(i). The study may be extended to incorporate the effects of elastic deformations and transient creep. The total strain in the disc will thus be obtained by the sum of elastic and creep induced strains, which would be estimated by using separate laws *i.e.* Hook's law and creep law.

(ii). The analysis may be extended for FGM disc having substantial thickness and thus eliminating the assumption of plane stress condition. The analysis will thus consider the effect of axial stress in the FGM disc.

(iii). The effect of residual stress, as induced during the processing of FGMs, may be investigated on the creep performance of FGM disc. Such an analysis will be based on Hoffman yield criterion, which takes into account the different yield strength exhibited by the FGMs under tension and compression.

(iv). The investigations may be carried out to further optimize the disc profile and reinforcement distribution, so as to minimize the weight of FGM disc for given operating conditions. The attempts can also be made to estimate the distribution of reinforcement in the FGM disc/disc thickness profile for achieving the desired variation of stresses in the disc.

(v). Attempts may be made to develop creep analysis based on micro-mechanical approach, which would be useful in investigating the role of fiber-matrix interfacial bonding on the creep response of FGM disc. The micro-mechanical approach consists of dividing the FGM into number of unit cells, with each cell consisting of two different regions *i.e.* pure matrix region and region containing reinforcement and its surrounding matrix. The stress distribution may be computed in these two different regions and integrated to estimate the overall creep rates in different unit cells located along the different radial locations of the FGM disc.

REFERENCES

[1]. Aboudi J., Pindera M. J. and Arnold S. M. (1999), Higher-order theory for functionally graded materials, *Composites: Part B*, 30(8), 777-832.

[2]. Abrate S. (2006), Free vibration, buckling, and static deflections of functionally graded plates, *Composites Science and Technology*, 66(14), 2383-94.

[3]. Afsar A. M. and Go J. (2010), Finite element analysis of thermoelastic field in a rotating FGM circular disk, *Applied Mathematical Modelling*, 34(11), 3309-20.

[4]. Akbari M. R. and Ghanbari J. (2015), Analytical solution of thermo-elastic stresses and deformation of functionally graded rotating hollow disc with radially varying thermo-mechanical properties under internal pressure, *Computers, Materials and Continua*, 45(3), 187-201.

[5]. Alexandrova N. and Alexandrov S. (2004), Elastic-plastic stress distribution in a plastically anisotropic rotating disk, *Journal of Applied Mechanics*, 71(3), 427-29.

[6]. Ali B. and Mostefa B. (2013), Thermomechanical modelling of disc brake contact phenomena *FME Transactions*, 41(1), 59-65.

[7]. Alman D. E. (2001), Properties of Metal-Matrix Composites, ASM Handbook, 21: Composites, ASM International, Ohio, 838-58.

[8]. Altan G., Topcu M., Bektas N. B. and Altan B. D. (2008), Elastic-plastic thermal stress analysis of an aluminum composite disc under parabolic thermal load distribution, *Journal of Mechanical Science and Technology*, 22(12), 2318-27.

[9]. Arya V. K. and Bhatnagar N. S. (1979), Creep analysis of rotating orthotropic discs, *Nuclear Engineering and Design*, 55(3), 323-30.

[10]. Asghari M. and Ghafoori E. (2010), A three-dimensional elasticity solution for functionally graded rotating disks, *Composite Structures*, 92(5), 1092-99.

[11]. Bache M. R., Evans W. J. and Uygur I. (1998), Fatigue life prediction for notch geometries in particle reinforced metal matrix composites, *Journal of Material Science and Technology*, 14(9-10), 1065–69.

[12]. Backofen W. A. (1972), Deformation Processing, Addison-Wesley Publishing Company, London.

[13]. Bayat M., Sahari B. B., Saleem M., Ali A. and Wong S. V. (2009a), Thermoelastic solution of a functionally graded variable thickness rotating disk with bending based on the first-order shear deformation theory, *Thin-Walled Structures*, 47(5), 568-82.

[14]. Bayat M., Sahari B. B., Saleem M., Dezvareh E. and Mohazzab A. H. (2011), Analysis of functionally graded rotating disks with parabolic concave thickness applying an exponential function and the Mori-Tranka scheme, *Mechanics Research Communications*, 35(5), 283-309.

[15]. Bayat M., Saleem M., Sahari B. B., Hamouda A. M. S. and Mahdi E. (2009b), Mechanical and thermal stresses in a functionally graded rotating disk with variable thickness due to radially symmetry loads, *International Journal of Pressure Vessels and Piping*, 86(6), 357-72.

[16]. Bayat M., Saleem M., Sahari B. B., Hamouda A. M. S. and Mahdi E. (2008), Analysis of functionally graded rotating disks with variable thickness, *Mechanics Research Communications*, 35(5), 283-309.

[17]. Bayat M., Saleem M., Sahari, B. B., Hamouda A. M. S. and Mahdi E. (2007), Thermo elastic analysis of a functionally graded rotating disk with small and large deflections, *Thin-Walled Structures*, 45(7-8), 677-91.

[18]. Bhatnagar N. S., Kulkarni P. S. and Arya V. K. (1986), Steady state creep of orthotropic rotating disks of variable thickness, *Nuclear Engineering and Design*, 91(2), 121-44.

[19]. Bhattacharya S., Singh I. V. and Mishra B. K. (2014), Fatigue life simulation of functionally graded materials under cyclic thermal load using XFEM, *International Journal of Mechanical Sciences*, 82, 41-59.

[20]. Bhowmick S., Misra D. and Saha K. N. (2010), Variational formulation based analysis on growth of yield front in high speed rotating solid disks, *International Journal of Engineering Science and Technology*, 2(4), 200-19.

[21]. Birman B., Chona R., Byrd L. W. and Henay M. A. (2008), Response of spatially tailored structures to thermal loading, *Journal of Engineering Mathematics*, 61(2-4), 201-17.

[22]. Bose T., Rattan M. and Chamoli N. (2017), Modeling the effect of thermal gradation on steady-state creep behavior of isotropic rotating disc made of functionally graded material, *International Journal of Mechanical, Aerospace, Industrial, Mechatronic and Manufacturing Engineering*, 11(5), 1126-31.

[23]. Budinski K. G. (2000), Engineering Materials, Properties and Selection, 5th Ed., Prentice Hall of India, India.

[24]. Bui T. Q., Do T. V., Ton L. H. T., Doan D. H., Tanaka S., Pham D. T., Van T. A. N., Yu T. and Hirose S. (2016), On the high temperature mechanical behaviour analysis of heated functionally graded plates using FEM and a new third-order shear deformation plate theory, *Composites Part B*, 92, 218-41.

[25]. Burden R. L. and Faires J. D. (2011). Numerical Analysis 9th Ed., Cengage Learning India Limited, Delhi, India.

[26]. Cadek J., Oikawa H. and Sustek V. (1995), Thershold creep behaviour of discontinuous aluminium and aluminium alloy matrix composites: An overview, *Materials Science and Engineering: A*, 190(1-2), 9-21.

[27]. Callioglu H. (2004), Stress analysis of an orthotropic rotating disc under thermal loading, *Journal of Reinforced Plastics and Composites*, 23(17), 1859-67.

[28]. Callioglu H. (2008), Stress analysis of functionally graded isotropic rotating discs, *Advanced Composites Letters*, 17(5), 147-53.

[29]. Callioglu H. (2011), Stress analysis of functionally graded rotating discs under mechanical load and a steady state temperature distribution, *Sadhana*, 36(1), 53-64.

[30]. Callioglu H., Bektas N. B. and Sayer M. (2011a), Stress analysis of functionally graded rotating discs analytical and numerical solutions, *Acta Mechanica Sinica,* 27(6), 950-55.

[31]. Callioglu H., Demir E. and Sayer M. (2011b), Thermal stress analysis of functionally graded rotating discs, *Scientific Research and Essays*, 6(16), 3437-46.

[32]. Callioglu H., Sayer M. and Demir E. (2011c), Stress analysis of functionally graded rotating discs under mechanical and thermal loads, *Indian Journal of Engineering and Material Sciences*, 18(2), 111-18.

[33]. Çallioğlu H., Sayer M. and Demir E. (2015), Elastic-plastic stress analysis of rotating functionally graded discs, *Thin-Walled Structures*, 94, 38-44.

[34]. Callıoglu H., Topcu M. and Tarakcilar A. R. (2006), Elastic-plastic stress analysis of an orthotropic rotating disc, *International Journal of Mechanical Sciences*, 48(9), 985-90.

[35]. Chamoli N., Rattan M. and Singh S.B. (2010), Effect of anisotropy on the creep of a rotating disc of Al-SiC_p composite, *International Journal of Contemporary Mathematical Sciences*, 5(11), 509-16.

[36]. Chang C. I. (1976), Stresses and displacements in rotating anisotropic disks with variable densities, *AIAA Journal*, 14(1), 116-18.

[37]. Clyne T. W. and Withers P. J. (1993), An Introduction to Metal Matrix Composites, Cambridge University Press, UK.

[38]. Dai T. and Dai H.-L. (2015), Investigation of mechanical behavior for a rotating FGM circular disk with a variable angular speed, *Journal of Mechanical Science and Technology*, 29(9), 3779-87.

[39]. Dai T. and Dai H.-L. (2016), Thermo-elastic analysis of a functionally graded rotating hollow circular disk with variable thickness and angular speed, *Applied Mathematical Modelling*, 40(17-18), 7689-707.

[40]. Deepak D., Gupta V. K. and Dham A. K. (2009), Impact of stress exponent on steady state creep in rotating composite disc, *Journal of Strain Analysis*, 44(2), 127-35.

[41]. Deepak D., Garg M. and Gupta V. K. (2015), Creep behavior of rotating FGM disc with linear and hyperbolic thickness profiles, *Kragujevac Journal of Science*, 37, 35-48.

[42]. Deepak D., Gupta V. K. and Dham A. K. (2010a), Creep modeling in functionally graded rotating disc of variable thickness, *Journal of Mechanical Science and Technology*, 24(11), 2221-32.

[43]. Deepak D., Gupta V. K. and Dham A. K. (2010b), Steady state creep in a rotating composite disc of variable thickness, *International Journal of Materials Research*, 101(6), 780-86.

[44]. Demir E., Callioglu H. and Sayer M. (2017), Elasto-plastic thermal stress analysis of functionally graded hyperbolic discs, *Structural Engineering and Mechanics*, 62, 587-93.

[45]. Dieter G. E. (1988), Mechanical Metallurgy, McGraw-Hill, London.

[46]. Durodala J. F. and Adlington J. E. (1997), Functionally graded materials properties for disks and rotors, *Key Engineering Materials*, 127-131, 1199-206.

[47]. Durodala J. F. and Attia O. (2000), Deformation and stresses in functionally graded rotating disks, *Composite Science and Technology*, 60(7), 987-95.

[48]. Dwivedi D. D., Gupta V. K. and Dham A. K. (2013), Investigating the effect of thickness profile of a rotating functionally graded disc on its creep behavior, *Journal of Thermoplastic Composite Materials*, 26(4), 461-75.

[49]. Eraslan A. N. (2003), Elastic-plastic deformations of rotating variable thickness annular disks with free, pressurized and radially constrained boundary conditions, *International Journal of Mechanical Sciences*, 45(4), 643-67.

[50]. Eraslan A. N. and Argeso H. (2002), Limit angular velocities of variable thickness rotating disks, *International Journal of Solids and Structures*, 39(12), 3109-30.

[51]. Eraslan A. N. and Orcan Y. (2002), On the rotating elastic-plastic solid disks of variable thickness having concave profiles, *International Journal of Mechanical Sciences*, 44(7), 1445-66.

[52]. Farshi B. and Bidabadi J. (2008), Optimum design of inhomogeneous rotating discs under secondary creep, *International Journal of Pressure Vessels and Piping*, 85(7), 507-15.

[53]. Finnie I. and Hellar W. R. (1959), Creep of Engineering Materials, McGraw Hill, New York.

[54]. Fitzpatrick M. E., Dutta M. and Edwards L. (1998), Determination by neutron diffraction of effect of plasticity on crack tip strains metal matrix composite, *Journal of Material Science and Technology*, 14(9-10), 980-86.

[55]. Gamer U. (1983), Tresca's yield condition and the rotating solid disk, *Journal of Applied Mechanics*, 50(3), 676-78.

[56]. Gamer U. (1984), Elastic-plastic deformation of the rotating solid disk, *Ingenieur-Archiv*, 54(5), 345-54.

[57]. Garg M., Salaria B. S. and Gupta V. K. (2012), Analysis of steady state creep in a functionally graded rotating disc of variable thickness, *Composites: Mechanics, Computations*, *Applications*, 3(2), 171-88.

[58]. Garg M. and Gupta V. K. (2015), Stress analysis of a variable thickness rotating FGM disc, *International Journal for Research in Applied Science & Engineering Technology*, *3*(*VI*). 24-28.

[59]. Garg M., Salaria B. S. and Gupta V. K. (2013a), Effect of disc geometry on the steady state creep in a rotating disc made of functionally graded materials, *Materials Science Forum*, 736, 183-91.

[60]. Garg M., Salaria B. S. and Gupta V. K. (2013b), Effect of reinforcement gradient on steady state creep in a variable thickness rotating disc made of non-linear FGM, *International Journal of Materials Engineering Innovation*, 4(1), 1-17.

[61]. Garg M., Salaria B. S. and Gupta V. K. (2013c), Effect of thermal gradient on steady state creep in a rotating disc of variable thickness, *Procedia Engineering*, 55, 542-47.

[62]. Garg M., Salaria B. S. and Gupta V. K. (2015), Modeling creep in a variable thickness rotating FGM disc under varying thermal gradient, *Engineering Computations: International Journal for Computer-Aided Engineering and Software*, 32(5), 1230-50.

[63]. Goel N., Garg M., Salaria B. S. and Gupta V. K. (2012), Finite element analysis of creep in a functionally graded rotating disc, *International Journal of Computer Aided Engineering and Technology*, 4(5), 432-44.

[64]. Gun H. (2008), Two-dimensional boundary element analysis of creep continuum damage problems with plastic effects, *Computational Material Science*, 41(3), 322-29.

[65]. Guo S., Li G. and Zhang J. (2014), Multiple reciprocity boundary face method for transient heat conduction in functionally graded materials, *WIT Transactions on Modelling and Simulation*, 56, 167-76.

[66]. Gupta A., Talha M., and Singh B. N. (2016), Vibration characteristics of functionally graded material plate with various boundary constraints using higher order shear deformation theory, *Composites Part B*, 94, 64-74.

[67]. Gupta S. K. and Dharmani R. L. (1979), Creep transition in thick-walled cylinder under internal pressure, *Journal of Applied Mathematics and Mechanics*, 59(10), 517-21.

[68]. Gupta S. K. and Pankaj (2007a), Creep transition in a thin rotating disc with rigid inclusion, *Defence Science Journal*, 57(2), 185-95.

[69]. Gupta S. K. and Pankaj (2007b), Thermo elastic-plastic transition in a thin rotating disc with inclusion, *Thermal Science*, 11(1), 103-18.

[70]. Gupta S. K. and Shukla R. K. (1994), Effect of non-homogeneity on elastic-plastic transition in a thin rotating disc, *Indian Journal of Pure and Applied Mathematics*, 25(10), 1089-97.

[71]. Gupta S. K., Sharma S. and Pathak S. (2000b), Creep transition in a thin rotating disc of variable density, *Defence Science Journal*, 50(2), 147-53.

[72]. Gupta S.K., Sharma S. and Pathak S. (2000a), Creep transition in a thin rotating disc having variable thickness and variable density, *Indian Journal of Pure and Applied Mathematics*, 31(10), 1235-48.

[73]. Gupta V. and Singh S. B. (2012), Creep analysis in anisotropic composite rotating disc with hyperbolically varying thickness, *Applied Mechanics and Materials*, 110-116, 4171-77.

[74]. Gupta V. and Singh S. B. (2014), Creep behavior in an anisotropy rotating disc of Al-SiC_w having varying thickness in presence of residual stress, *ARPN Journal of Engineering and Applied Sciences*, 9(8), 1367-75.

[75]. Gupta V. K., Kumar V. and Ray S. (2005b), Modeling creep in a rotating disc with linear and quadratic composition gradients, *Engineering Computations*, 26(4), 400-21.

[76]. Gupta V. K., Kwatra N. and Ray S. (2007), Artificial neural network modeling of creep behavior in a rotating composite disc, *Engineering Computations*, 24(2), 151-64.

[77]. Gupta V. K., Singh S. B., Chandrawat H. N. and Ray S. (2003), Creep in an isotropic rotating disc of Al-SiC composites, *Indian Journal of Pure and Applied Mathematics*, 34, 1797-807.

[78]. Gupta V. K., Singh S. B., Chandrawat H. N. and Ray S. (2004a), Steady state creep and material parameters in a rotating disc of Al-SiC_p composite, *European Journal of Mechanics A/Solids*, 23(2), 335-44.

[79]. Gupta V. K., Singh S. B., Chandrawat H. N. and Ray S. (2004b), Creep behavior of a rotating functionally graded composite disc operating under thermal gradient, *Metallurgical and Materials Transactions* A, 35(4), 1381-91.

[80]. Gupta V. K., Singh S. B., Chandrawat H. N. and Ray S. (2005a), Modeling of creep behavior of a rotating disc in the presence of both composition and thermal gradients, *Journal of Engineering Materials and Technology*, 127(1), 97-105.

[81]. Gupta V. K., Singh S.B. and Ray S. (2009b), Role of reinforcement geometry on the steady state creep behavior of a rotating composite disc, *Multidisciplinary Modeling in Materials and Structures.* 5(2), 139-50.

[82]. Gupta V.K., Kumar V. and Ray S. (2009a), Modeling creep in a rotating disc with linear and quadratic composition gradients, *Engineering Computations*, 26(4), 400-21.

[83]. Güven U. (1992), Elastic-plastic stresses in a rotating annular disk of variable thickness and variable density, *International Journal of Mechanical Sciences*, 34(2), 133-38.

[84]. Güven U. (1995), On the applicability of Tresca's yield condition to the linear hardening rotating solid disk of variable thickness, *Journal of Applied Mathematics and Mechanics*, 75(5), 397-98.

[85]. Guven U. and Altay O. (2000), Elastic plastic solid disk with non-uniform heat source subjected to external pressure, *International Journal of Mechanical Sciences*, 42(5), 831-42.

[86]. Guven U. and Celik A. (2001), On transverse vibrations of functionally graded isotropic linearly elastic rotating solid disks, *Mechanics Research Communications*, 28(3), 271-76.

[87]. Hasan Z., Pandey R. K. and Sehgal D. K. (2011), Wear characteristics in Al-SiC particulate composites and the Al-Si piston alloy, *Journal of Minerals & Materials Characterization & Engineering*, 10(14), 1329-35.

[88]. Hassani A., Hojjati M. H., Farrahi G. H. and Alashti R. A. (2012), Semi-exact solution for thermo-mechanical analysis of functionally graded elastic-strain hardening rotating disks, *Communications in Nonlinear Science and Numerical Simulation*, 17(9), 3747-62.

[89]. Hassani A., Hojjati M. H., Farshi G. and Alashti, R. A. (2011), Semi-exact solutions for thermo-mechanical analysis of functionally graded rotating disks, *Composite Structures*, 93(12), 3239-51.

[90]. Hojjati M. H. and. Hassani A. (2008), Theoretical and numerical analysis of rotating discs of non-uniform thickness and density, *International journal of pressure vessels and piping*, 85(10), 694-700.

[91]. Horgan C. O. and Chan A. M. (1999), The pressurized hollow cylinder or disk problem for functionally graded isotropic linearly elastic materials, *Journal of Elasticity*, 55(1), 43-59.

[92]. Hunt W. H. (2000), Metal Matrix Composites, Comprehensive Composite Materials, Editor-T W Clyne, 6, Elsevier, USA, 57-66.

[93]. Jabbari M., Ghannad M. and Nejad M. Z. (2016), Effect of thickness profile and FG function on rotating disks under thermal and mechanical loading, *Journal of Mechanics*, 32(1), 35-46.

[94]. Jagtap K. R., Lal A. and Singh B. N. (2013), Thermomechanical elastic post-buckling of functionally graded materials plate with random system properties, *International Journal for Computational Methods in Engineering Science and Mechanics*, 14(3), 175-94.

[95]. Jahed H. and Bidabadi J. (2003), An axisymmetric method of creep analysis for primary and secondary creep, *International Journal of Pressure Vessels and Piping*, 80(9), 597-606.

[96]. Jahed H., Farshi B. and Bidabadi J. (2005), Minimum weight design of inhomogeneous rotating discs, *International Journal of Pressure Vessels and Piping*, 82(1), 35-41.

[97]. Jain R., Ramachandra K. and Simha K. R. Y. (1999), Rotating anisotropic disc of uniform strength, *International Journal of Mechanical Sciences*, 41(6), 639-48.

[98]. Kaw A. K. (2006), Mechanics of Composite Materials, 2nd Ed. CRC Press, Taylor and Francis Group, New York.

[99]. Kennedy D., Cheng R. K. H., Wei S. and Alcazar A. F. J. (2016), Equivalent layered models for functionally graded plates, *Computers and Structures*, 174, 113-21.

[100]. Khan A. S. and Huang S. (1995), Continuum Theory of Plasticity, John Wiley and Sons, Inc, New York.

[101]. Kollman F. G. (1981), Rotating elasto-plastic disc interference fits, *Journal of Mechanical Design*, 103(1), 61-66.

[102]. Kollman F. G. (1984), Welle-Nabe-Verbindungen. Konstruktionsbücher, 32nd Ed., Springer, Berlin.

[103]. Kordkheili S. A. H. and Livani M. (2013), Thermoelastic creep analysis of a functionally graded various thickness rotating disk with temperature-dependent material properties. *International Journal of Pressure Vessels and Piping*, 111-112, 63-74.

[104]. Lepeshkin A. (2012), Investigations of thermal barrier coatings for turbine parts, Ceramic Coatings, In -Applications in Engineering (Editor-Prof. Feng Shi), InTech, Croatia.

[105]. Li Y. and Langdon T.G. (1997), Creep behavior of an Al-6061 metal matrix composite reinforced with alumina particulates, *Acta Materialia*, 45(11), 4797-806.

[106]. Li Y. and Langdon T.G. (1999), An examination of a substructure-invariant model for the creep of metal matrix composites, *Materials Science and Engineering: A*, 265(1-2), 276-84.

[107]. Li Y. and Mohamed F. A. (1997), An investigation of creep behavior in an SiC-2124 Al composite, *Acta Materialia,* 45(11), 4775-85.

[108]. Liu S., Yu T., Bui T. Q. and Xia S. (2017a), Size-dependent analysis of homogeneous and functionally graded microplates using IGA and a non-classical Kirchhoff plate theory, *Composite Structures*, 172, 34-44.

[109]. Liu S., Yu T., Bui T. Q., Yin S., Thai D. K. and Tanaka S. (2017b), Analysis of functionally graded plates by a simple locking-freequasi-3D hyperbolic plate isogeometric method, *Composites Part B*, 120, 182-96.

[110]. Loghman A., Arani G. A., Shajari A. R. and Amir S. (2011), Time-dependent thermoelastic creep analysis of rotating disk made of Al–SiC composite, *Archive of Applied Mechanics*, 81(12), 1853-64.

[111]. Lubhan D. and Felger R. P. (1961), Plasticity and Creep of Material, Wiley, New York.

[112]. Ma B. M. (1959), A creep analysis of rotating solid disks, *Journal of the Franklin Institute*, 267(2), 167-68.

[113]. Ma B. M. (1960), A further creep analysis for rotating solid disks of variable thickness, *Journal of the Franklin Institute*, 269(5), 408-19.

[114]. Ma B. M. (1961), Creep analysis for rotating solid disks of variable thickness and temperature, *Journal of the Franklin Institute*, 271(1), 40-55.

[115]. Ma B. M. (1964), A power function creep analysis for rotating solid disks having variable thickness and temperature, *Journal of the Franklin Institute*, 277(6), 593-612.

[116]. Ma Z. Y. and Tjong S. C. (2001), Creep deformation characteristics of discontinuously reinforced aluminium-matrix composites, *Composites Science and Technology*, 61(5), 771-86.

[117]. Mahamood R. M., Akinlabi E. T., Shukla M. and Pityana S. (2012), Functionally graded material: An Overview, Proceedings of the World Congress on Engineering, July 4-6, 2012, London, U.K.

[118]. Malkin I. (1934), Design and calculation of steam turbine disc wheels, *Journal of Applied Mechanics*, 56(8), 585-600.

[119]. Meyers M. A. and Chawla K. K. (2009), Mechanical Behavior of Materials, 2nd Ed., Cambridge University Press, UK.

[120]. Mirzana I. M., Rao G. K. M., Sadaq S. I., Dasari K., and Kumari N. B. V. L. (2016), Behavioural study of a functionally graded material disk subjected to pressure conditions, *International Journal on Mechanical Engineering and Robotics*, 4(2), 39-45.

[121]. Mohamed F. A., Park K. T. and Lavernia E. J. (1992), Creep behaviour of discontinuous SiC-Al composites, *Materials Science and Engineering: A*, 150(1), 21-35.

[122]. Nath Y. and Sandeep K. (1998), Effect of transverse shear on static and dynamic buckling of anti-symmetrically laminated polar orthotropic shallow spherical shells, *Composite Structures,* 40(1), 67-72.

[123]. Naumenko K. and Altenbach H. (2007), Modelling of creep for structural Analysis, Springer Berlin Heidelberg, New York.

[124]. Nejad M. Z., Abedi M., Lotfian M. H. and Ghannad M. (2013), Elastic analysis of exponential FGM disks subjected to internal and external pressure, *Central European Journal of Engineering*, 3(3), 459-65.

[125]. Nie G. J. and Batra R. C. (2010), Stress analysis and material tailoring in isotropic linear thermoelastic incompressible functionally graded rotating disks of variable thickness, *Composite Structures*, 92(3), 720-29.

[126]. Nie G. J. Zhong Z. and Batra R. C. (2011), Material tailoring for orthotropic elastic rotating disks.*Composites Science and Technology*, 71(3), 406-14.

[127]. Nieh T. G. (1984), Creep rupture of a silicon carbide reinforced aluminium composite, *Metallurgical and Materials Transactions: A*, 15(1), 139-45.

[128]. Nieh T. G., Xia K. and Langdon T. G. (1988), Mechanical properties of discontinuous SiC reinforced aluminum composite at elevated temperature, *Journal of Engineering Materials and Technology*, 110(2), 77-82.

[129]. Orcan Y. and Eraslan A. N. (2002), Elastic-plastic stresses in linearly hardening rotating solid disks of variable thickness, *Mechanics Research Communications*, 29(4), 269-81.

[130]. Orlando J. A. and Filho G. (2004), A lower bound to the creep rupture time of pressurized thick cylinders, *International Journal of Mechanical Sciences*, 46(4), 527-39.

[131]. Padture N. P., Gell M. and Jordan E. H. (2002), Thermal Barrier Coatings for Gas-Turbine Engine Applications. *Science*, 296(5566), 280-84.

[132]. Pankaj (2009), Elastic-plastic transition stresses in an isotropic disc having variable thickness subjected to internal pressure, *International Journal of Physical Sciences*, 4(5), 336-42.

[133]. Pankaj and Bansal S. R. (2008a), Creep transition in a thin rotating disc having variable density with inclusion, *World Academy of Science, Engineering and Technology*, 38, 33-42.

[134]. Pankaj and Bansal S. R. (2008b), Elastic-plastic transition in a thin rotating disc with inclusion, *World Academy of Science, Engineering and Technology*, 38, 43-47.

[135]. Park K. T. and Mohamed F. A. (1995), Creep strengthening in a discontinuous SiC-Al composite, *Metallurgical and Materials Transactions A*, 26(12), 3119-29.

[136]. Park K. T., Lavernia E. J. and Mohamed F.A. (1990), High temperature creep of silicon carbide particulate reinforced aluminum, *Acta Metallurgica et Materialia*, 38(11), 2149-59.

[137]. Pei Y. C., Tan Q.C., Zhuang Q. W. and Ma J. C. (2013), Elastic-plastic stresses in rotating connection disk under temperature rise and transmitted torque, *International Journal of Mechanical Sciences*, 69, 141-49.

[138]. Peng X. L. and Li X. F. (2012), Effects of gradient on stress distribution in rotating functionally graded solid disks, *Journal of Mechanical Science and Technology*, 26(5), 1483-92.

[139]. Pitcher P. D., Shakesheff A. J. and Lord J. D. (1998), Aluminum based metal matrix composites for improved elevated temperature performance, *Journal of Materials Science and Technology*, 14(9-10), 1015-23.

[140]. Ramnath B. V., Elanchezhian C., Annamalai R. M., Aravind S., Atreya T. S. A., Vignesh V. and Subramanian C. (2014), Aluminium Metal Matrix Composites - A Review, *Reviews on Advanced Materials Science*, 38, 55-60.

[141]. Rattan M., Chamoli N. and Singh S. B. (2010), Creep Analysis of an Isotropic Functionally Graded Rotating Disc, *International Journal of Contemporary Mathematical Sciences*, 5(9), 419-31.

[142]. Rattan M., Kaushik A., Chamoli N. and Bose T. (2016), Steady state creep behavior of thermally graded isotropic rotating disc of composite taking into account the thermal residual stress, *European Journal of Mechanics A/Solids*, 60, 315-26.

[143]. Reddy T. Y. and Srinath H. (1974), Elastic stresses in a rotating anisotropic annular disc of variable thickness and variable density, *International Journal of Mechanical Sciences*, 16(2), 85-89.

[144]. Rees D. W. A. (1999), Elastic-plastic stresses in rotating discs by von Mises and Tresca, *Journal of Applied Mathematics and Mechanics*, 79(4), 281-88.

[145]. Rohatagi P. K., Liu Y., and Ray S. (1992), Friction and wear of metal-matrix composites, ASM Handbook (Editor-Scott, D.Henry), 18, 802-11.

[146]. Sayman O. (2006), Stress analysis of a thermoplastic composite disc under uniform temperature distribution, *Journal of Thermoplastic Composite Materials*, 19(1), 61-77.

[147]. Sen F. and Aldas K. (2009), Elastic-plastic thermal stress analysis in a thermoplastic composite disc applied linear temperature loads via FEM, *Advances in Engineering Software*, 40(9), 813-19.

[148]. Sen F. and Sayer M. (2006), Elasto-plastic thermal stress analysis in a thermoplastic composite disc under uniform temperature using FEM, *Mathematical and Computational Applications*, 11(1), 31-39.

[149]. Sen F., Pekbey Y. and Sayman O. (2007), Elastic-plastic stress analysis of a thermoplastic composite disc under parabolic temperature distribution, *Indian Journal of Engineering and Material Sciences*, 14(4), 282-88.

[150]. Seth B. R. (1966), Measure concept in mechanics, *International Journal of Non-Linear Mechanics*, 1(1), 35-40.

[151]. Shakesheff A. J., and Purdue G. (1998), Designing metal matrix composites to meet their target: Particulate reinforced aluminum alloys for missile applications, *Journal of Material Science and Technology*, 14(9-10), 851-56.

[152]. Shanmugavel P., Bhaskar G. B., Chandrasekaran M., Mani P. S. and Srinivasan S. P. (2012), An overview of fracture analysis in functionally graded materials, *European Journal of Scientific Research*, 68(3), 412-39.

[153]. Sharma J. N., Sharma D. and Kumar S. (2012), Stress and strain analysis of rotating FGM thermoelastic circular disk by using FEM, *International Journal of Pure and Applied Mathematics*, 74(3), 339-52.

[154]. Sharma S. and Sahni M. (2008), Creep analysis of thin rotating disc under plane stress with no edge load, *WSEAS Transactions on Applied and Theoretical Mechanics,* 3(7), 725-38.

[155]. Sharma S. and Sahni M. (2009), Elastic-plastic transition of transversely isotropic thin rotating disc, *Contemporary Engineering Sciences*, 2(9), 433-40.

[156]. Sharma S. and Sahni M. (2011), Elastic-plastic analysis for finite deformation of a rotating disk having variable thickness with inclusion, *International Journal of Mathematical, Computational, Physical, Electrical and Computer Engineering*, 5(3) 217-26.

[157]. Sharma S. and Yadav S. (2013), Finite difference solution of elastic-plastic thin rotating annular disk with exponentially variable thickness and exponentially variable density, *Journal of Materials*, 1-9.

[158]. Sharma S., Sahai I. and Kumar R. (2013), Creep transition of a thin rotating annular disk of exponentially variable thickness with inclusion and edge load, *Procedia Engineering*, 55, 348-54.

[159]. Shen H. S. (2009), Functionally Graded Materials - Nonlinear Analysis of Plates and Shells, CRC Press, Taylor and Francis Group, New York.

[160]. Shen H. S. (2014), Postbuckling of FGM cylindrical panels resting on elastic foundations subjected to lateral pressure under heat conduction, *International Journal of Mechanical Sciences*, 89, 453-61.

[161]. Shukla R. K. (1996), Creep transition in a thin rotating non-homogeneous disc, *Indian Journal of Pure and Applied Mathematics*, 27(5), 487-98.

[162]. Shukla R. K. (1997), Elastic-Plastic transition in a compressible cylinder under internal pressure, *Indian Journal of Pure and Applied Mathematics,* 28(2), 277-88.

[163]. Shukla R. K. (2000), Elastic-plastic transitional stresses in a non-homogeneous disc with variable thickness subjected to internal pressure, *Indian Journal of Pure and Applied Mathematics*, 31(6), 713-20.

[164]. Singh S. B. (2008), One parameter model for creep in a whisker reinforced anisotropic rotating disc of Al-SiC_w composite, *European Journal of Mechanics A/Solids*, 27(4), 680-90.

[165]. Singh S. B. and Rattan M. (2010), Creep analysis of an isotropic rotating Al-SiC_p composite disc taking into account the phase-specific thermal residual stress, *Journal of Thermoplastic Composite Materials*, 23(3), 299-312.

[166]. Singh S. B. and Ray S. (2001), Steady-state creep behavior in an isotropic functionally graded material rotating disc of Al-SiC composite, *Metallurgical and Materials Transactions A*, 32(7), 1679-85.

[167]. Singh S. B. and Ray S. (2002), Modeling the anisotropy and creep in orthotropic Aluminium-Silicon carbide composite rotating disc, *Mechanics of Materials*, 34(6), 363-72.

[168]. Singh S. B. and Ray S. (2003a), Creep analysis in an isotropic FGM rotating disc of Al-SiC composite, *Journal of Materials Processing Technology*, 143-144, 616-22.

[169]. Singh S. B. and Ray S. (2003b), Newly proposed yield criterion for residual stress and steady state creep in an orthotropic composite rotating disc, *Journal of Materials Processing Technology*, 143-144, 623-28.

[170]. Singh T. and Gupta V. K. (2011), Effect of anisotropy on steady state creep in functionally graded cylinder.*Composite Structures*, 93(2), 747-58.

[171]. Singh T. P. and Sahni M. (2016), Study of strength of rotating discs of innovative composite material with variable thickness, Proceedings of the International Multi Conference of Engineers and Computer Scientists, Vol. II, March 16-18, 2016, Hong Kong.

[172]. Stouffer D. C. and Dame L. T. (1996), Inelastic Deformation of Metals, John Wiley and Sons, 197-205.

[173]. Surappa M. K. (2003), Automotive applications of aluminium matrix composites, International Conference on Advances in Materials and Processes for Industrial Applications, ASM International, Pune Chapter, Sep. 25-26, Pune, India, 3-6.

[174]. Talha M. and Singh B. N. (2015), Stochastic vibration characteristics of finite element modelled functionally gradient plates, *Composite Structures,* 130, 95-106.

[175]. Thakur P. (2009), Elastic-plastic transition in a thin rotating disc having variable density with inclusion, *Structural Integrity and Life*, 9(3), 171-79.

[176]. Thakur P. (2010a), Elastic-plastic transition stresses in a thin rotating disc with rigid inclusion by infinitesimal deformation under steady-state temperature, *Thermal Science*, 14(1), 209-19.

[177]. Thakur P. (2010b), Creep transition stresses in a thin rotating disc with shaft by finite deformation under steady-state temperature, *Thermal Science*, 14(1), 425-36.

[178]. Thakur P. (2011), Effect of transition stresses in a disc having variable thickness and Poisson's ratio subjected to internal pressure, *WSEAS Transactions on Applied and Theoretical Mechanics*, 6(4), 147-59.

[179]. Thakur P. (2012), Stresses in a thin rotating disc of variable thickness with rigid shaft, *Journal of Technology for Plasticity,* 37(1), 1-14.

[180]. Thakur P., Kaur J. and Singh S. B. (2015), Mathematical model in a thin non-homogeneous rotating disc for isotropic material with rigid shaft by using Seth's transition theory, *Kragujevac Journal of Science*, 37(1), 11-22.

[181]. Thakur P., Singh S. B. and Kaur J. (2013), Thickness variation parameter in a thin rotating disc by finite deformation, *FME Transactions*, 41, 96-102.

[182]. Thakur P., Singh S. B. and Kaur J. (2014), Elastic-plastic stresses in a thin rotating disk with shaft having density variation parameter under steady-state temperature, *Kragujevac Journal of Science*, 36(1), 5-17.

[183]. Thawait A. K., Sondhi L., Sanyal S. and Bhowmick S. (2017), An investigation of stresses and deformation states of clamped rotating functionally graded disks, *Journal of Theoretical and Applied Mechanics*, 55(1), 189-98.

[184]. Timoshenko S. P. and Goodier J. N. (1970), Theory of Elasticity, McGraw-Hill, New York.

[185]. Tjong S. C. and Ma Z. Y. (2000), Microstructural and mechanical characteristics of in situ metal matrix composites, *Materials Science and Engineering*, 29(3-4), 49-113.

[186]. Tutuncu N. (1995), Effect of anisotropy on stresses in rotating discs, *International Journal of Mechanical Sciences*, 37(8), 873-81.

[187]. Vandana and Singh S. B. (2011), Modeling anisotropy and steady state creep in a rotating disc of Al-SiC_p having varying thickness, *International Journal of Scientific & Engineering Research*, 2(10), 1-10.

[188]. Viola E. and Tornabene F. (2009), Free vibrations of three parameter functionally graded parabolic panels of revolution, *Mechanics Research Communications*, 36(5), 587-94.

[189]. Wahl A. M. (1956), Analysis of creep in rotating disks based on the Tresca criterion and associated flow rule, *Journal of Applied Mechanics*, 23, 231-38.

[190]. Wahl A. M. (1957), Stress distributions in rotating disks subjected to creep at elevated temperature, *Journal of Applied Mechanics*, 79, 299-305.

[191]. Wahl A. M. (1958), Further studies of stress distribution in rotating disks and cylinders under elevated-temperature creep conditions, *Journal of Applied Mechanics*, 80, 243-50.

[192]. Wahl A. M. (1962), Application of the modified bailey equations for creep under biaxial tension stress. 4^{th} U. S. National Congress of Applied Mechanics, Berkeley, California.

[193]. Wahl A. M., Sankey G. O., Manjoine M. J. and Shoemaker E. (1954), Creep test of rotating discs at elevated temperature and comparison with theory, *Journal of Applied Mechanics*, 21, 225-35.

[194]. Wang S. S. (1983), Fracture mechanics for delamination problems in composite materials, *Journal of Composite Materials*, 17(3), 210-23.

[195]. Wattanasakulpong N., Prusty B. G. and Kelly D. W. (2011), Thermal buckling and elastic vibration of third-order shear deformable functionally graded beams, *International Journal of Mechanical Sciences*, 53(9), 734-43.

[196]. Yeh K.Y. and Han R. P. S. (1994), Analysis of high-speed rotating disks with variable thickness and inhomogeneity, *Journal of Applied Mechanics*, 61(1), 186-91.

[197]. Yoshioka H., Suzumura Y., Cadek J., Zhu S. J. and Milicka K. (1998), Creep behaviour of ODS aluminium reinforced by silicon carbide particulates: ODS Al-30 SiC_p composite, *Materials Science and Engineering: A*, 248(1-2), 65-72.

[198]. You L. H., Tang Y. Y., Zhang J. J. and Zheng C. Y. (2000), Numerical analysis of elastic-plastic rotating disks with arbitrary variable thickness and density, *International Journal of Solids and Structures*, 37(52), 7809-20.

[199]. You L. H., You X. Y., Zhang J. J. and Li J. (2007), On rotating circular disks with varying material properties, *Journal of Applied Mathematics and Physics*, 58(6), 1068-84.

[200]. Yue T. M., Du J. H. and Man H. C. (1998), High power Nd-YAG laser welding of SiC particle reinforced aluminum alloy 2124, *Journal of Material Science and Technology*, 14(9-10), 906-12.

[201]. Zafarmand H. and Hassani B. (2014), Analysis of two-dimensional functionally graded rotating thick disks with variable thickness, *Acta Mechanica*, 225(2), 453-64.

[202]. Zenkour A. M. (2006), Thermoelastic solutions for annular disks with arbitrary variable thickness, *Structural Engineering and Mechanics*, 24(5), 515-28.

[203]. Zenkour A. M. (2007), Elastic deformation of the rotating functionally graded annular disk with rigid casing, *Journal of Materials Science*, 42(23), 9717-24.

[204]. Zenkour A. M. (2009), Stress distribution in rotating composite structures of functionally graded solid disks, *Journal of Materials Processing Technology*, 209(7), 3511-17.

[205]. Zenkour A. M. and Mashat D. S. (2010), Analytical and numerical solutions for a rotating annular disk of variable thickness, *Applied Mathematics*, 1, 431-38.

[206]. Zhou F. and Ogata A. (2002), Elastic solutions for a solid rotating disk with cubic anisotropy, *Journal of Applied Mechanics*, 69(1), 81-83.